The biologically active conformation of peptide 11

by Gerard Joseph Ostheimer

A thesis submitted in partial fulfillment of the requirements for the degree of Master of Science in Chemistry
Montana State University

Abstract:
The biological activities of biopolymers are a function of their three dimensional (3D) structure. Therefore, establishing the biologically active 3D structure of a biopolymer can provide unique insights into the mechanism by which that biopolymer functions. Peptide 11, a synthetic peptide, which is derived from the sequence of the basement membrane glycoprotein, laminin, disrupts metastatic invasion of tumor cells through the basement membrane matrix. Peptide 11 functions by interacting with the 67 kDa high affinity laminin receptor found on the surface of metastatic tumor cells (Iwamoto et al, 1987, Graf et al, 1987a, Graf et al, 1987b). In order to determine the structural properties responsible for its interaction with the 67 kDa high affinity laminin receptor, peptide 11 was studied by two-dimensional 1H-1H nuclear magnetic resonance spectroscopy (NMR). NMR provides a powerful means of structure elucidation for biopolymers in solution (Wuthrich, 1986, Kessler et al., 1988, Wuthrich, 1989). Results of the application of NMR to determine the biologically active conformation of peptide 11 are presented in this thesis.

THE BIOLOGICALLY ACTIVE CONFORMATION OF PEPTIDE 11

by

Gerard Joseph Ostheimer

A thesis submitted in partial fulfillment
of the requirements for the degree

of

Master of Science

in

Chemistry

Montana State University
Bozeman, MT

December 1992

APPROVAL

of a thesis submitted by

Gerard Joseph Ostheimer

This thesis has been read by each member of the thesis committee and has been found to be satisfactory regarding content, English usage, format, citations, bibliographic style, and consistency, and is ready for submission to the College of Graduate Studies.

2/3/93
Date

Edward A. Neuschatz
Chairperson, Graduate Committee

Approved for the Major Department

2/3/93
Date

John R Quast
Head, Major Department

Approved for the College of Graduate Studies

2/3/93
Date

R K Brown
Graduate Dean

STATEMENT OF PERMISSION TO USE

In presenting this thesis in partial fulfillment of the requirements for a master of science degree from Montana State University, I agree that the Library shall make it available to borrowers under the rules of the Library. Brief quotations from this thesis are allowable without special permission, provided that accurate acknowledgement of source is made.

Permission for extensive quotation from or reproduction of this thesis may be granted by my major professor, or in his absence, by the Dean of Libraries when, in the opinion of either, the proposed use of the material is for scholarly purposes. Any copying or use of the material in this thesis for financial gain shall not be allowed without my written permission.

Signature M Ostheimer

Date 12/6/92

TABLE OF CONTENTS

TABLE OF CONTENTS - continued

LIST OF TABLES

LIST OF FIGURES

LIST OF FIGURES - continued

ABSTRACT

The biological activities of biopolymers are a function of their three dimensional (3D) structure. Therefore, establishing the biologically active 3D structure of a biopolymer can provide unique insights into the mechanism by which that biopolymer functions. Peptide 11, a synthetic peptide, which is derived from the sequence of the basement membrane glycoprotein, laminin, disrupts metastatic invasion of tumor cells through the basement membrane matrix. Peptide 11 functions by interacting with the 67 kDa high affinity laminin receptor found on the surface of metastatic tumor cells (Iwamoto *et al.*, 1987, Graf *et al.*, 1987a, Graf *et al.*, 1987b). In order to determine the structural properties responsible for its interaction with the 67 kDa high affinity laminin receptor, peptide 11 was studied by two-dimensional ^{1}H-^{1}H nuclear magnetic resonance spectroscopy (NMR). NMR provides a powerful means of structure elucidation for biopolymers in solution (Wüthrich, 1986, Kessler *et al.*, 1988, Wüthrich, 1989). Results of the application of NMR to determine the biologically active conformation of peptide 11 are presented in this thesis.

CHAPTER 1

INTRODUCTION

The Use of NMR to Study Peptide Conformation

The use of NMR to study the conformation of short, linear peptides, such as peptide 11, when free in aqueous solution, has several inherent difficulties (Wright *et al.*, 1988). The energy barriers separating low energy backbone conformations of short, linear peptides have been estimated to be on the order of 1-3 kilocalories per mole (Zimmerman *et al.*, 1977). Such low energy barriers between conformations permit short peptides to sample conformation space on the millisecond or shorter timescale (reviewed by Rose et al., 1985). As short peptides are constantly in the process of sampling conformation space, only a fraction of the molecules possess compact conformations at any one time.

The timescale of NMR experiments is on the order of milliseconds; therefore, molecular structures must exist for greater than milliseconds in order to be directly studied by solution state NMR. Short peptides explore conformation space rapidly on the NMR timescale. As a result of their rapid exploration of conformation space, the structural parameters of short peptides measured by NMR are an average of all different compact peptide conformations as well as the conformations of "unfolded" peptides in the process of exploring conformation space. Properties of interest to

biopolymer structure elucidation that are detectable by NMR include inter-proton distances, bond angles, chemical shifts, and the presence of hydrogen bonding. These parameters are all subject to the aforementioned time averaging.

NOESY of Short, Linear Peptides Free in Solution

Inter-proton distances can be measured by monitoring the through space dipolar magnetic cross-relaxation between the protons of interest (Jeener *et al.*, 1979, Macura and Ernst, 1980, Ernst *et al.*, 1987). This through space dipolar coupling is referred to as the nuclear Overhauser effect (NOE). NOE intensity is a function of the average distance between the two nuclei (r_{ij}), the correlation time (τ_c) of the molecule, and the mixing time (τ_m).

$$NOE \propto \langle r_{ij}^{-6} \rangle \cdot f(\tau_c) \cdot g(\tau_m)$$

Because the nuclear Overhauser effect diminishes rapidly with distance ($\propto \langle r_{ij}^{-6} \rangle$), the maximum inter-proton distance measureable in solution is approximately 5 Å.

The NOEs of short peptides free in solution are weighted towards compact conformations. Unless $r_{ij} < 3.5$ Å the NOE interaction will typically not be sufficiently strong to observe even if a long mixing time is employed (Dyson *et al.*, 1988a,b). This reduction in the range of NOE detection from 5.0 Å to 3.5 Å results from the NOE dependence on the rotational correlation time (τ_c) of the inter-proton vectors of the molecule under study. τ_c is a function of the viscosity of the solvent (η), the radius of the molecule (a) and the temperature of the solvent (T). For spherical molecules in solution:

$$\tau_c = 4\pi a^3/3kT$$

(k = Boltzmann's constant). When studied with high field (300 MHz $\geq \omega_0 \geq$ 600 MHz) NMR spectrometers, small molecules, with short τ_c ($\sim 10^{-11}$ sec.) exhibit strong positive NOEs, and large molecules, with long τ_c ($\sim 10^{-8}$ sec.) exhibit strong negative NOEs (Fig. 1). Short peptides, in non-viscous solvents, possess intermediate correlation times which result in values of $\omega_0 t_c \leq 1$ (ω_0 = experimental proton resonance frequency), for which NOE intensity is a minimum (Ernst *et al.*, 1987).

The range of measureable r_{ij} in short peptides free in solution is ≤ 3.5 Å. In an extended peptide, both non-sequential inter-residue distances and the sequential inter-residue distances $d_{NN}(i,i+1)$ and $d_{\beta N}(i,i+1)$, which range from 1.5 Å to 4.5 Å, will be greater than 3.5 Å. Therefore, detection of inter-residue NOEs indicates the existence of compact peptide conformations in solution. However, of the many low energy compact conformations accessible to a peptide free in aqueous solution (Zimmerman *et al.*, 1977), only a few, if any, very closely related conformations are likely to be responsible for its biological activity. Unfortunately, it is impossible to quantitate by solution NMR what fraction of the free peptide conformer population is biologically active. Therefore, it is not possible to specify the biologically active conformation of a short, linear peptide solely by NMR spectroscopy of the peptide free in solution.

Transferred Nuclear Overhauser Effect Spectroscopy

A short flexible peptide ligand need only possess its biologically active

Figure 1. NOE Intensity Dependence on Correlation Time (τ_c).

When studied at high magnetic fields, inter-proton NOE intensity is large and negative for $\tau_c < \sim 10^{-9}$ s and large and positive for $\tau_c > \sim 10^{-11}$ s. If τ_c is in between this range ($\omega_0\tau_c \approx 1$), then inter-proton NOE intensity is at a minimum. The τ_c of peptide 11 is in the range for which NOE intensity is a minimum.

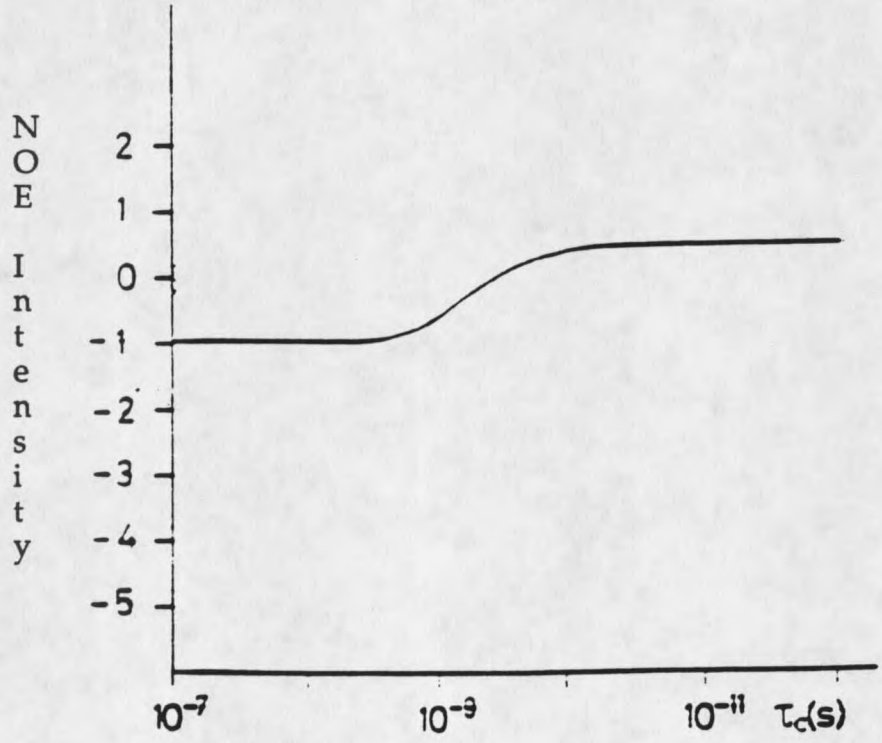

conformation when it is bound to its receptor. Evidence for the structure of a peptide ligand when bound to its receptor can be determined by using the 1D time-dependent intramolecular transferred Nuclear Overhauser Effect (TRNOE)(Balaram *etal.*, 1972a, Balaram *et al.*, 1972b, Clore and Gronenborn, 1982, Clore and Gronenborn, 1983) or the 2D intramolecular TRánsferred Nuclear Overhauser Effect SpectroscopY (TRNOESY, Clore and Gronenborn, 1986, Campbell and Sykes, 1991a, Campbell and Sykes, 1991b). For large molecules, such as cell surface receptors like the 67 kDa high-affinity laminin receptor, $\tau_c > 10^{-8}$ seconds and $\omega_0\tau_c >> 1$. The long correlation time of large molecules results in extremely efficient magnetic cross-relaxation between protons but very broad linewidths. The efficient magnetic cross-relaxation of small molecules when bound to the large molecule results in the small molecule exhibiting strong negative NOEs (Fig. 1).

When a ligand binds to its receptor its correlation time slows from its value free in solution to a value close to that of the receptor. The rate of cross-relaxation between the protons i and j (W_{ij}) of the peptide increases as a result of receptor binding. Receptor bound magnetic cross-relaxation rates (W_{ijB}) are far greater than the magnetic cross-relaxation rates of the peptide free in solution (W_{ijF}). Therefore, NOE intensities of receptor bound peptides build much faster than NOE intensities of peptides free in solution. Unfortunately, it is not possible to directly observe the peptide by solution state NMR when it is bound to a large receptor protein. The long τ_c of molecules which are 50 kilo-Daltons (kDa) or larger exhibit line widths that are too broad to be observed by NMR. However, if the peptide ligand were to dissociate from its receptor, then its τ_c would decrease to its shorter free in

solution value, and the peptide would again be NMR observable.

The magnetic cross-relaxation between protons of a short peptide is significantly slower when it is free in solution. Therefore, the distribution of magnetization that results from rapid nuclear Overhauser cross-relaxation in the bound state, and the structural information the magnetization contains, is lost more slowly in the free peptide. The receptor bound magnetization, and the structural information contained therein, can be measured by NOESY. Through chemical exchange, the information concerning the bound state has been "transferred" to the free state where it can be measured. For this transferral to be effective, the peptide ligand must exchange rapidly between the free and the bound state relative to the rate of magnetic longitudinal relaxation (T_1 relaxation) of the free peptide.

As cross-relaxation rates are relatively rapid for large molecules, unwanted spin diffusion can occur between the protons of the peptide ligand, while it is receptor bound. Spin diffusion alters NOE intensities in complex ways, and consequently disrupts attempts to use NOE intensity to calculate r_{ij}. Recently, Campbell and Sykes have evaluated the effects of mixing time (τ_m), receptor bound correlation time (τ_{cB}), and fraction of bound peptide (p_B) on TRNOESY intensity and on the inter-proton distances calculated from these intensities (Campbell and Sykes, 1991a). They found spin diffusion to occur quite rapidly on the NMR timescale. The effects of τ_m, τ_{cB}, and p_B are additive, so each can be considered independently. Spin diffusion is maximized at long τ_m, long τ_c, and high p_B. In order to achieve a decent signal-to-noise ratio, Campbell and Sykes suggest that "it is best to use very low p_B values but work at a reasonable τ_m" (ie. $\leq$ 200 ms). In the discussion of

their results they provide the following example, "for a protein of $M_r \approx 80{,}000$ Da one need only bind 5% of the peptide to achieve both a huge enhancement in the size of the TRNOE and a linear buildup of magnetization for reasonable mixing times."

If the p_B is relatively small (ie. < 5%), then interference from NMR detection of the free ligand might be anticipated. For small p_B both the chemical shift ($\delta_{obs} = p_F\delta_F + p_B\delta_B$) and the linewidth ($\Delta\nu_{obs} = p_F\Delta\nu_F + p_B\Delta\nu_B$) will be dominated by the free peptide (Campbell and Sykes, 1991b). However, due to the difference in cross-relaxation rates mentioned earlier ($W_{ijB} >> W_{ijF}$), the observed NOEs will be TRNOE dominated, $NOE(\tau_m) \approx -[p_F W_{ijF} + p_B W_{ijB}]\tau_m \approx -[p_B W_{ijB}]\tau_m$, at "reasonable" τ_m (Campbell and Sykes, 1991b). Interestingly, for a p_B as low as 0.5% the distances derived from TRNOE cross peak intensity correspond quite well to the inter-proton distances of the bound peptide (Campbell and Sykes, 1991a). As opposed to NOEs measured from short peptides free in solution, TRNOESY distance measurements relate directly to the bound, biologically active conformation, and can therefore be used to provide information on the biologically active conformation of a short peptide. TRNOESY has been used to gain insights concerning the interactions between fibrinogen derived peptides and thrombin (Ni *et al.*, 1989a-1989c), the interactions of troponin I and troponin C (Campbell and Sykes, 1991a), the different conformations of peptides when bound to the chaperones DnaK and GroEL (Landry *et al.*, 1992) and in other systems, as well.

The Biological Activity of Peptide 11

Laminin is the primary glycoprotein of basement membranes (Timpl *et al.*, 1979; Chung *et al.*, 1979). It is composed of three chains: A (440,000 kDa), B1 (225,000 kDa), and B2 (205,000 kDa), which combine to form a cruciform shaped structure (Engel *et al.*, 1981). Various domains of laminin have been shown to promote attachment to basement membranes, migration through basement membranes, and growth and differentiation of certain cell types (reviewed by Beck *et al.*, 1990, Goodman, 1992, and Starkey, 1990). Metastatic ability has been shown to correlate with the expression of 67 kDa high-affinity laminin receptor (Terranova *et al.*, 1983, Wewer *et al.*, 1986). High concentrations of this cell surface receptor improve the ability of these cells to attach to, and to subsequently migrate through, basement membranes. Metastatic cells employing the 67 kDa high-affinty laminin receptor to adhere to the basement membrane interact with the laminin B1 chain near its intersection with the other two chains (Graf *et al.*, 1987a). The 67 kDa high-affinity laminin receptor is not the only means by which metastatic cells interact with laminin. Other laminin receptors include the a6β1 (Ramos *et al.*, 1991) and a7β1 (Kramer *et al.*, 1991) integrins.

Peptide 11, CDPGYIGSR, which corresponds to residues 924-933 of the laminin B1 chain has been shown to inhibit the attachment of tumor cells to laminin (Graf *et al.*, 1987a), inhibit migration of tumor cells through a basement membrane matrix Matrigel ©, Ostheimer *et al.*, 1992), which is a reconstitution of a urea extraction of basement membranes (Kleinman *et al.*, 1986), and decrease tumor lung colony formation *in vivo* (Iwamoto *et al.*, 1987, Ostheimer *et al.*, 1992). The minimum sequence necessary for biological

activity is YIGSR. Either deletion of tyrosine or substitution of lysine or glutamine for arginine is sufficient to destroy YIGSR activity (Graf *et al.*, 1987b). The amide form of peptide 11, CDPGYIGSR-NH_2, is more active (Iwamoto, *et al.*, 1987), and hereafter, the name peptide 11 will refer to the amide form, which was the form of the peptide used in this work. The biological effects of Peptide 11 are believed to result from binding to the 67 kDa high affinity laminin receptor found on the metastatic cells, blocking the normal laminin binding site, and thereby reducing the capacity of the metastatic cells to adhere to basement membranes via laminin (Iwamoto *et al.*, 1987, Ostheimer *et al.*, 1992).

Prior Computational Studies of Peptide 11 Conformation

The YIGSR region of peptide 11 has been previously investigated by molecular dynamics (MD) (Brandt-Rauf *et al.*, 1989, McKelvey *et al.*, 1991). However, as neither of the two previous studies incorporated experimentally derived structural information into their calculations, the structures they propose for YIGSR are strictly predictions.

Brandt-Rauf *et al.* calculated the lowest energy conformation of N-Acetyl-YIGSR-$NHCH_3$ using the modelling software, ECEPP (Empirical Conformational Energy for Polypeptides and Proteins, Scheraga, 1984). They predicted that the backbone conformation of the YIGSR sequence would correspond to regions C-D-D^*-D-D of a Zimmerman ϕ,ψ plot (Zimmerman *et al.*, 1977). A Zimmerman ϕ,ψ plot is a Ramachandran plot, to which regions corresponding to conformational energy minima have been assigned a single letter code. Unstarred letters indicate ø to be in the range, $-180^\circ \leq \phi \leq 0^\circ$, and

starred letters indicate ϕ to be in the range, $0° \leq \phi \leq 180°$. C-D-D*-D-D consists of a bend about the glycine residue held in place by a hydrogen bond between the NH_2 of the arginine side chain and the backbone C=O of tyrosine.

McKelvey *et al.* calculated the lowest energy conformation N-Acetyl-YIGSR-$NHCH_3$ using the molecular mechanics program CHARMM (Chemistry at HARvard Macromolecular Mechanics, Brooks *et al.*, 1983). McKelvey *et al.* predicted that for dielectric constants ranging from 1 to 10 that the conformation of the YIGSR sequence would correspond to Zimmerman regions CA-A-A-F-E/C. CA being a previously undefined region of the Zimmerman plot found between regions C and A. CA-A-A-F-E/C corresponds to a partial helical conformation, which McKelvey *et al.* found to be stabilized by hydrogen bonds between the NH_2 of the arginine side chain and the C=O of tyrosine, isoleucine, and glycine. Although Brandt-Rauf *et al.* and McKelvey *et al.* both predicted YIGSR to adopt a bent conformation, the type of bend differed greatly between the predictions of the two groups.

<u>The Use of Amino Acid Substitution to Determine the Biologically Active Conformation of Peptide 11</u>

The prediction of a turn about the glycine of YIGSR is not unexpected. Glycine lacks a side chain and is therefore achiral. Because glycine does not possess a side chain, it is free to explore all four quadrants of ϕ,ψ space. In contrast, the side chains of l-stereoisomeric amino acids sterically forbid them from adopting conformations corresponding to quadrant IV of a ϕ,ψ plot. Consequently, glycine frequently plays the role of a hinge, allowing protein backbones to make tight turns and bends not allowed by other amino acids.

The predictions of a glycine centered YIGSR bend by Brandt-Rauf *et al.*

and McKelvey *et al.* can be tested by substituting chiral amino acids for the achiral glycine. Substitution of d-alanine and l-alanine for Gly_7 would prevent the backbone of peptide 11 from adopting conformations at its seventh residue corresponding to ϕ,ψ quadrants III and IV, respectively. The d-$alanine_7$ analog, CDPGYI(dA)SR-NH_2 (d-analog), was found to be as capable as the native peptide 11 of inhibiting cell migration *in vitro* at high concentrations (0.10 mM) and to be more effective than peptide 11 at lower concentrations (0.0125 mM) (Fig. 2). The increased activity of the d-analog at low peptide concentrations is thought to be at least partly due to the fact that d-Ala_7 is more resistant to protease activity than the native Gly_7. The presence of proteases was expected as intact cells are present in the *in vitro* assay employed to determine peptide activity.

In contrast, the l-$alanine_7$ analog, CDPGYI(lA)SR-NH_2 (l-analog), was found to be considerably less active than peptide 11 and the d-analog at both low and high concentrations (Fig. 2). The different activities of the d and l-analogs suggests that the biological activity of peptide 11 results in part from the conformation of the YIGSR region of the molecule. To test this hypothesis 2D ^1H-^1H NMR spectroscopy was employed to measure structural parameters of peptide 11, the d-analog, and the l-analog when free in solution and when bound to the 67 kDa high affinity laminin receptor. The structural information derived from NMR was incorporated into molecular dynamics simulations of the peptides in order to generate candidate structures for the biologically active conformation of peptide 11.

As per the earlier discussion of short, linear peptides free in aqueous solution, it is typically not possible to directly determine the biologically

Figure 2. Dose Dependent (mM) Inhibition(%) of Metastatic Cell Migration *in vitro* by Peptide 11, the D-analog, and the L-analog.

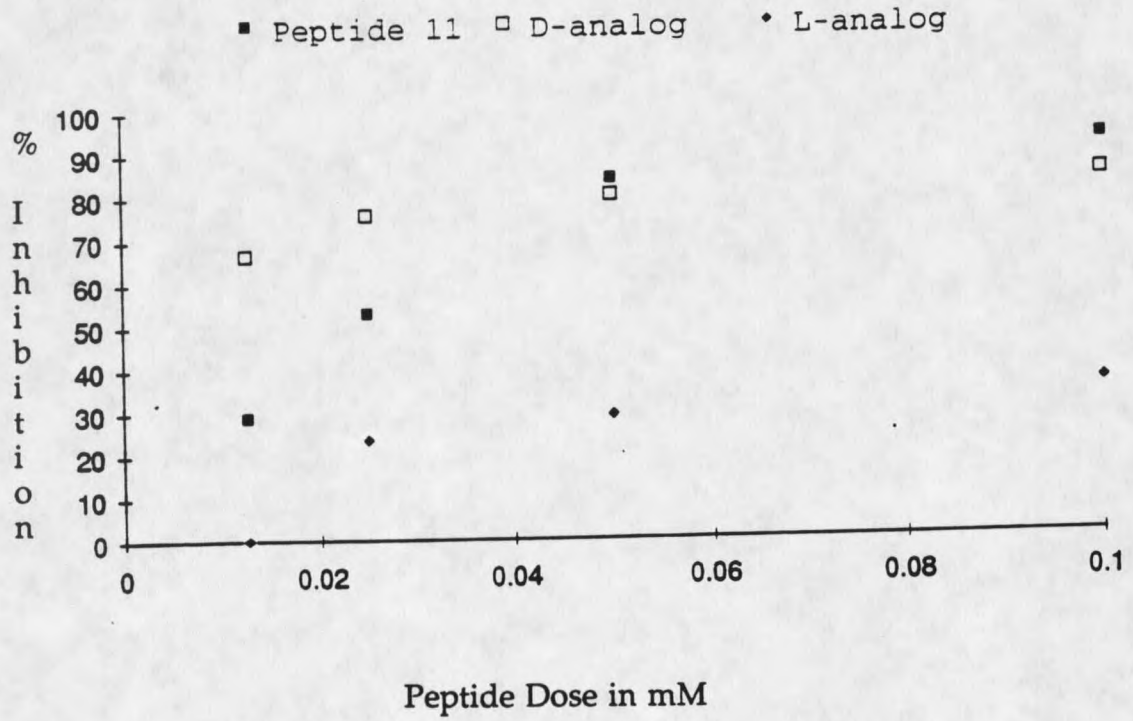

active conformation of a short peptide when it is free in solution. However, in this system, it was believed that a comparison of the free in solution candidate conformations of peptide 11 with the free in solution candidate conformations of the equally active and less active analogs might suggest conformational properties responsible for the biological activity of peptide 11.

NMR spectroscopy indicated that peptide 11 and the d-analog behaved similarly, and simultaneously quite differently from the l-analog when free in solution. When the NMR derived distance constraints were incorporated into molecular dynamics simulations quite similar conformations for peptide 11 and the d-analog were generated. The conformations generated for the l-analog were very different from those preferred by peptide 11 and the d-analog. These conformations, and the data used to derive them, will be described and discussed below.

TRNOESY experiments successfully indicated the receptor bound conformation of peptide 11 and the d and l-analogs. Based on TRNOESY cross peak patterns, it was possible to identify the secondary structures possessed by the bound peptides. In order to visualize the peptide conformations, TRNOE intensities were converted into inter-proton distances, which were then employed to restrain molecular dynamics simulations. The peptide conformations generated by the molecular dynamics are presented, and their biological relevance are discussed below.

Other groups of researchers are employing NMR spectroscopy to elucidate the structure/function relationships of peptides derived from proteins involved in cell adhesion. Data exists concerning peptides containing the RGD (arginine-glycine-aspartic acid) sequence (Reed *et al.*, 1988,

Bogusky *et al.*, 1992) and non-RGD cell adhesion promoting peptides from collagen, fibrinogen, and laminin (Mayo *et al.*, 1991, Mayo *et al.*, 1990, Burke *et al.*, 1991).

CHAPTER 2

MATERIALS AND METHODS

Peptide Synthesis

Peptide 11, the d-alanine$_7$ analog (d-analog), and the l-alanine$_7$ analog (l-analog) were synthesized, purified, and analyzed by Craig Johnson at the MSU Peptide Synthesis Facility. Peptides were synthesized on a Milligen 9050 Peptide Synthesizer using standard FMOC chemistry with Bop/Hobt activation. DMF, DCM, acetic anhydride, and piperidine were of spectrophotomeric grade as supplied by Aldrich Chemical Co. Peptides were purified by HPLC using a Vydac C18 reverse phase preparatory column, and analyzed on a Vydac C18 reverse phase analytical column. Peptide purity was estimated to be greater than or equal to 90%. Molecular weights were checked by probe FAB mass spectrometry, which was performed by Joe Sears at the MSU Mass Spectrometry Facility.

Isolation of the 67 kDa high-affinity laminin receptor

All samples of the 67 kDa high-affinity laminin receptor were prepared by Terry Landowski and Jean Starkey. The 67 kDa high-affinity laminin receptor was isolated from EHS mouse tumor using a modified laminin extraction process (Timpl *et al.*, 1979). EHS tumor was propagated by subcutaneous transplant in C57BL/6 mice. Tumors were harvested after having grown to be approximately 1.5 to 2.0 cm in diameter. Harvested

material was washed extensively in 4° C Tyrode's calcium and magnesium free saline and stored at -20° C until used.

Tumor thawed at 4° C was covered with an equal volume of ice cold buffer containing 3.4 M NaCl, 0.05 M Tris-HCl, pH 7.4, 0.01 M ethylenediaminetetraacetic acid (EDTA) plus the protease inhibitors Benzamidine, N-ethylmaleamide (NEM), and phenylmethanesulfonyl flouride (PMSF). The preparation was homogenized on ice for approximately 20 minutes with a Polytron homogenizer, centrifuged for 10 minutes at 12,000 x g, and the supernatent discarded. Homogenization was repeated 2-3 times until the material became a thick slurry, which was then suspended in 10 volumes (v/v) of 0.5 M NaCl, 0.05 M Tris, pH 7.4, and the same protease inhibitors. Basement membrane components were extracted by mechanical stirring overnight at 4° C, followed by centrifugation for 20 minutes at 10,000 x g. The supernatant was made 1.7 M in NaCl and stirred on ice for 2 hours to precipitate type IV collagen, which was then removed by 30 minutes of centrifugation at 10,000 x g. The supernatent was dialyzed against a solution of 2 M urea, 0.05 M Tris-HCl, pH 8.6. Silver-stained SDS-Page electrophoresis of the urea treated material showed it to consist predominantly of laminin and a band characteristic of the 67 kDa high-affinity laminin receptor. Minor additional bands were present at 90, 55, and 40 kDa (data not shown).

Laminin receptor was then extracted from the urea treated material by the method of Folch et al. (1957). The material extracted from EHS tumor was mixed with 20 volumes of chloroform:methanol (2:1, v/v) and mechanically stirred at room temperature for one hour, after which time it was allowed to

partition into aqueous and organic phases. The organic phase, which contained the laminin receptor, was collected through the bottom of a separatory funnel. Great care was taken to exclude the aqueous phase and interfacial material, which is predominantly laminin. Rotary evaporation was then used to reduce the volume of organic solvent. Renaturation of the receptor was achieved through exchange of the urea by the following series of dialysis steps: three changes of 1 M urea in methanol, three changes of 89% water, 10% methanol, 1% NP-40 in Dulbecó's phosphate buffered saline (DPBS), and four changes of 95% methanol. Dialysis into methanol was necessary to reduce the detergent concentration. The presence of detergent in the isolated material disrupted NMR spectroscopy of the peptides in the presence of receptor. The solution was then frozen at -70° C, lyophilized to dryness, and stored at -20° C.

Silver stained SDS-Page with a 5% to 15% acrylamide gradient of the final material revealed a single band at 67 kDa with a negligible amount of non-specific background (Fig. 3). In the gel presented in figure 3, lane A contained the molecular weight standards, lanes B and D contained material that had been reduced and lanes C and E contained unreduced material. The lower intensity of lanes B and D resulted from the lower concentrations of material found in the reduced solutions. The material extracted from tumor was reduced by heating for one hour at 80° C in a solution that was 20% glycerol, 2% sodium dodecyl sulfate (SDS), 2% beta-mercapto ethanol, and 0.05 M Tris-HCl, pH 8.6. The white powder produced by the extraction process, was used in TRNOESY NMR experiments without further purification.

Figure 3. SDS-Page of the Material Extracted From EHS Tumor.

The molecular weights (kDa) of the standard in lane A are given. The material in lanes B and D was reduced. Non-denatured material was run in lanes C and E.

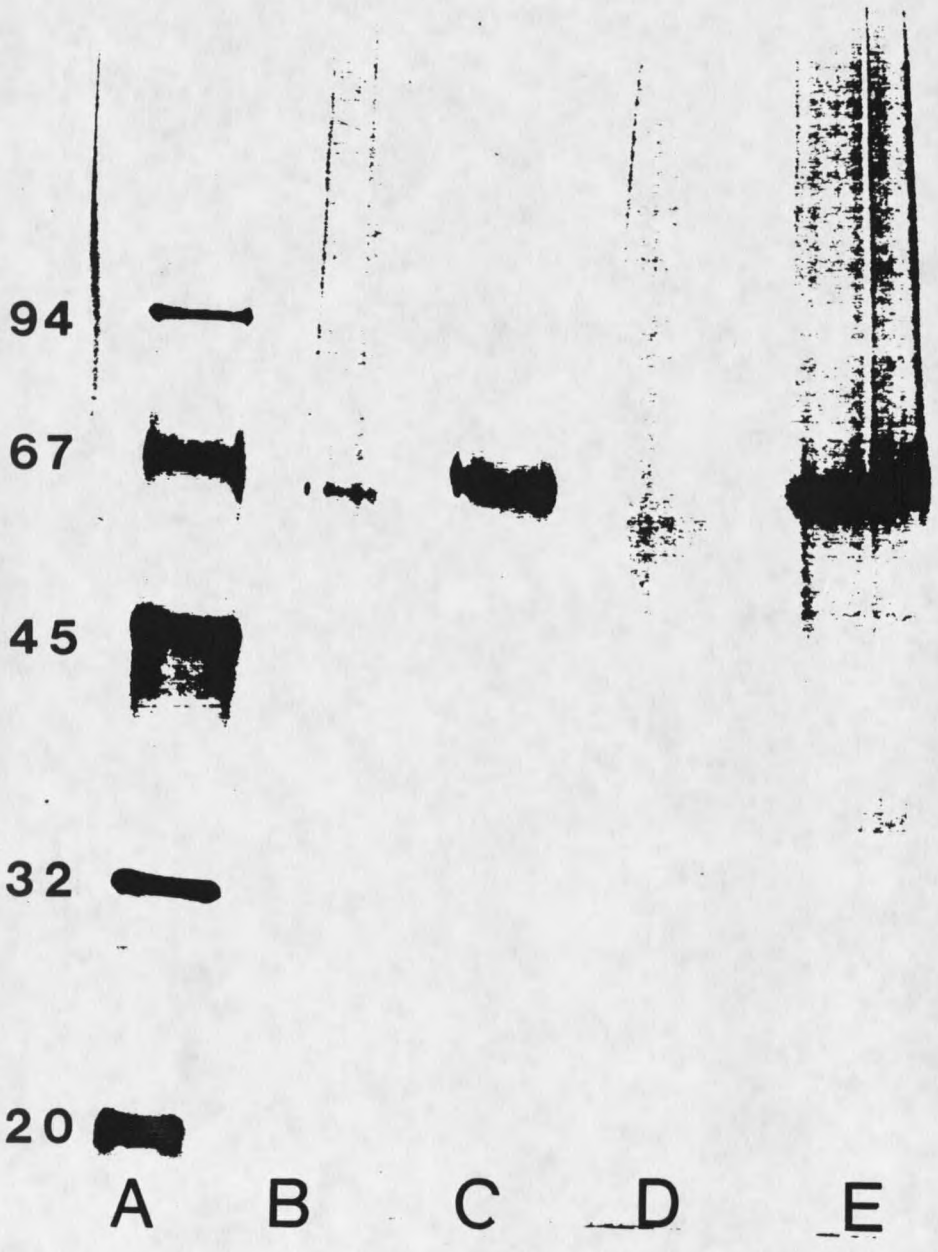

Composition of Solution State NMR Samples

NMR spectroscopy of peptide 11, the d-analog, and the l-analog freein solution was performed on two sets of samples. The peptide concentration in both sets of NMR sample was approximately 10 mM. The first set of peptide 11, d-analog, and l-analog samples was dissolved in 90% H_2O/10% D_2O, 100 mM NaCl, 10 mM KPO_4, and 5 mM $MgCl_2$. Sodium azide at 0.02% was included as a bacteriocide. The pH of these solutions was in the range of 4.5 to 5, not correcting for isotope effects. The second set of peptide samples was dissolved in 90% Dulbeco's phosphate buffered saline (DPBS), which is 150 mM NaCl, 2.5 mM KCl, 1 mM $CaCl_2$, 0.5 mM $MgCl_2 \cdot 6\ H_2O$, 6.5 mM $Na_2HPO_4 \cdot 2\ H_2O$, 1.5 mM KH_2PO_4, and 10% D_2O. The pH of these samples was in the range of 7 to 7.6. The chemical shift standard employed was 3-(trimethylsilyl) propionic acid-2,2,3,3-d_4 (TSS).

NMR spectroscopy of peptides in the presence of the 67 kDa high-affinity laminin receptor was performed on samples which were ~1 mM in peptide and ~0.04 mM in receptor. The 67 kDa high-affinity laminin receptor has limited solubility in aqueous solution, and 3 mg per ml was the maximum attainable receptor concentration. As the receptor has a molecular weight of 67 kDa, it was assumed that the receptor was essentially pure and therefore the concentration was approximately 0.04 mM. Peptide 11 in the presence of receptor were made using both of the solutions used to study the peptides free in solution. The pH of these solutions was 5.0 and 7.6 respectively. Solutions of the d and l-analogs in the presence of receptor were made solely with DPBS. The pH of these solutions was 7.6 as well. DPBS was employed to study peptide in the presence of the receptor, because the 67 kDa

high-affinity laminin receptor appears to be more stable in aqueous solution in the presence of the divalent cations Ca^{2+} and Mg^{2+} (Jean Starkey and Terry Landowski, unpublished data).

The ratio of peptide to receptor in the NMR samples yields a $p_B \leq 2.5\%$. Although this p_B is relatively small, the TRNOESY cross peaks would be expected to be dominated by the bound form of the peptide due to the long τ_c expected for the 67 kDa high-affinity laminin receptor (Campbell and Sykes, 1991a). A low p_B produces the beneficial effect of reducing spin diffusion. As a result, the inter-proton distances of peptide 11, and the d and l-analogs derived from TRNOE peak intensities may reasonably be employed to calculate the receptor-bound peptide conformations; provided that the mixing times used are "reasonable" (Campbell and Sykes, 1991a).

NMR Spectroscopy Experimental Parameters

All NMR experiments were acquired at 500 MHz on a Bruker AM 500 with a 5 mm proton selective probe. The temperature of the sample was maintained at 274 K by a Eurotherm temperature control unit. Performing NMR spectroscopy of short, linear peptides in aqueous solution at low temperatures retards the exchange of amide protons, and increases the correlation time of the free peptide (Campbell and Sykes, 1991a). All spectra were acquired over a spectral width of 5263.16 Hz with the carrier frequency centered on the H_2O resonance. All spectra consisted of 512 t1 experiments, each with 2048 data points. 64 scans were time averaged per t1 experiment. Quadrature detection in t1 was achieved using time-proportional phase incrementation (TPPI) (Bodenhausen *et al.*, 1980, Marion and Wüthrich,

1983). At the experimental conditions described above, the longitudinal relaxation times (T_1) for the protons in the peptides ranged from 300 to 550 ms (Table 1). As an effective relaxation delay is 1 to 5 · T_1, 1 second relaxation delay was deemed sufficient.

Table 1. Longitudinal Relaxation Times (T_1) of the Different Species of Protons Found in Peptide 11.

Proton	T_1 (ms)
CH_3	300
CH_2	300
CH	450
aromatic	550
NH	350

TOtal Correlation SpectroscopY (TOCSY) (Bax and Davis, 1985b, Bax, 1989, Cavanagh and Rance, 1990) incoporating the MLEV-17 spin lock sequence at a field strength of 10 kHz, and ROtating frame nuclear Overhauser Effect SpectroscopY (ROESY) (Bothner-By *et al.*, 1984, Bax and Davis, 1985a, Neuhaus and Keeler, 1986) utilizing a spin lock of 2.5 kHz for 200 ms, were utilized to assign the spectra. In these experiments the water resonance was suppressed by low power irradiation coherent with the transmitter phase during the relaxation delay.

Nuclear Overhauser Effect SpectroscopY (NOESY) (Jeener *et al.*, 1979) and transferred Nuclear Overhauser Effect Spectroscopy (TRNOESY) (Clore and Gronenborn, 1983, Campbell and Sykes, 1991a, Campbell and Sykes, 1991b) experiments were performed to estimate inter-proton distances. Water suppression in these experiments was obtained by Jump and Return (J+R)

detection (Plateau and Gueron, 1982). The pulse sequence of J+R NOESY experiments is presented in figure 4. By adjusting the receiver phase and incorporating a suitable delay immediately prior to signal detection it is possible to generate 2D J+R NOESY experiments that are in phase. Phasing with instrumental parameters is known as hardware phasing, a technique which greatly improved the ability to detect NOESY peaks in the resulting spectra by noticeably flattening the baseline. When processing the spectra only minor software phase corrections were necessary.

Processing of NMR Data

2D NMR data sets were processed on a Silicon Graphics 4D25TG workstation using the NMR processing software package, FELIX version 2.05 (© Hare Research Inc.). The 2 K by 0.5 K experimental data sets were converted to 1 K by 1 K matrices by deleting the imaginary points from the f2 dimension and zero filling the t1 dimension. Prior to Fourier transforming

Figure 4. J+R NOESY Pulse Sequence and Phase Cycling.

Pulse Sequence

D - 90°(PH1) - t1 - 90°(PH2) - t_m - 90°(PH3) - t_1 - 90°(PH4) - t_2 - t2(PH5)

Delays	Phase Cycles
D = 1 sec. relaxation delay	PH1 = 0 0 2 2 0 0 2 2
t1 = 2D evolution period	PH2 = (8) 5
t_m = mixing time	PH3 = 0 1 0 1 2 3 2 3
t_1 = 170 µsec. J+R delay	PH4 = 2 3 2 3 0 1 0 1
t2 = aquisition.	PH5 = 0 1 2 3 0 1 2 3
t2 = first order phase delay	

(FT) t1 experiments (FIDs), a sine bell convolution difference (K=24) was applied at the carrier frequency to reduce residual water signals (Marion *et al.*, 1989). FIDs were also multiplied by a $\pi/6$ shifted sine bell window function in t2 to enhance resolution and an unshifted sine bell window function in t1. After transformation and phasing in the t2 dimension, a fifth order polynomial baseline correction algorithm was applied in f2. The data from experiments with jump and return detection were corrected for peak intensity distortion in f2 using a reciprocal sine correction function before transformation in the t1 dimension (Dratz and Lambert, unpublished).

Determination of Average Inter-Proton Distances

NOE and TRNOE intensities were converted into inter-proton distances so that experimentally estimated $\langle r_{ij} \rangle$ could be used to constrain molecular dynamics simulations. The average inter-proton distances of the compact conformations of peptide 11, the d-analog, and the l-analog free in solution were estimated from NOESY spectra with a t_m of 400 ms. NOESY cross peak volumes were measured using the NMR processing software, FELIX version 2.05 (© Hare Research, Inc., 1990).

Average inter-proton distances were then calculated according to the NOE intensity $r_{ij}^{-1/6}$ distance dependence using the $P_3\beta H^1$-$P_3\beta H^2$ NOE intensity and the known 1.89 Å inter-proton distance as a reference. $r_{ij} = 1.89 \text{ Å} \cdot (NOE_{P3\beta H1\text{-}P3\beta H2}/NOE_{ij})^{1/6}$ The NOE between the geminal β protons of proline was isolated in the NOESY spectra of peptide 11, the d-analog, and the l-analog and its intensity was readily measured. Using the $P_3\beta H^1$-$P_3\beta H^2$ NOE as a reference successfully predicted other known inter-

proton distances, such as the distance (1.76 Å) between the geminal γ protons of isoleucine ($I_6\gamma H_2^1$-$I_6\gamma H_2^2$). The inter-proton distances from sequential inter-residue NOE intensities (ie. $X_i\alpha H$-$Y_{i+1}NH$ and $X_i\beta H$-$Y_{i+1}NH$) were consistently predicted to be within their allowed ranges.

As has been discussed previously, the NOEs measured from a short peptide free in aqueous solution are indicative only of r_{ij} averaged largely over the most compact conformations of the peptide. In addition, intra-residue spin diffusion could have reduced the $P_3\beta H^1$-$P_3\beta H^2$ NOE intensity, which would result in the calculated distances being too short. Therefore, the $\langle r_{ij} \rangle$ calculated from the equation presented earlier should not be considered a precise measurement. In order to provide flexibility to the predicted inter-proton distances, after a distance was measured it was assigned to a 0.5 Å range. For example, if the $\langle r_{ij} \rangle$ was measured to be 2.65 Å, then r_{ij} was assigned to the range: 2.5 Å $\leq r_{ij} \leq$ 3.0 Å. The shortest range used was 1.5 Å - 2.0 Å and the longest was 3.5 Å - 4.0 Å. The longest range employed was 3.5 Å - 4.0 Å, because it is difficult to detect NOEs between protons which are greater than 3.5 Å apart in short, linear peptides free in aqueous solution (Wright *et al.*, 1988).

The method by which TRNOESY cross peaks were converted into inter-proton distances was quite different than the method used for free in solution NOE intensities. TRNOESY experiments were performed with 50 ms, 100 ms, 200 ms, and 400 ms mixing times. The range of inter-proton distance assigned to two protons was based on the length of the mixing time required for the cross peak to be detectable. If a NOE was first detectable using a 50, 100, or 200 ms mixing time, then r_{ij} was assigned to the range 2.0 - 2.5 Å,

2.5 - 3.0 Å, or 3.0 - 3.5 Å, respectively. If a sequential NOE was absent from the τ_m = 200 ms experiment, then a lower limit of 3.0 Å was assigned to r_{ij}. If a sequential NOE was absent from the τ_m = 400 ms experiment, then a lower limit of 3.5 Åwas assigned to r_{ij}. Incorporating lower limits has been shown to improve the accuracy of the subsequently computer generated structures (Fesik *et al.*, 1987, Olejniczak *et al.*, 1988). This mixing time based assignment of inter-proton distances is analogous to the strategy employed by Ni *et al.* to determine the conformation of residues 7-16 of the human fibrinogen Aa chain when bound to thrombin (Ni *et al.*, 1989b).

Incorporation of Pseudo-atoms

With the exception of the β protons of Asp_2, it was not possible to stereo-specifically assign NOEs involving geminal proton pairs. Hence it was necessary to employ pseudo-atoms to incorporate r_{ij} involving groups of protons into molecular dynamics (Wüthrich, 1983). Pseudo-atoms were defined for all methyl groups, the a protons of glycine, geminal β (except for Asp_2) and γ protons, and for the protons in positions 2 and 6 of the tyrosine ring. The ranges of possible sequential inter-proton distances are different if pseudo-atoms are used. For example, the distance between $X_i\beta H_2$ and $Y_{i+1}NH$ can range between 2.26 and 4.35 Å, but if the geminal β protons are replaced with a pseudo-atom, $X_i\beta H$, then the possible range is changed to between 2.50 - 4.10 Å. Consequently, pseudo-atom corrections are typically added to r_{ij} prior to incorporation into molecular dynamics simulations (Wüthrich, 1983).

Prior to incorporation of experimentally derived r_{ij} ranges into

molecular dynamics simulations of peptide 11 and the d and l-analog, the r_{ij} range assigned to a proton pair involving a pseudo atom was compared to the possible range of distance between the proton and the pseudo-atom. With the exception of the tyrosine 2,6 ring protons, all experimentally determined r_{ij} fell within the range of sterically allowed proton to pseudo-atom distances. For example, the accessible distance between $D_2\alpha H$ and and the pseudo-atom $P_3\delta H$ ranges between 2.38 and 4.18 Å, and in the bound conformation of peptide 11 this distance was predicted to be in the range of 2.50 to 3.00 Å. In this instance, the experimental range (2.50- 3.00 Å) not only falls within the theoretically accessible range (2.38 - 4.18 Å), but the experimentally derived restraint restricts the atoms involved to a fraction of their accessible range. For restraints involving the 2,6 ring protons of tyrosine the lower limit was unchanged but it was necessary to raise the upper limit by 0.50 Å.

Molecular Dynamics

Separate molecular dynamics (MD) simulations of the peptides were performed using distance constraints derived from either the free in solution or the receptor bound NMR in order to study the characteristics of the biologically active conformation of peptide 11. MD simulations were performed on a Silicon Graphics 4D25TG workstation using the software package, Discover (© BIOSYM Technologies, Inc.), and analyzed using the software package, InsightII (© BIOSYM Technologies, Inc.).

Molecular dynamics was performed with a step size of 1 fs. All MD utilized the Consistent Valence Forcefield (CVFF, Dauber-Osguthorpe, 1988) with no charges or cross terms. Charges were not incorporated into MD,

because the resultant electrostatic forces could potentially have prevented the peptides from adopting conformations with good agreement to the NOE derived inter-proton distance constraints. As the simulated temperature was high, 500 K, harmonic bond stretching potentials were used to avoid bond rupture. Peptide omega bonds were held in the trans conformation by a torsional force constant of 200 kcal/rad^2. The peptide protonation was simulated to be that which is found in a solution of pH 5.0 or pH 7.0 in order to match the NMR experimental conditions.

Molecular dynamics was initiated at a temperature of 300 K for 100 fs. Following this initial warming of the molecule, the temperature was raised to 500 K and MD performed for 100 ps. The conformation of the peptide was archived at picosecond intervals. At the conclusion of the dynamics simulation, each archived conformation was energy minimized using steepest decent for 100 iterations. Continued minimization after 100 iterations failed to change the conformation of the peptides; therefore, the observed conformation was assumed to have converged.

Separate simulations of the peptides were performed with and without NOE derived distance constraints. Unconstrained MD was performed as a control to insure that the distance constraints did excessively bias the peptide from exploring conformational space. Constrained peptides were aided in exploring conformational space by using multiple starting conformations (β sheet, right handed and left handed a helix). Ramachandran plots (ϕ,ψ plots) were generated from the archived conformations to aid in visualizing the peptide's exploration of conformation space during the MD simulations.

NOE derived distance restraints consisted of a flat-bottomed potential

with a width equal to the experimentally determined inter-proton distance range. The NOE constraints on the protons allowed them to move freely within this range. Above and below the accepted range a restraining force was applied in order to move the protons toward the accepted range. The restraining force increased from 0 to 1000 Kcal/Å over the width of the enforcement ranges, which were 0.50 Å above and below the accepted inter-proton range.

The archived conformations were analyzed on the basis of their agreement to the NOE derived inter-proton distances. Total deviation from the experimentally estimated inter-proton distances was determined by monitoring the inter-proton distance of restrained protons, subtracting the average of the experimentally estimated inter-proton distance, and summing the deviation of every pair of restrained protons from its experimentally estimated value.

CHAPTER 3

PEPTIDE 11 IN AQUEOUS SOLUTION

Peptide 11, the d-alanine$_7$ analog (d-analog), and the l-alanine$_7$ analog (l-analog) were studied free in solution with two-dimensional ^{1}H-^{1}H nuclear magnetic resonance spectroscopy. Peptide proton resonances were assigned using TOCSY and ROESY spectra. The amino acid side chain spin system connectivities were first categorized using TOtal Correlation SpectroscopY (TOCSY). Comparison of the chemical shifts of the side chain protons with their random coil values (Bundi and Wüthrich, 1979) and the spin system connectivities provided an indication as to the identity of each spin system. Resonance assignments were confirmed by comparison of the sequential connectivity of the backbone protons αH_i-NH_{i+1} found in ROESY spectra (Figs. 5-7) with the known sequences of the synthetic peptides. The resonance assignments for peptide 11, the l-analog, and the d-analog are illustrated in figures 8-10 and listed in tables 2-5, respectively. The chemical shifts of the proton resonances of peptide 11, the d-analog, and the l-analog exhibit distinct patterns which are indicative of conformational behavior that deviates from random coil.

Figure 5. Peptide 11 Sequential Backbone Connectivity as Shown by ROESY.

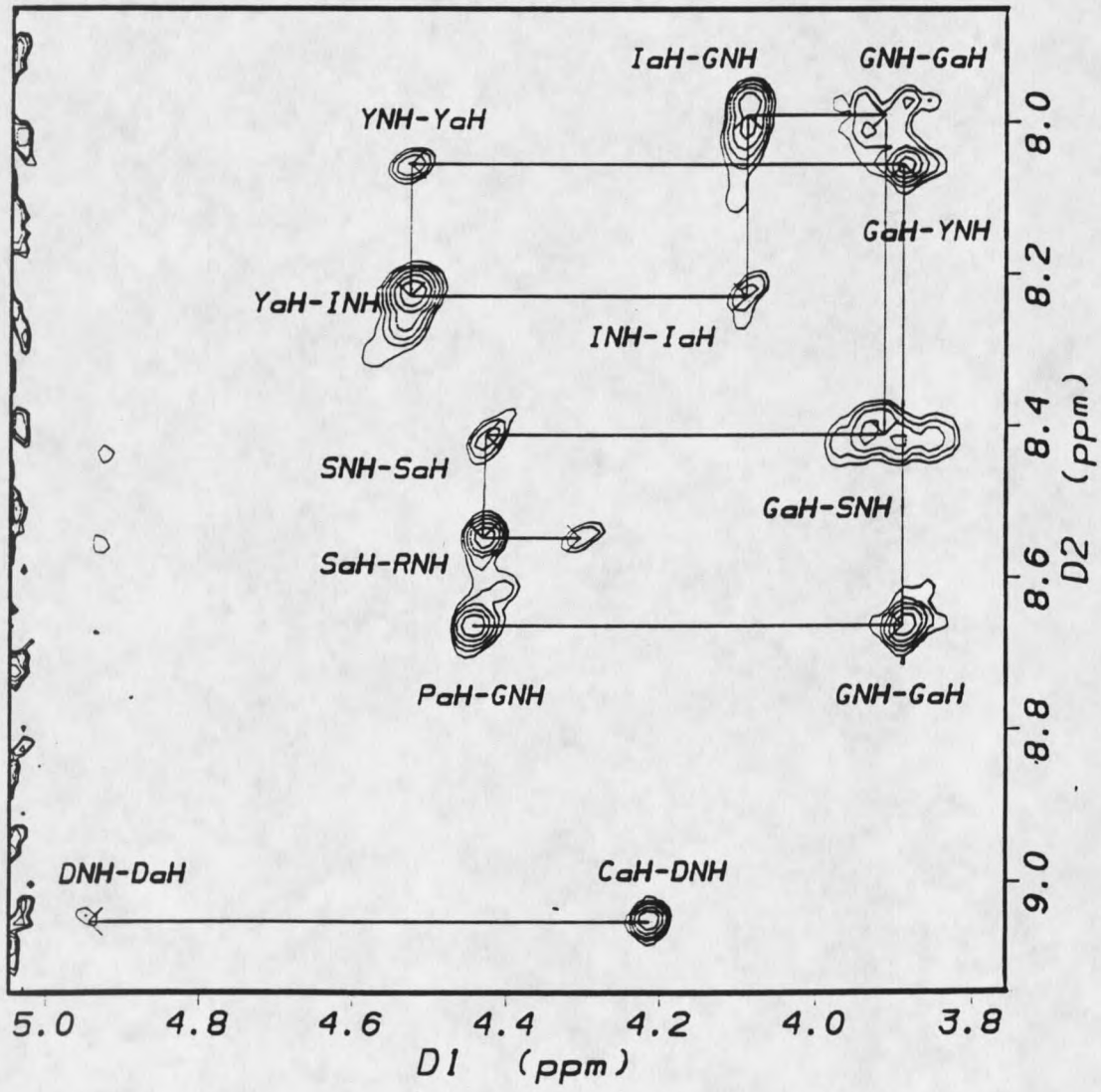

Figure 6. D-analog Sequential Backbone Connectivity as Shown by ROESY.

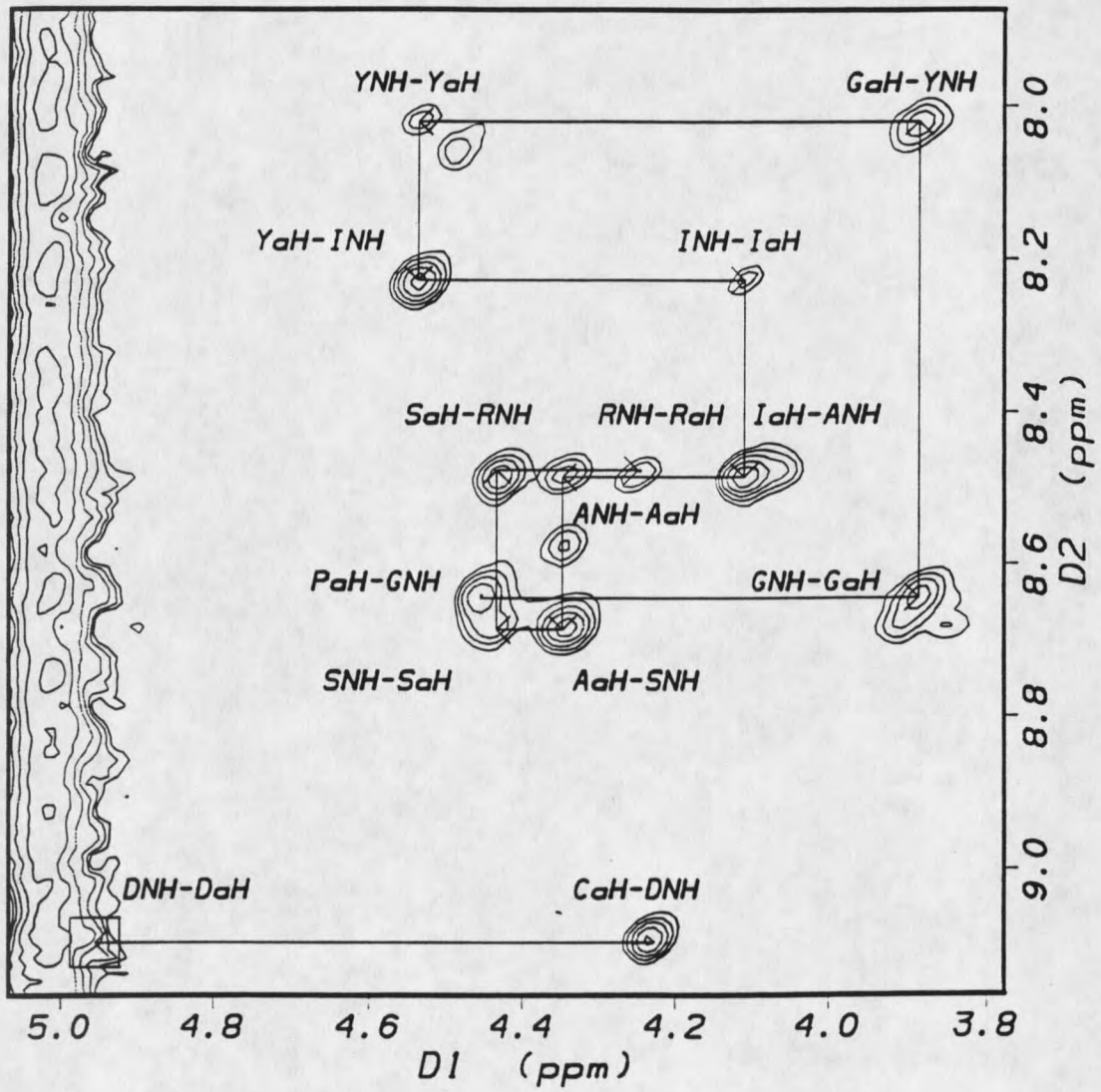

Figure 7. L-analog Sequential Backbone Connectivity as Shown by ROESY.

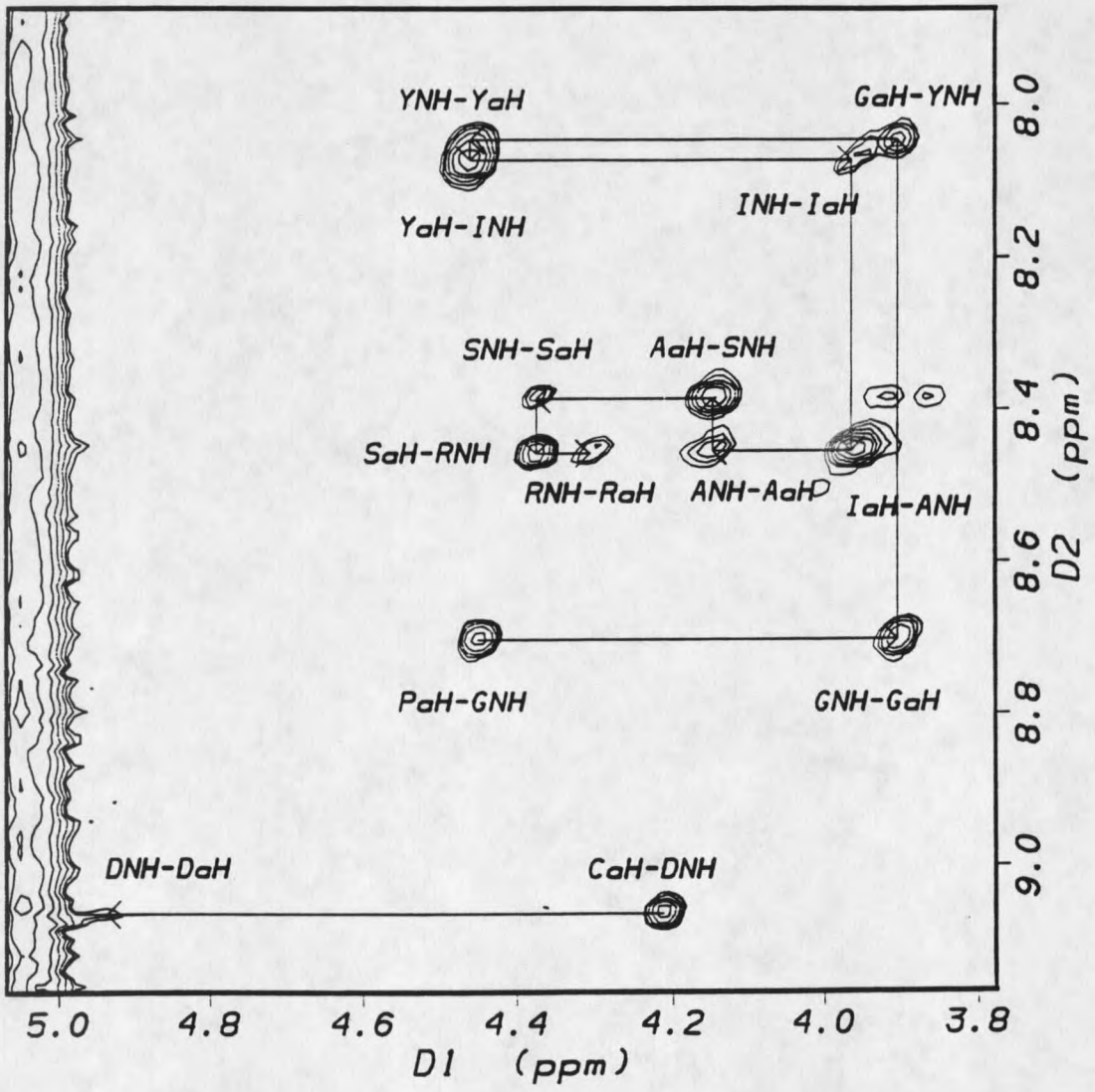

Figure 8. The Proton Assignments of Peptide 11 as Shown by TOCSY.

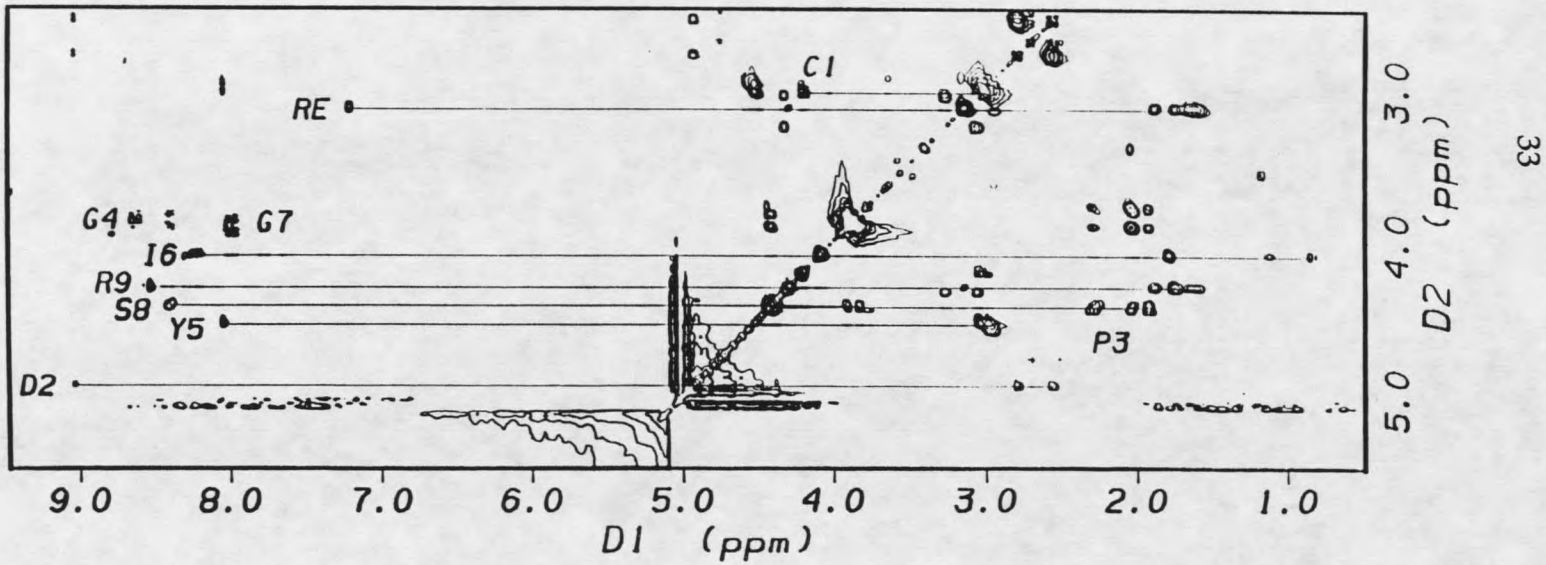

Figure 9. The Proton Assignments of the D-analog as Shown by TOCSY.

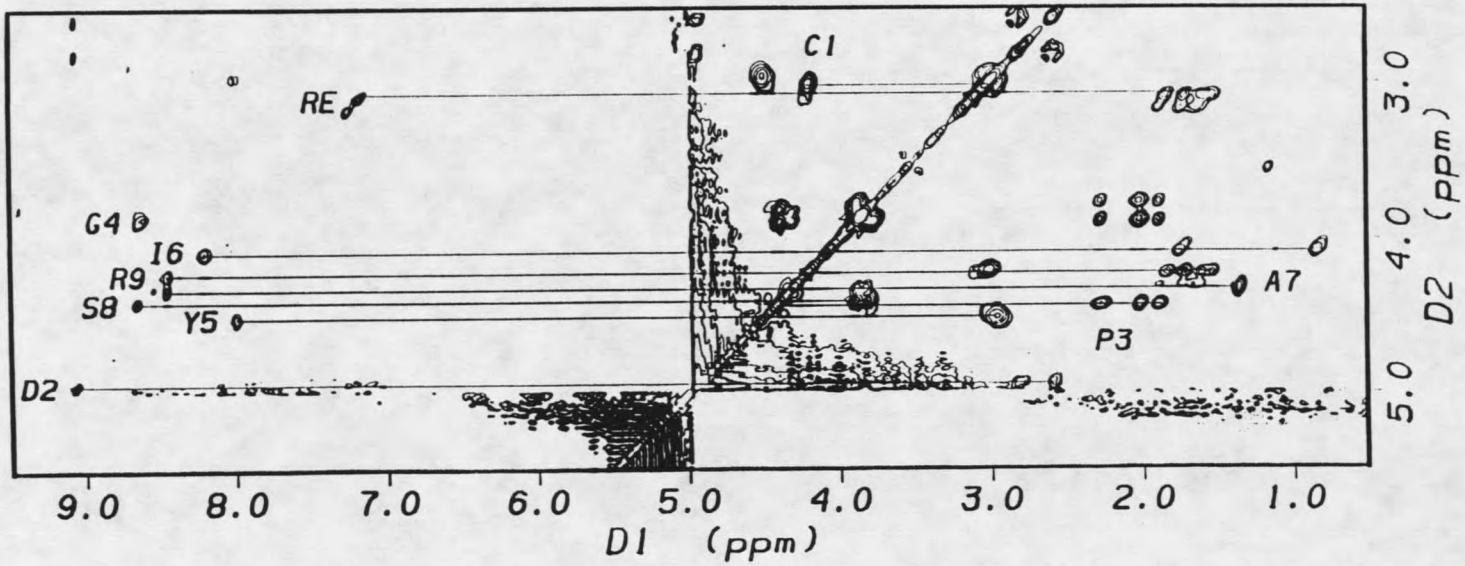

Figure 10. The Proton Assignments of the L-analog as Shown by TOCSY.

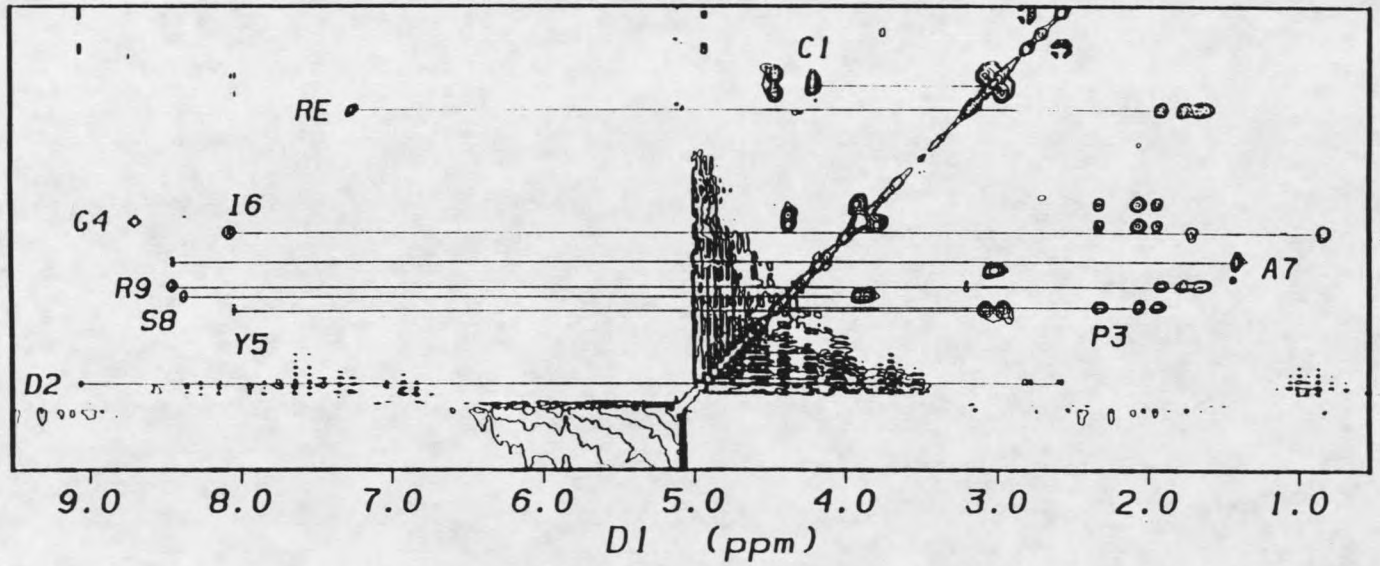

Table 2. The Chemical Shifts (ppm) of the Protons in Peptide 11 Compared to Random Coil Values*.

	NH	ΔRC	αH	ΔRC	βH	additional
Cys 1			4.21	-0.48	3.00	
					3.00	
Asp 2	9.05	+0.63	4.94	+0.46	2.67	
					2.80	
Pro 3			4.45		1.93	γCH_2 2.03
					2.31	δCH_2 3.79, 3.91
Gly 4	8.66	+0.27	3.89			
Tyr 5	8.06	-0.12	4.53		2.99	C2,6H 7.12
					3.06	C3,5H 6.81
Ile 6	8.23		4.09	-0.14	1.79	γCH_2 1.13, 1.42
						γCH_3 0.86
						δCH_3 0.85
Gly 7	7.99	-0.40	3.94			
			3.97			
Ser 8	8.42		4.43		3.84	
					3.91	
Arg 9	8.55	+0.28	4.30		1.76	γCH_2 1.59, 1.64
					1.89	δCH_2 3.14
						εNH 7.19
						NH_2 6.47, 6.90
NH_2	7.30					
	7.60					

* Bundi and Wüthrich, 1979.

Table 3. The Chemical Shifts (ppm) of the Protons in the D-analog Compared to Random Coil Values*.

	NH	ΔRC	αH	ΔRC		βH	additional
Cys 1			4.23	-0.45		3.05	
						3.05	
Asp 2	9.06	+0.66	4.96	+0.46	2.60		
						2.83	
Pro 3			4.43			1.91	γCH_2 2.03
						2.29	δCH_2 3.79, 3.89
Gly 4	8.62	+0.23	3.86	+0.11			
Tyr 5	8.00	-0.18	4.51			2.97	C2,6H 7.07
						3.00	C3,5H 6.80
Ile 6	8.21		4.09	-0.14		1.77	γCH_2 1.14, 1.46
							γCH_3 0.87
							δCH_3 0.84
Ala 7	8.47	+0.22	4.32			1.39	
Ser 8	8.66	+0.28	4.41			3.83	
						3.90	
Arg 9	8.46	+0.19	4.23	-0.17		1.74	γH_2 1.58, 1.63
						1.85	δCH_2 3.09
							εNH 7.18
							NH_2 6.48, 6.90
NH_2 10	7.30						
	7.53						

* Bundi and Wüthrich, 1979.

Table 4. The Chemical Shifts (ppm) of the Protons in the L-analog Compared to Random Coil Values*.

	NH	ΔRC	αH	ΔRC	βH	additional
Cys 1			4.23	-0.45	3.05	
					3.05	
Asp 2	9.05	+0.65	4.94	+0.45	2.59	
					2.81	
Pro 3			4.46		1.95	γCH_2 2.07
					2.33	δCH_2 3.81, 3.94
Gly 4	8.68	+0.29	3.91			
Tyr 5	8.04	-0.14	4.48	-0.12	2.99	C2,6H 7.11
					3.09	C3,5H 6.83
Ile 6	8.06	-0.14	3.97	-0.26	1.72	γCH_2 1.14, 1.46
						γCH_3 0.85
						δCH_3 0.84
Ala 7	8.44	+0.19	4.17	-0.18	1.43	
Ser 8	8.37		4.39		3.80	
					3.93	
Arg 9	8.46	+0.19	4.32		1.77	γCH_2 1.58, 1.66
					1.92	δCH_2 3.13
						εNH 7.26
						NH_2 6.51, 6.96
NH_2 10	7.32					
	7.66					

* Bundi and Wüthrich, 1979.

Chemical Shift Behavior

The chemical shift of a proton is a result of its magnetic environment, which is in turn a reflection of the chemical environment. The chemical environment of a peptide proton is affected by peptide conformation; therefore, proton chemical shift contains information regarding peptide conformation. Recently, Wishart *et al.* created a means of predicting protein secondary structure by an analysis of the chemical shift of protein a protons (Wishart *et al.*, 1992). These authors found that an unbroken sequence of amino acid residues whose a protons resonate 0.1 ppm downfield of a specific value for each amino acid indicates that those residues form a β sheet, and that an unbroken sequence of amino acid residues whose protons resonate 0.1 ppm upfield of the same value indicates that those residues form an a helix. This simple set of rules is remarkably adept at predicting protein secondary structure. The predictive power of the Wishart *et al.* rules clearly demonstrates that structural information is contained in proton chemical shifts. However, as their work is based on an analysis of small proteins (10-30 kDa), it is not expected to be applicable to linear peptides as short as peptide 11, which are likely to exist in a range of conformations.

Bundi and Wüthrich tabulated the proton chemical shifts of amino acids which were incorporated into the third position of the synthetic peptide H-GGXA-OH (Bundi and Wüthrich, 1979). H-GGXA-OH is not long enough to adopt a high population of compact conformations in aqueous solution. The highly flexible state of such short peptides is referred to as random coil. The chemical shift values tabulated by Bundi and Wüthrich are assumed to be close to the proton resonance values of random coil (RC) peptides. A direct

means of predicting the secondary structure of short peptides analogous to the Wishart *et al.* rules for small proteins has not been devised. This is not surprising, as few short peptides have a firmly defined secondary structure when free in solution. However, if a backbone proton displays a chemical shift which deviates significantly from its accepted random coil value, then it is likely that the peptide backbone in the vicinity of this proton possesses a significant population of non-random compact conformations unless some other rationalization of the shift is apparent such as an aromatic ring current from a spatially close aromatic side chain.

The backbone proton chemical shift behavior of peptide 11, the d-analog, and the l-analog provided information concerning their respective conformations in aqueous solution. Several backbone protons possessed chemical shifts that deviated from random coil values. Deviations from random coil greater than 0.1 ppm ($\Delta RC > 0.1$ ppm) are indicated in the resonance assignment tables (Tables 2-4). The protons of the $Cys_1\alpha H$ through Tyr_5NH region of all three peptides possess nearly identical chemical shifts. The similarity of these chemical shifts suggests that the CDPG region of all three peptides behaves similarly when free in solution.

Commencing with $Tyr_5\alpha H$, chemical shifts of the three different analogs are affected by the identity of the seventh residue. The chemical shifts of $Tyr_5\alpha H$, Ile_6NH, and $Ile_6\alpha H$ in peptide 11 and the d-analog are nearly identical, but are shifted upfield by 0.08, 0.15, and 0.12 ppm respectively in the l-analog. The chemical shift of the amide proton of the seventh residue in each peptide differed significantly from its random coil value. The -0.40 ΔRC of Gly_7NH is a significant deviation from random coil values. This ΔRC of

Gly_7NH suggests that peptide 11 exhibits a large population of conformers which possess a non-random conformation about Gly_7. A relatively stable bend about Gly_7, such as was predicted by Brandt-Rauf *et al.* or McKelvey *et al.*, might yield such a large ΔRC.

In addition to the ΔRC of Gly_7NH, the complexity of the Gly_7NH-$Gly_7\alpha H$ further suggested that peptide 11 possessed a large population of non-random conformers about Gly_7. The Gly_7NH and $Gly_7\alpha H$ resonances were split by their mutual J^3 coupling and the two a protons were split by their large geminal coupling constant to yield the pattern of eight cross peaks observed in the ROESY (Fig. 5), TOCSY (Fig. 8), and NOESY (Fig. 11) spectra of peptide 11. In the d-analog (Figs. 6, 9, and 12) and the l-analog (Fig. 7, 10, and 13) this complex peak was conspicuously absent, which supported the assignment of this complex peak to Gly_7. The strength of the J^3 coupling of this peak suggested that the conformation of Gly_7 was constrained in some way. Again, a high population of peptide 11 conformers with a turn about Gly_7 could be responsible for the observed non-random coil behavior of Gly_7.

$Gly_7\alpha H$ of peptide 11 and $Ala_7\alpha H$ of the d-analog possessed random coil chemical shifts, while $Ala_7\alpha H$ of the l-analog did not. The d-analog Ser_8NH resonates 0.28 ppm downfield of the l-analog Ser_8NH. It is unclear why a change in chirality of the preceding residue would directly affect the amide proton, unless the peptide backbone conformation had been affected by the chirality of the preceding alanine. Arg_9NH and $Arg_9\alpha H$ behaved similarly in all three peptides.

The YIXS backbone protons of peptide 11 and the d-analog exhibit parallel chemical shift behavior, which suggests that these peptides possess

similar conformation populations in this region when free in solution. In addition, the differences in chemical shift exhibited by the l-analog imply that its YIXS conformations differ from those of peptide 11 and the d-analog. Interestingly, peptide 11 and the d-analog are more biologically active than the l-analog (Fig. 2). This parallel of YIXS chemical shift behavior with the peptides' biological activity, is consistent with the premise that peptide 11 and the d-analog possess a YIXS conformation, different from the l-analog, that is responsible for their greater biological activity.

Two Spin Systems are Assignable to the CDPG Regions of the Peptides Free in Solution at pH ~5

The chemical shifts of the protons of the two spin systems assignable to Cys_1, Asp_2, Pro_3, and Gly_4 of peptide 11, the d-analog, and the l-analog are presented in Table 5.

There are multiple possible causes for presence of these two spin systems. The presence of incorrectly synthesized peptides could account for the additional spin systems. Alternatively, no reducing agent was incorporated into the NMR samples; therefore, inter-peptide di-sulfide bonds involving Cys_1 could form. Peptides involved in inter-peptide di-sulfide bonds would exhibit different chemical shifts than peptides not involved in inter-peptide bonds. The two spin systems of Cys_1 could be due to a mixture of monomeric and di-sulfide bonded dimeric peptides. The two species of the peptides could possess significant populations of compact conformers with very different conformations. These different peptide conformations would manifest themselves in the NMR spectra as two sets of unique spin systems.

Table 5. The Chemical Shifts of the Two Spins Systems of Cys_1 Found in the Free Peptides at pH ~5.

	Peptide 11		d-analog		l-analog	
$C_1\alpha H$	4.33	4.22	4.35	4.22	4.34	4.22
$C_1\beta H^1$	3.08	3.03	3.07	3.04	3.06	3.04
$C_1\beta H^2$	3.28	3.03	3.28	3.04	3.27	3.04
D_2NH	9.19	9.05	9.24	9.06	9.20	9.05
$D_2\alpha H$	5.00	4.94	5.01	4.96	5.00	4.94
$D_2\beta H^1$	2.59	2.57	2.60	2.59	2.55	2.58
$D_2\beta H^2$	2.83	2.79	2.84	2.82	2.83	2.80
$P_3\alpha H$	4.40	4.45	4.40	4.46	4.43	4.39
$P_3\delta H^1$	3.83	3.80	3.82	3.78	3.81	3.83
$P_3\delta H^2$	3.91	3.91	3.90	3.90	3.93	3.93
G_4NH	8.61	8.66	8.62	8.59	8.63	8.66

The existence of two spin systems in the CDPG regions of the peptides can alternatively be explained by cis/trans isomerization of the Asp_2-Pro_3 peptide bond. Proline isomerization has been well characterized in small peptides (Mayo *et al.*, 1991). However, it is unlikely that the two different splittings of the β protons observed in Cys_1 (Table 6) could be caused by the different conformers that would be generated by isomerization about the Asp_2-Pro_3 peptide bond. The β splitting of Cys_1 is caused by the sulfur; therefore, the two different β splittings observed in Cys_1 are most likely due to changes in the chemistry of the Cys_1 sulfur. The pK_a of the Cys_1 sulfur is 8.33; therefore, at a pH of ~5, changes in protonation could not be the source of the change in chemistry of the Cys_1 sulfur. The most likely cause of the two different chemical states of the Cys_1 sulfur at pH ~5 is the formation of inter-peptide di-sulfide bonds. Whether or not the formation of these inter-peptide di-sulfide bonds could result in two Asp_2, Pro_3, and Gly_4 spin systems is

unclear. It is possible that the two spin systems observed in the CDPG region of the peptides free in solution at pH ~5 could be due to a combination of both inter-peptide di-sulfide bond formation and cis/trans isomerization about the Asp_2-Pro_3 peptide bond.

As the three peptides exhibited two spin sytems, it was necessary to choose one for the purpose of structure elucidation by NOESY and subsequent molecular dynamics calculations. The spin system in which the Asp_2NH diagonal peak possessed the greatest intensity was chosen. It was assumed that the greater diagonal peak intensity indicated that this spin system corresponded to the dominant molecular species in the NMR sample. The spin systems used in the structure elucidation of peptide 11, the d-analog, and the l-analog corresponded to Asp_2NH chemical shifts of 9.05, 9.06, and 9.05, respectively (Table 5).

NOESY of the Peptides Free in Aqueous Solution

The average conformations of peptide 11, the d-analog, and the l-analog free in solution were investigated by nuclear Overhauser effect NMR spectroscopy (NOESY). Peptide 11 and its analogs are comparatively short; their backbones are approximately 29 Å in length. Approximating peptide 11 as a sphere with a radius of 7 Å the τ_c of peptide 11 in an aqueous solution at 274 K is 0.4 nanoseconds. For peptide 11 studied at these conditions in a 500 MHz spectrometer, $\omega_0\tau_c$ is approximately 0.2. If the correlation time of a molecule is such that $\omega_0\tau_c \approx 1$ (Fig. 1), then inter-proton NOEs of that molecule are weak and difficult to observe (Ernst et al., 1987). As peptide 11 and the d and l-analog possess $\omega_0\tau_c \approx 0.2$, if an NOE is observed in one of

these molecules, then it is a reflection of a compact conformation ($\langle r_{ij} \rangle < 3.5$ Å, Wright *et al.*, 1988).

The NMR experiment that is better suited to the measurment of the inter-proton nuclear Overhauser effect in molecules the size of peptide 11 is ROtating frame nuclear Overhauser Effect SpectroscopY or ROESY (Bothner-By *et al.*, 1984, Bax and Davis, 1985a). Unfortunately, the intensity of ROESY cross peaks are frequently contaminated by magnetization which was transferred through bonds during the spin lock (Neuhaus and Keeler, 1986). These contaminated peaks may confuse attempts at structure determination. The ROESY spectra of peptide 11 and the d and l-analogs appeared to exhibit through bond magnetization contamination. Consequently, the intensities of ROESY cross peaks in these spectra were not used to estimate the inter-proton distances of peptide 11, the d-analog, and the l-analog.

Dyson *et al.* performed a meticulous NMR spectroscopy study of over 50 short peptides free in aqueous solution (Dyson *et al.*, 1988a). In the course of their study they found that short peptides "invariably" exhibit αH_i-NH_{i+1} NOE connectivity. The consistent observation of these peaks can be explained by the flexibility of the short peptides. The conformations of most short peptides free in aqueous solution are not rigidly maintained. Instead short peptides tend to fluctuate between low energy compact conformations insuring the existence of a significant peptide population in which the αH_i and NH_{i+1} are not forced apart. Only in tight secondary structures, such as a type I turn, is the peptide backbone in a conformation such that some of the αH_i and NH_{i+1} are forced more than 4 Å apart (Billeter *et al.*, 1982).

In contrast to the invariability of αH_i-NH_{i+1} NOEs, relatively few of

the peptides studied by Dyson *et al.* possessed NH_i-NH_{i+1} connectivity. In addition, the peptides which did possess NH_i-NH_{i+1} connectivity were also the peptides that exhibited large populations of compact conformations. Based on this correlation, Wright, Dyson, and Lerner proposed that the presence of both αH_i-NH_{i+1} and NH_i-NH_{i+1} sequential NOE connectivities at a specific site of a peptide indicates that this portion of the peptide possesses a large population of compact conformers (Wright *et al.*, 1988). Similarly, a peptide with a high population of extended conformers exhibits strong sequential αH_i-NH_{i+1} NOEs and lacks NH_i-NH_{i+1} NOEs. While NOE patterns in free short peptides are indicative of specific conformations, the information concerning average inter-proton distance derived from these NOEs is not expected to be sufficient to determine with precision the structure of these compact conformations (Wright *et al.*, 1988).

When free in solution, peptide 11 and its analogs demonstrate similar properties as the peptides studied by Dyson *et al.* For all three peptides it is possible to follow the αH_i-NH_{i+1} connectivity from $Cys_1\alpha H$ to Arg_9NH in both NOESY and ROESY spectra at any mixing time (Figs. 11-13 and 5-7). The sequential backbone connectivity is perforce broken at Asp_2NH-Pro_3NH, because proline does not possess an amide proton.

For peptide 11 and the d-analog it is possible to follow the NH_i-NH_{i+1} connectivity from G_4NH-R_9NH in NOESY experiments with $\tau_m \geq 400$ ms (Figs. 14-16). The l-analog displays similar connectivity, but the Y_5NH-I_6NH NOE is absent. In all peptides, NH_i-NH_{i+1} connectivity cannot exist prior to G_4, becauseneither Cys_1 nor Pro_3 possess an amide proton. Cys_1 is the amino terminal residue and consequently its nitrogen is in the NH_3^+ state. The

Figure 11. Peptide 11 Sequential Backbone Connectivity as Found in NOESY.

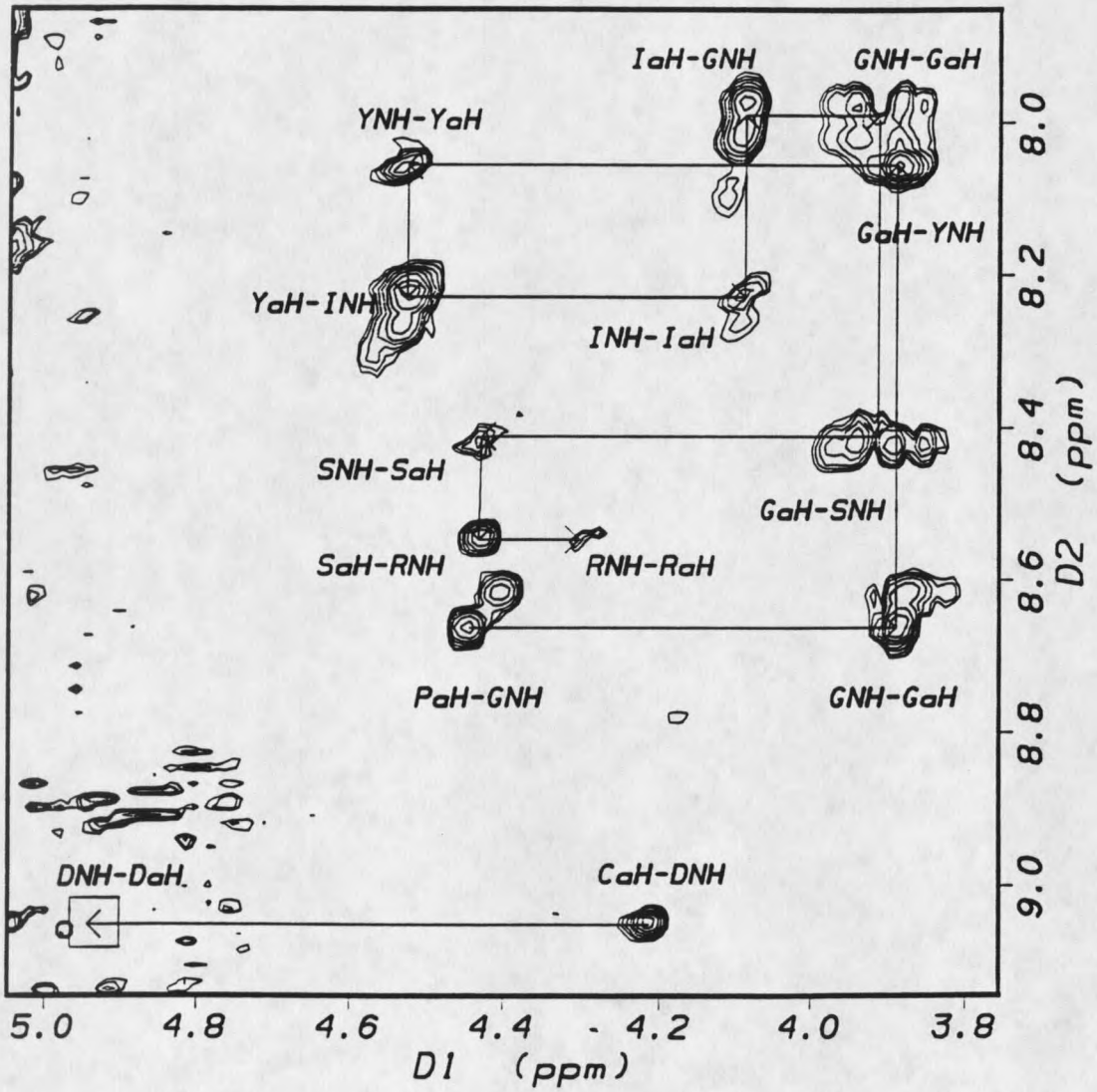

Figure 12. D-analog Sequential Backbone Connectivity as Found in NOESY.

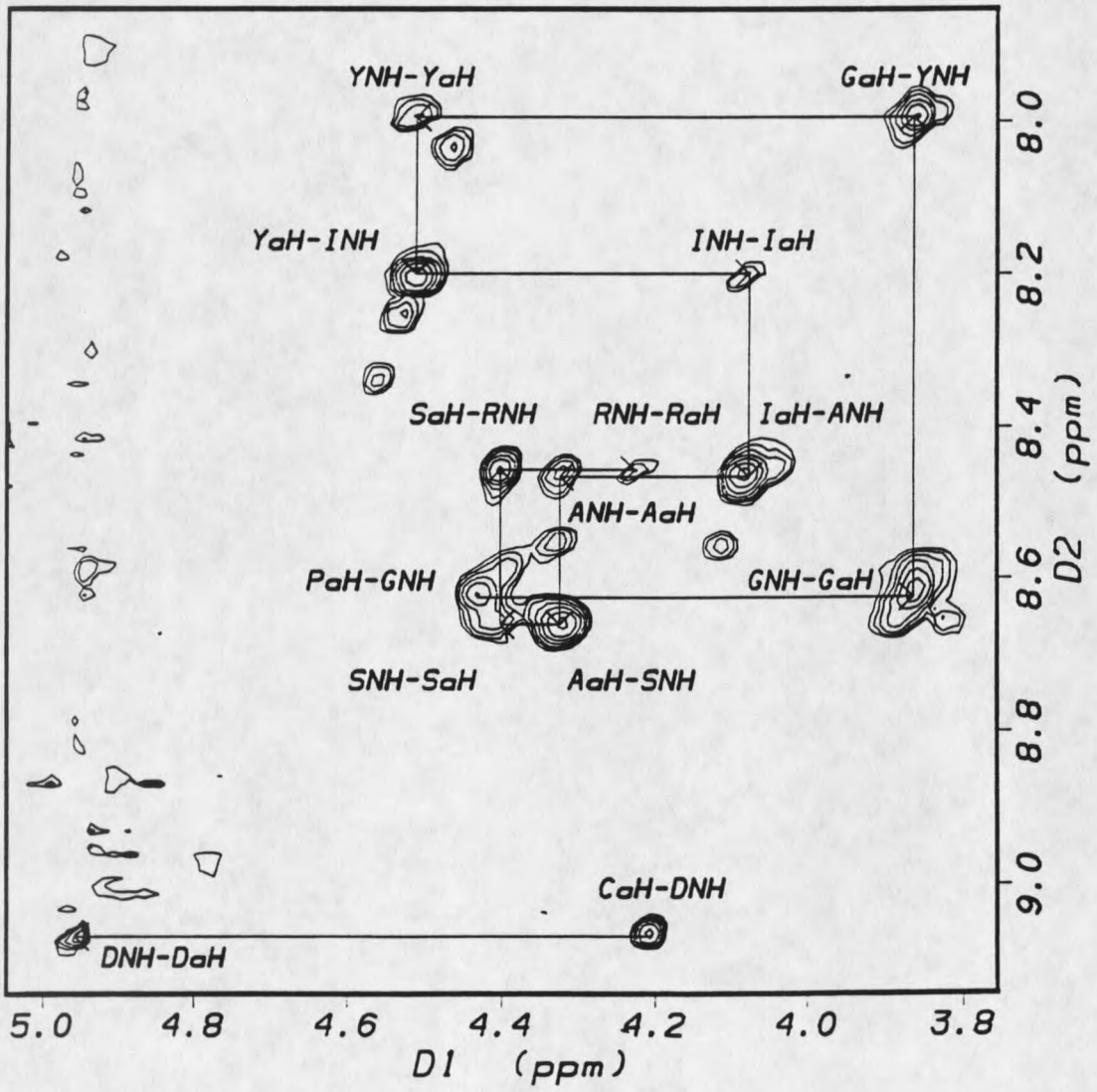

Figure 13. L-analog Sequential Backbone Connectivity as Found in NOESY.

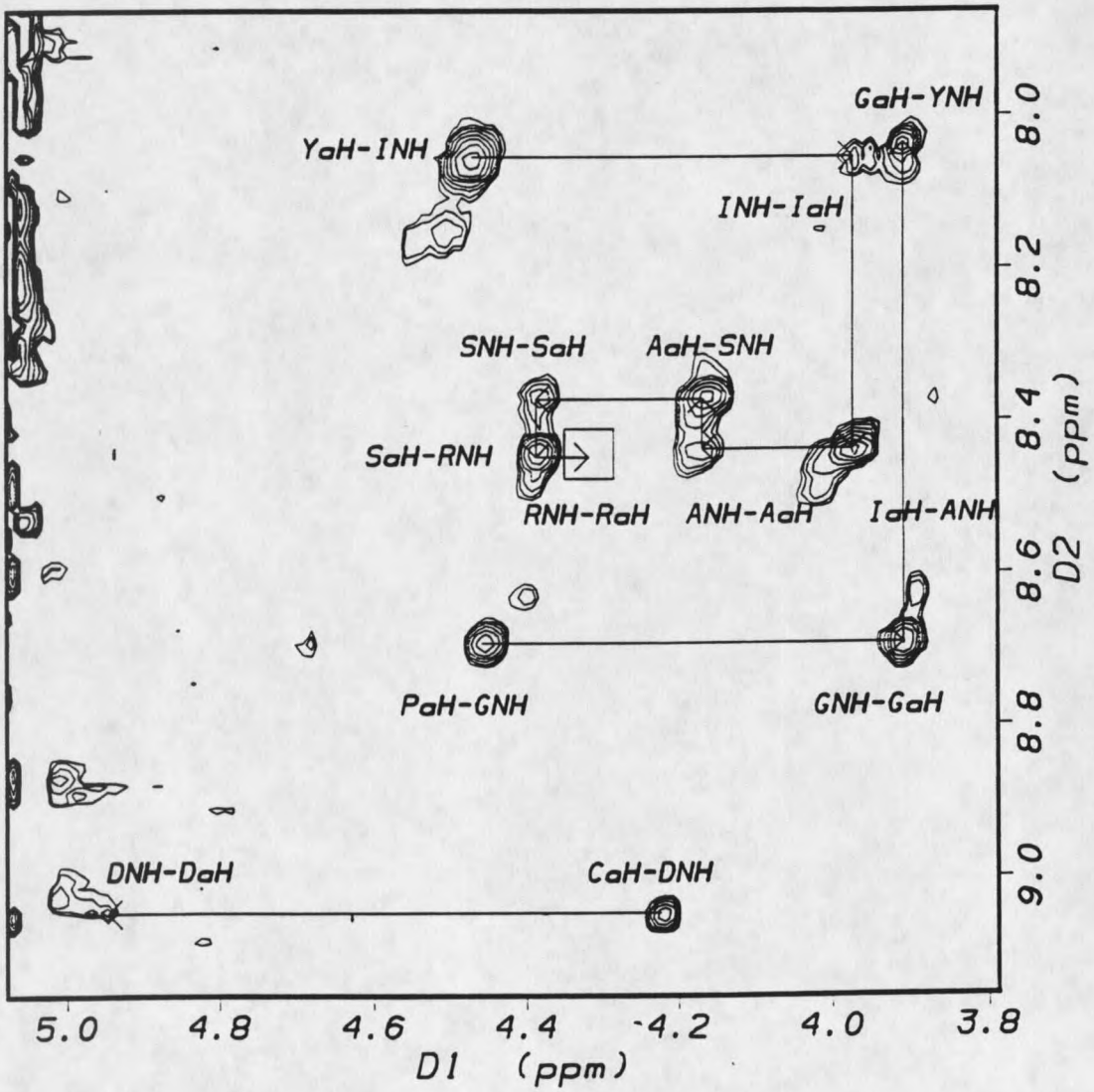

Figure 14. The NH_i-NH_{i+1} NOE Connectivity of Peptide 11.

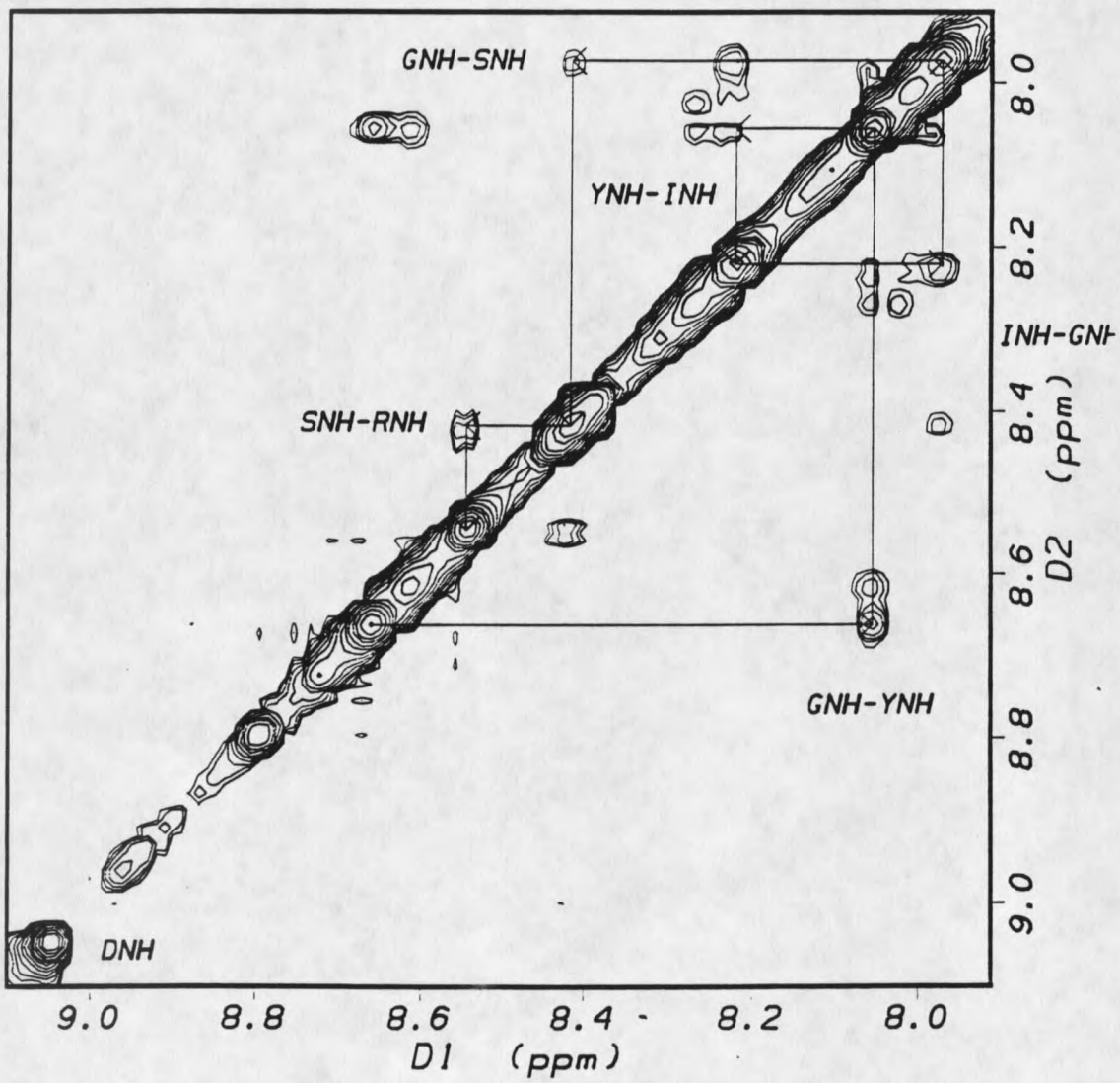

Figure 15. The NH_i-NH_{i+1} NOE Connectivity of the D-analog.

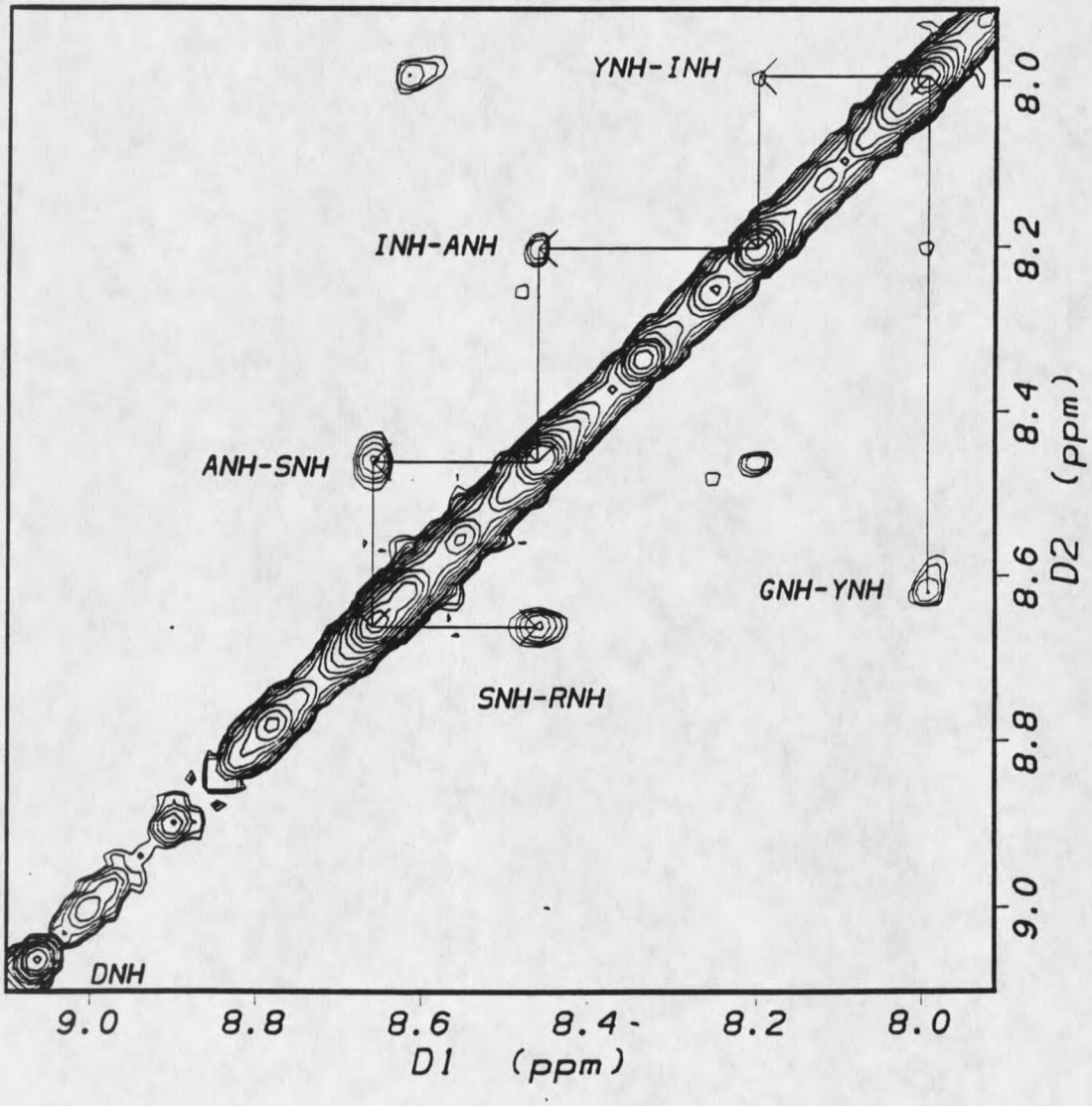

Figure 16. The NH_i-NH_{i+1} NOE Connectivity of the L-analog.

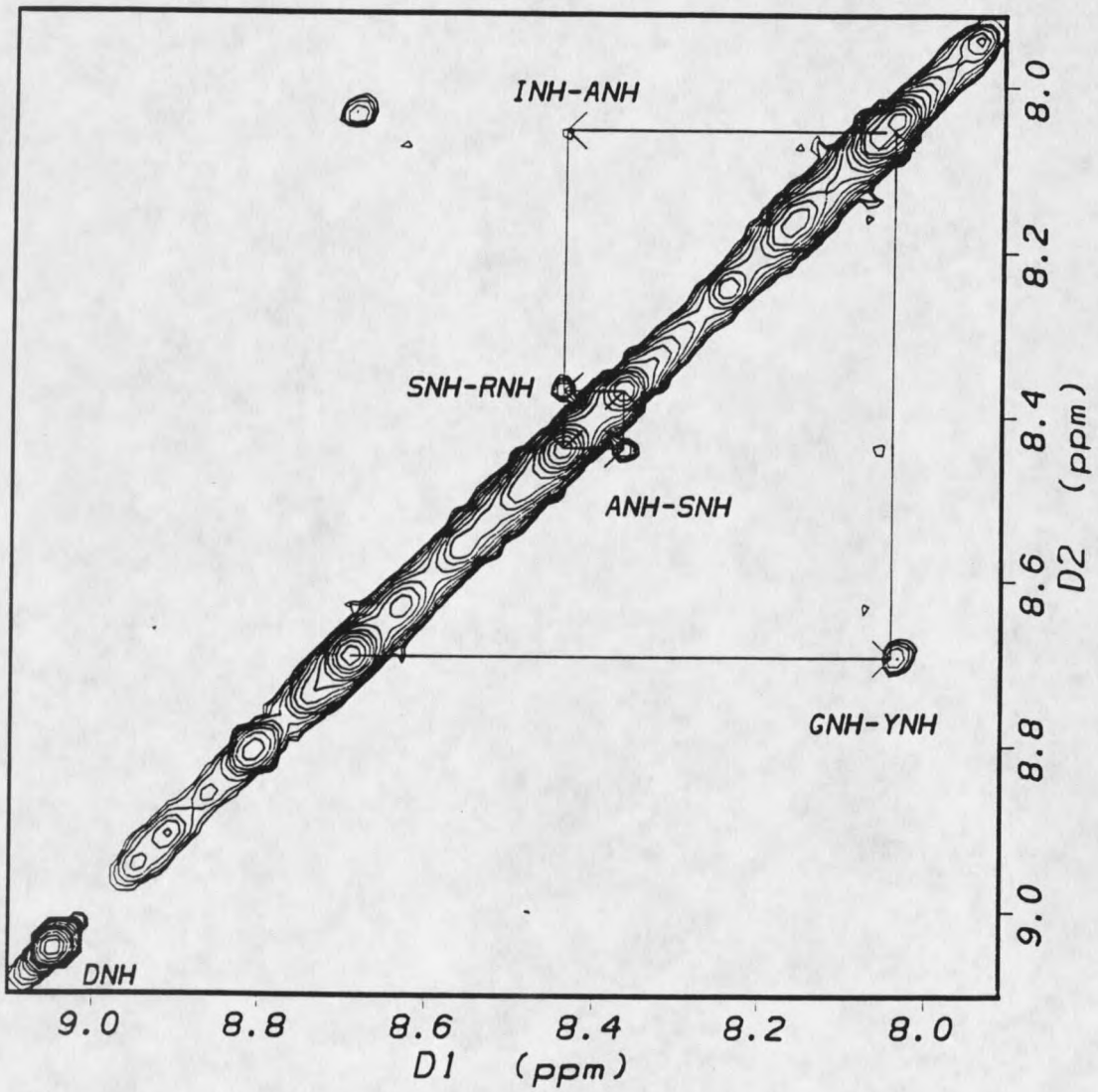

protons of NH_3^+ exchange with water rapidly on the NMR time scale; therefore, they are NMR invisible.

The spectra of the analogs contains a degree of ambiguity with regards to the extent of the connectivity. For both the d-analog and the l-analog, the resonances of A_7NH (8.47 ppm) and R_9NH (8.48 ppm) overlap. Both of these residues are sequential to Ser_8. Therefore, if both A_7NH-S_8NH and S_8NH-R_9NH gave NOESY cross peaks, then these peaks would overlap. In both NOESY spectra of the d-analog and the l-analog there is a cross peak that can be assigned to either A_7NH-S_8NH or S_8NH-R_9NH (Figs. 15-16). As this cross peak is relatively intense, it is likely to be composed of two overlapping cross peaks.

The intensity of NH_i-NH_{i+1} NOEs is dependent on the identity of the seventh residue (Figs. 15-16). The NH_i-NH_{i+1} NOEs of the d-analog are slightly weaker than those of peptide 11, and the corresponding NOEs of the l-analog are significantly weaker than both peptide 11 and the d-analog. The one exception to this trend is G_4NH-Y_5NH which is strong in all three spectra. The intensity of the Y_5NH-I_6NH NOE is especially dependent on the identity of the seventh residue. In the d-analog it is the most weakened of the NH_i-NH_{i+1} NOEs, and in the l-analog it is absent. Based on the aforementioned observations of Wright *et al.* (1988) concerning the presence of NH_i-NH_{i+1} NOEs in small peptides it would appear reasonable to propose that peptide 11 and the d-analog possess a significant population of compact conformers in solution, while the l-analog does not. NH_i-NH_{i+1} based implication of high populations of peptide 11 and d-analog compact conformers is in agreement with the YIXSR chemical shift behavior of peptide 11 and the d and l-analogs.

The final type of sequential NOE connectivity observed is βH_i-NH_{i+1}. Free in solution, peptide 11 possesses $C_1\beta H_2$-D_2NH, $P_3\beta H_2$-G_4NH, $Y_5\beta H_2$-I_6NH, and $I_6\beta H$-G_7NH NOEs (Fig. 17). The d and l-analogs free in solution possess $Y_5\beta H_2$-I_6NH, $I_6\beta H$-A_7NH, and $A_7\beta H_3$-S_8NH NOEs (Figs. 18 and 19). None of the peptides possesses the $S_8\beta H$-R_9NH NOE.

Substituting alanine for Gly_7 introduces a side chain adjacent to the bulky side chain of Ile_6. The chirality of the substituted alanine (A_7) affects the conformation of the Ile_6 side chain. The d-analog exhibits both I_6NH-$I_6\gamma H_2$ NOEs but no I_6NH-$I_6\gamma H_3$ NOE (Fig. 18), while the l-analog exhibits the I_6NH-$I_6\gamma H_3$ NOE and only one of the two possible I_6NH-$I_6\gamma H_2$ NOEs (Fig. 19). The d-analog Ile_6 side chain NOE behavior more closely resembles that of peptide 11. Free peptide 11 exhibits strong I_6NH-$I_6\gamma H_2$ NOEs, and although peptide 11 exhibits an I_6NH-$I_6\gamma H_3$ NOE, it is weaker than the I_6NH-$I_6\gamma H_2$ NOEs (Fig. 17).

Molecular Dynamics

In order to visualize the structural information provided by the NMR data, molecular dynamics simulations (MD) incorporating NOESY derived distance constraints were performed. For every MD simulation the agreement of the structures generated to the predicted inter-proton distances was monitored. Energy minimized candidate conformations of the peptides generated by the high temperature (500 K) MD were chosen on the basis of agreement with the NOESY derived distance constraints (Figs. 20-22) and total energy (Figs. 23-25). Conformations with both good agreement to the NOESY predicted $\langle r_{ij} \rangle$ and comparatively low total energy were chosen.

Figure 17. The NH_i-βH_i and βH_i-NH_{i+1} NOE Connectivity of Peptide 11.

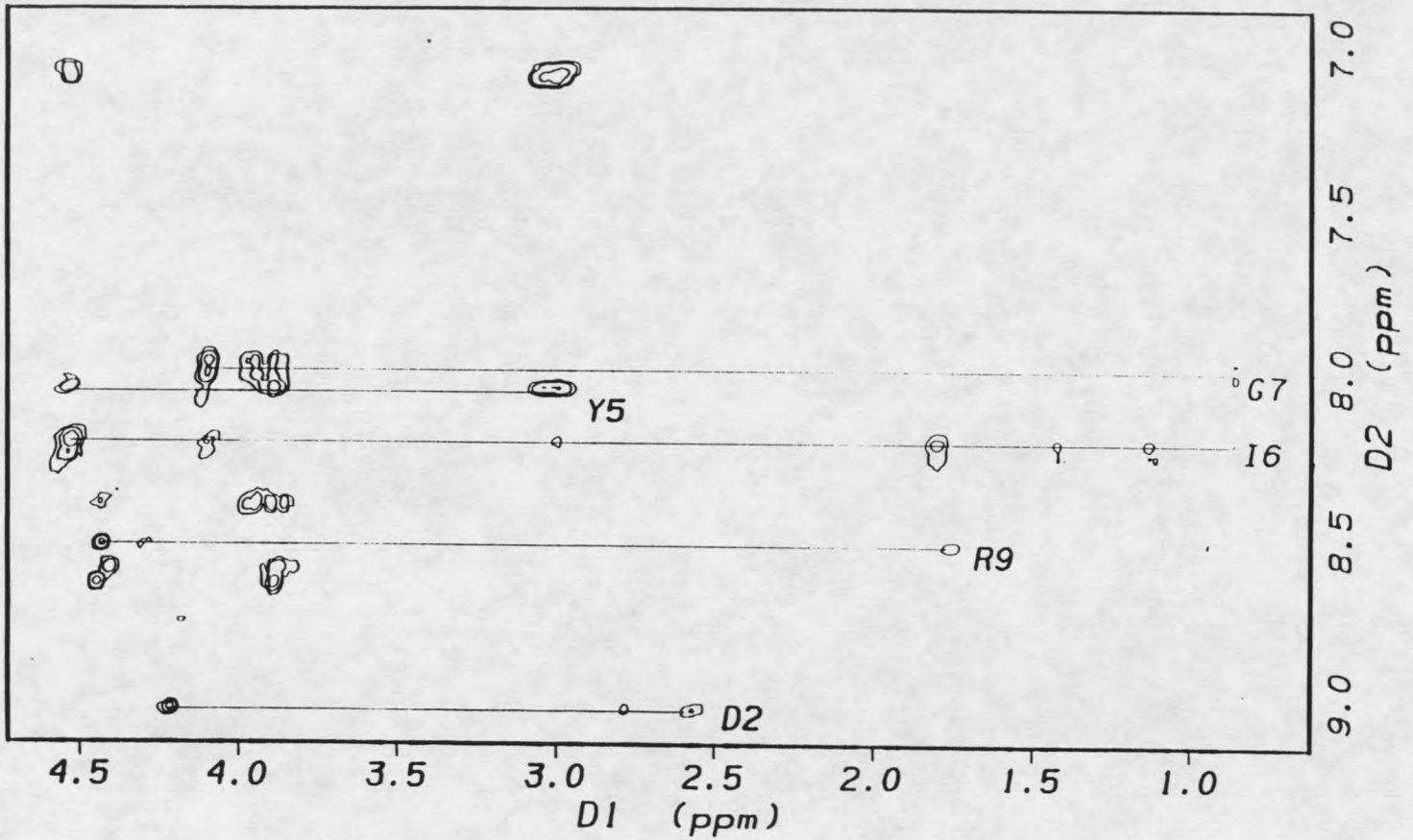

Figure 18. The NH_i-βH_i and βH_i-NH_{i+1} NOE Connectivity of the D-analog.

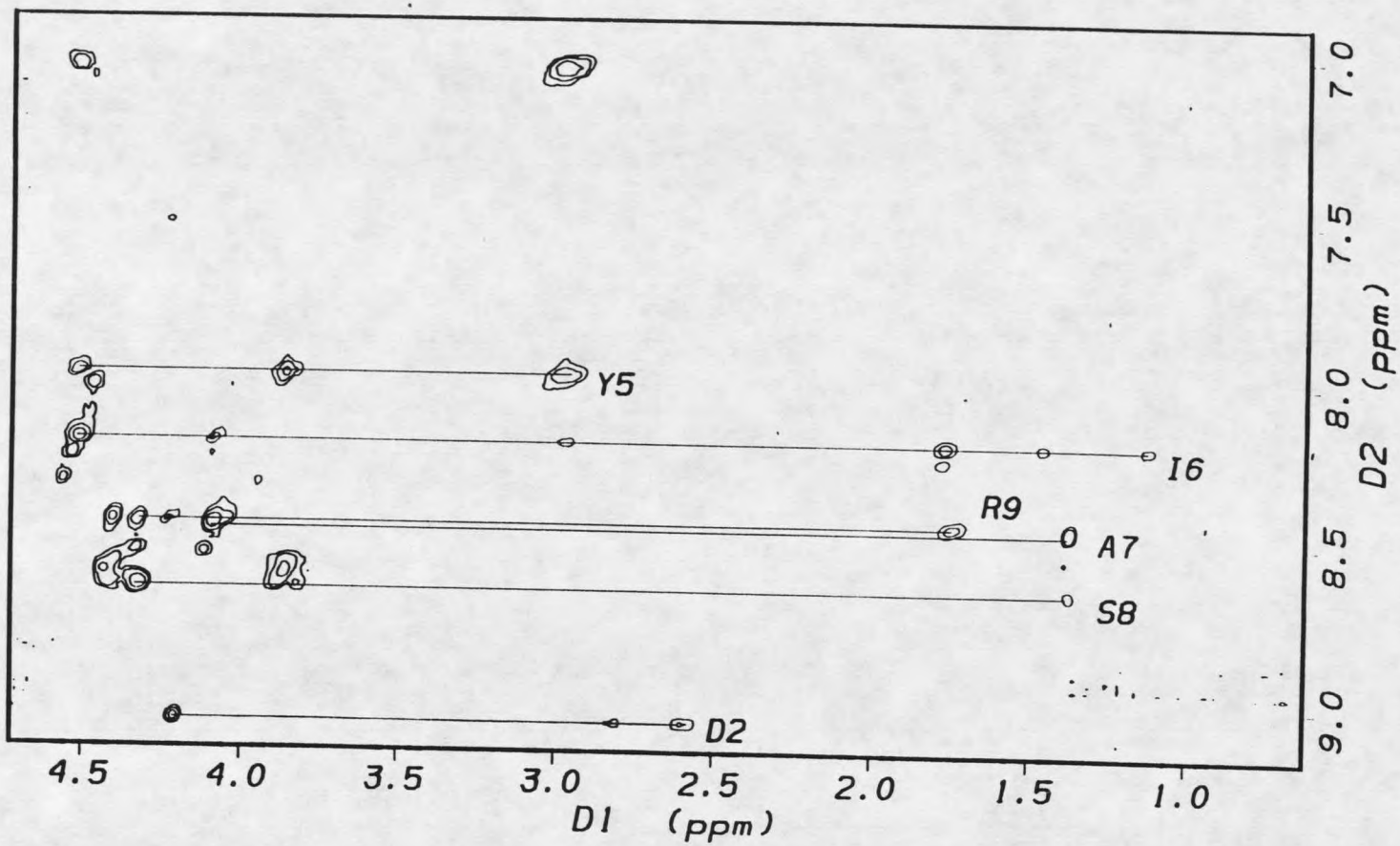

Figure 19. The NH_i-βH_i and βH_i-NH_{i+1} NOE Connectivity of the L-analog.

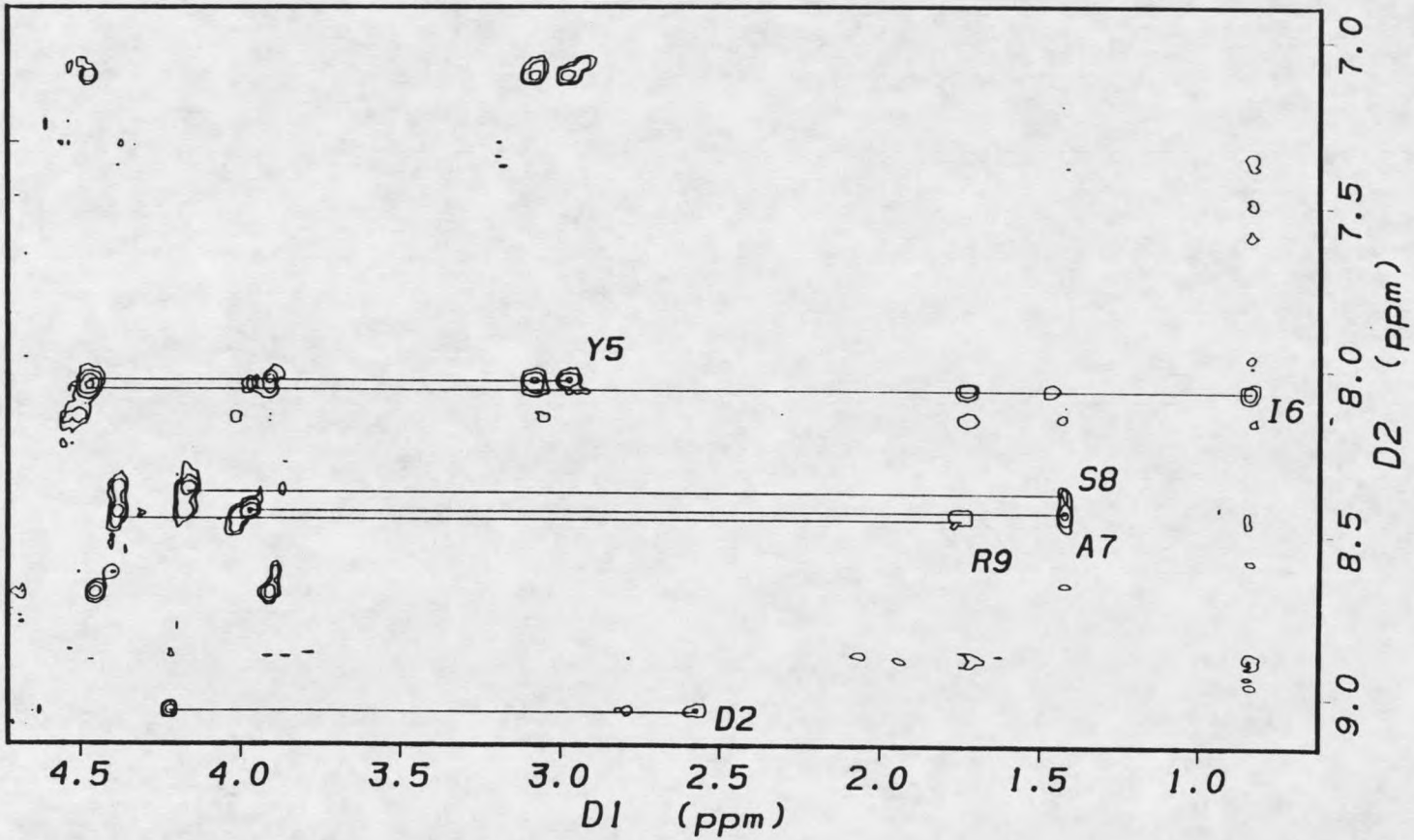

Figure 20. Free Peptide 11 NOE Deviation.

The Total Deviation in Å of Peptide 11 Inter-proton Distances From the Free in Solution NOESY Derived Distance Constraints as a Function of the Time Elapsed by the Molecular Dynamics Simulation.

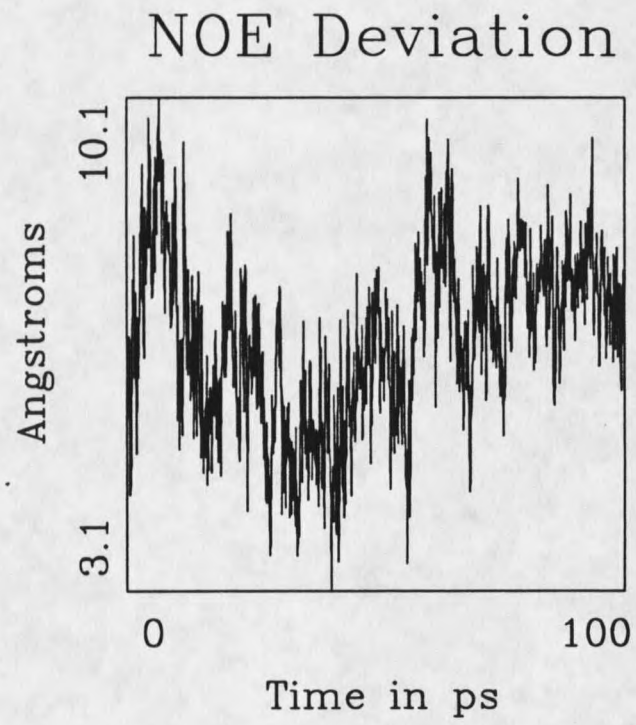

Figure 21. Free D-analog NOE Deviation.

The total deviation (Å) of d-analog inter-proton distances from the free in solution NOESY derived distance constraints as a function of the time (ps) elapsed by the molecular dynamics simulation.

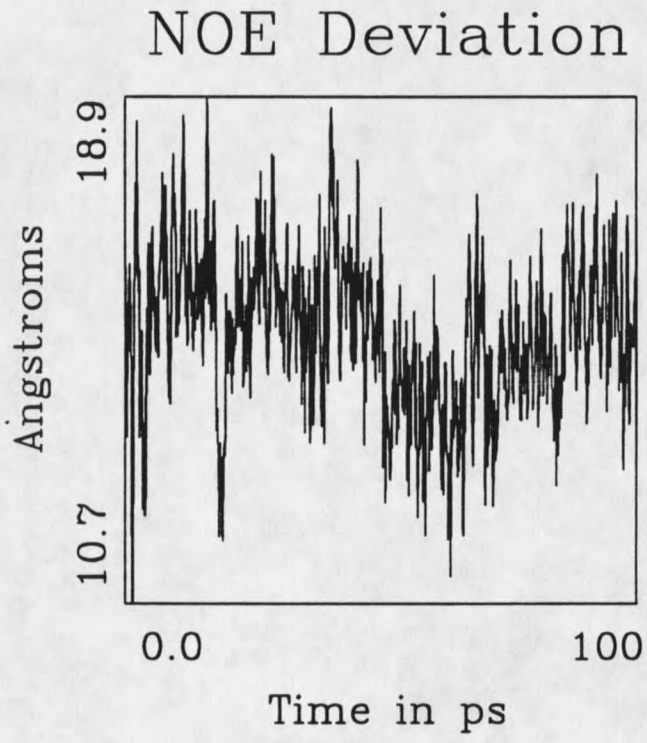

Figure 22. Free L-analog NOE Deviation.

The total deviation (Å) of l-analog inter-proton distances from the free in solution NOESY derived distance constraints as a function of the time (ps) elapsed by the molecular dynamics simulation.

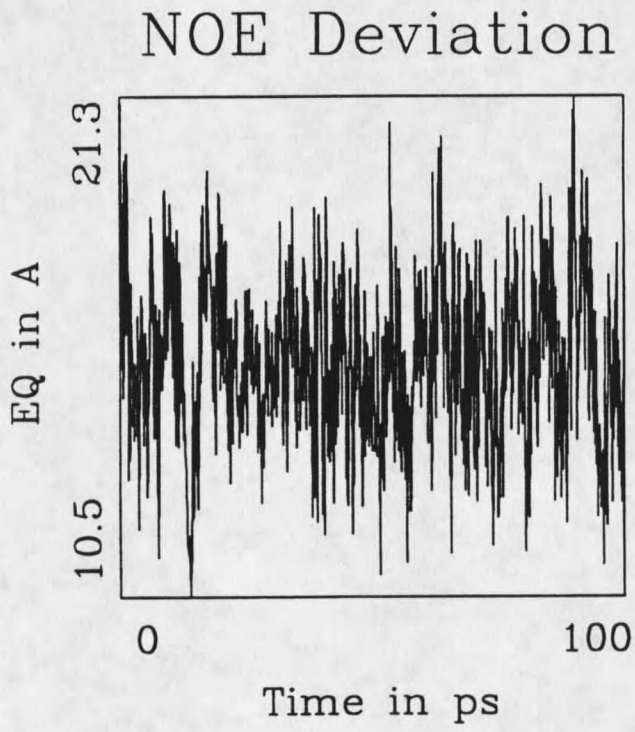

Figure 23. Free Peptide 11 Energy.

The total kinetic and potential energy (Kcal) of peptide 11 as a function of the time (ps) elapsed by the molecular dynamics simulation.

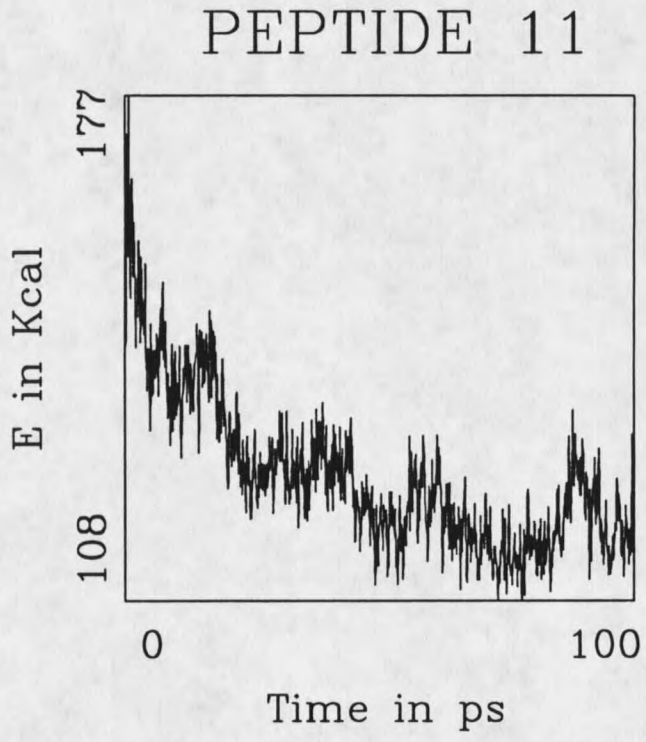

Figure 24. Free D-analog Energy.

The total kinetic and potential energy (Kcal) of the d-analog as a function of the time (ps) elapsed by the molecular dynamics simulation constrained by free in solution NOESY derived distance constraints.

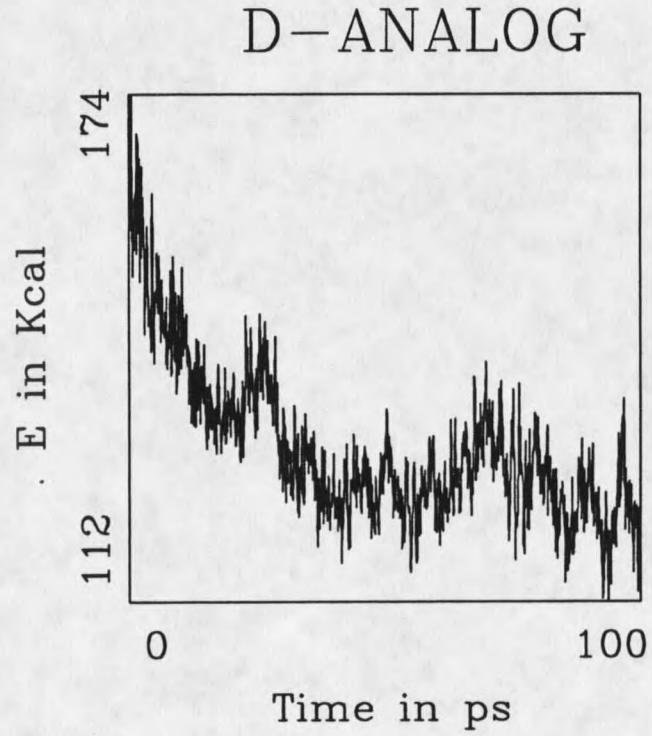

Figure 25. Free L-analog Energy.

The total kinetic and potential energy (Kcal) of the l-analog as a function of the time (ps) elapsed by the molecular dynamics simulation constrained by free in solution NOESY derived distance constraints.

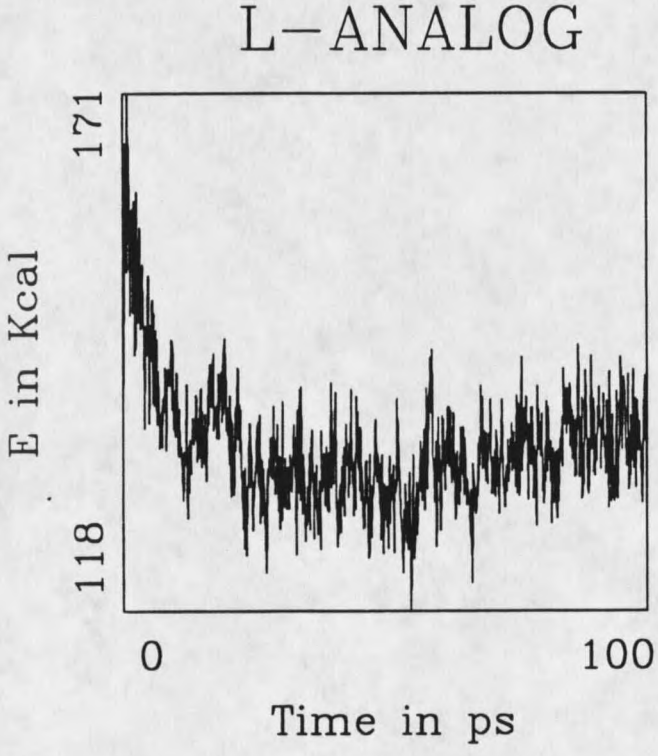

Candidate conformations for peptide 11 and the d and l-analogs are presented in figures 26-27, 28-29, and 30-31, respectively. The small tetrahedrons present in all figures of the peptides are the pseudo-atoms used to constrain groups of protons which were not stereo-specifically assigned. The inter-proton distances of these conformations agreed well with their NOESY predicted values. Deviation from predicted $\langle r_{ij} \rangle$ averaged less than 0.4 Å per constraint over the 35 to 40 constraints utilized per peptide.

The conformational similarities suggested in the NMR spectra of peptide 11 and the d-analog are clearly expressed in their respective constrained MD structures. Both peptide 11 (Figs. 26-27) and the d-analog (Figs. 28-29) adopt many compact conformations in the NOE constrained MD simulations, which possess a bend in the YIXSR region. In contrast, the YIXSR region of the l-analog does not appear to favor any one compact conformation (Figs. 30-31).

When employing molecular dynamics simulations to discern the biologically active conformation of a biopolymer, it is important to sample conformation space. In order to increase the sampling of conformation space, MD simulations of peptide 11 and the d and l-analogs were performed at the simulated temperature of 500 K. An elevated temperature, such as 500 K, increases the kinetic energy of the molecule, and consequently the rate at which the molecule traverses the conformational energy surface. In addition, three different starting conformations of peptide 11 and the d and l-analogs were employed: a β sheet, a right handed a helix, and a left handed a helix. The conformations with the best NOE agreement that resulted from the different starting structures were indistinguishable.

Figure 26. Peptide 11 Free in Solution.

The conformation adopted by peptide 11 after 55.9 ps of molecular dynamics constrained by free in solution NOESY derived distance constraints.

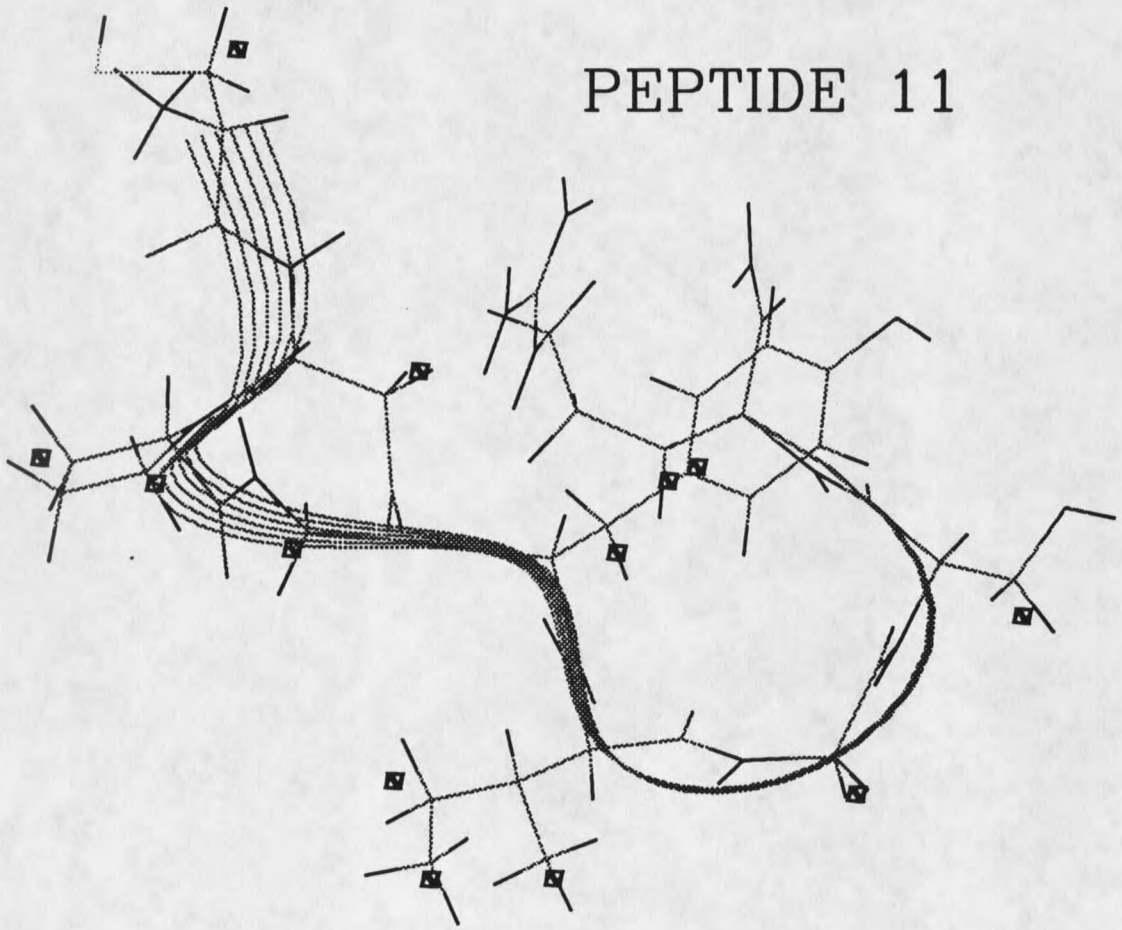

Figure 27. Peptide 11 Free in Solution.

The conformation adopted by peptide 11 after 96.5 ps of molecular dynamics constrained by free in solution NOESY derived distance constraints.

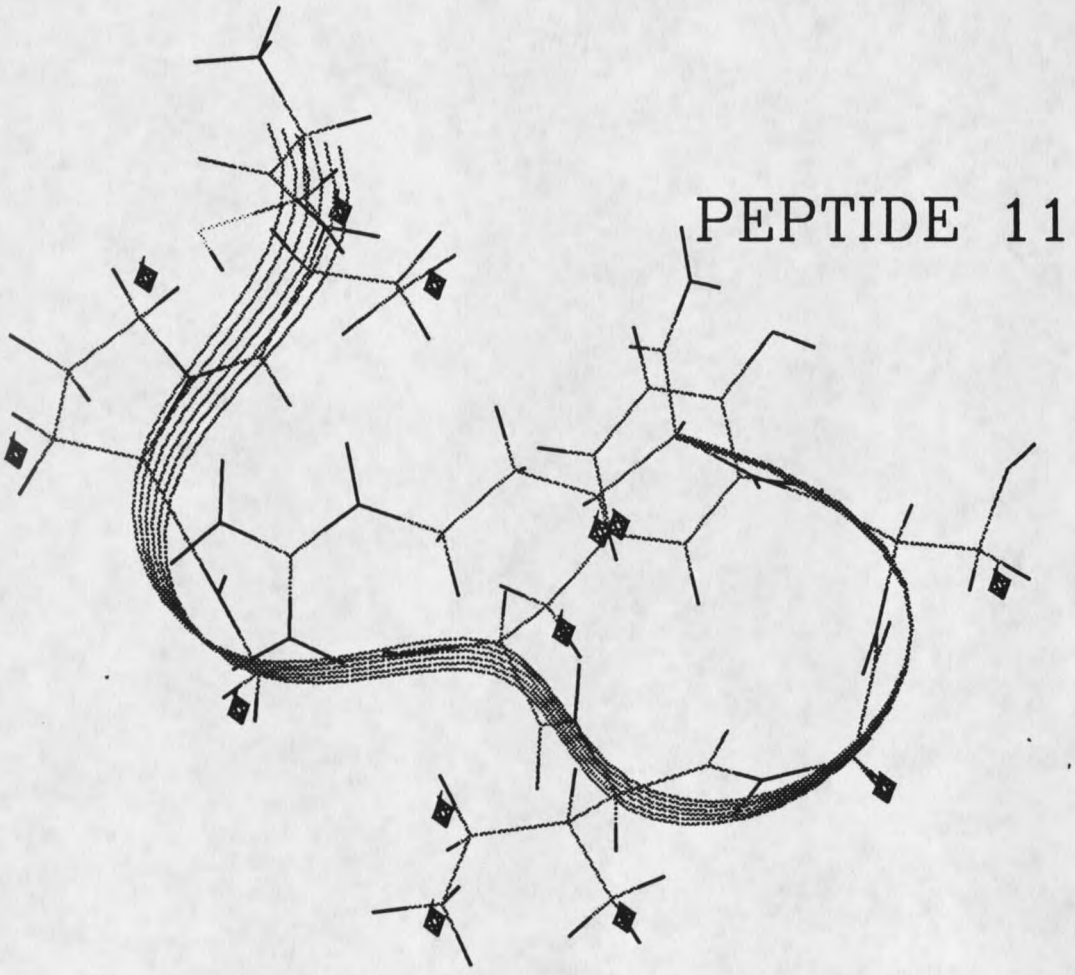

Figure 28. The D-analog Free in Solution.

The conformation adopted by the d-analog after 63.5 ps of molecular dynamics constrained by free in solution NOESY derived distance constraints.

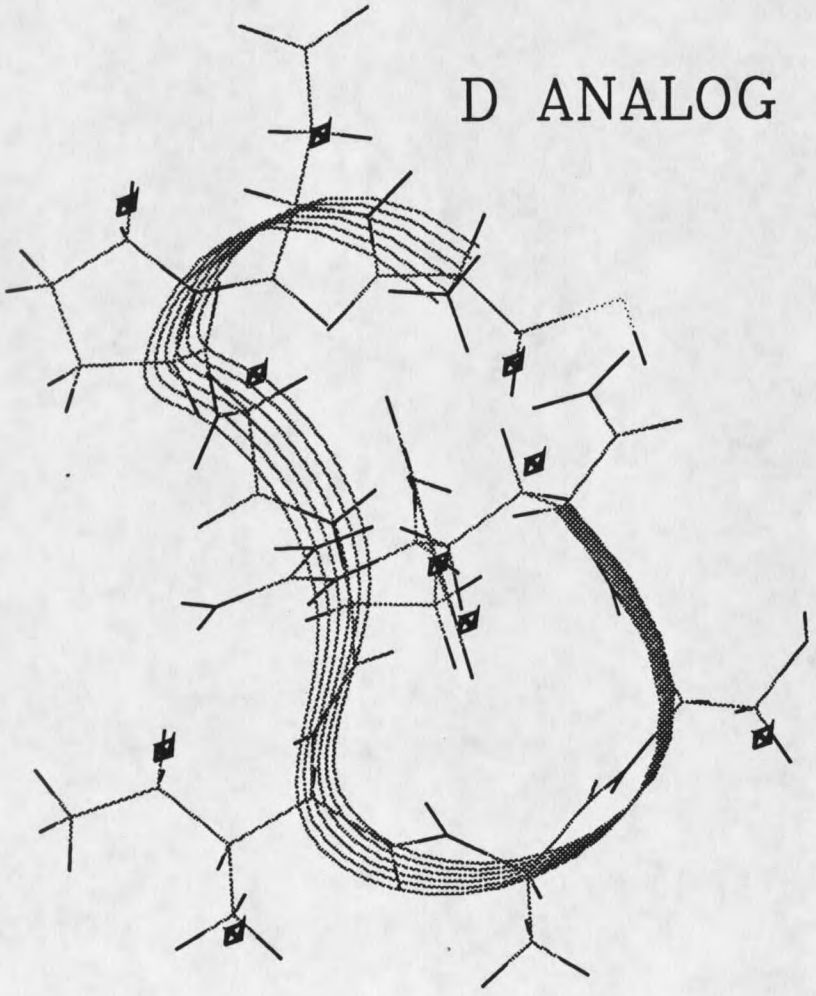

Figure 29. The D-analog Free in Solution.

The conformation adopted by the d-analog after 84.2 ps of molecular dynamics constrained by free in solution NOESY derived distance constraints.

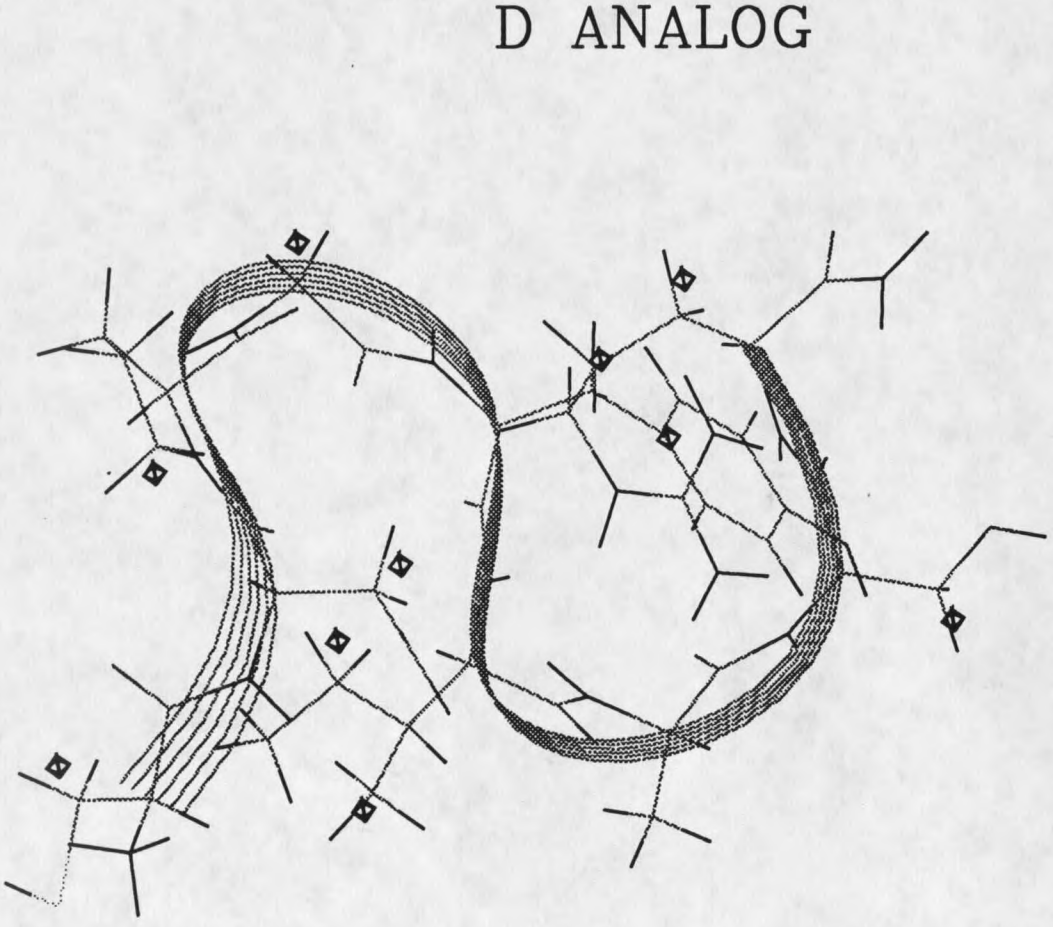

Figure 30. The L-analog Free in Solution.

The conformation adopted by the l-analog after 82.0 ps of molecular dynamics constrained by free in solution NOESY derived distance constraints.

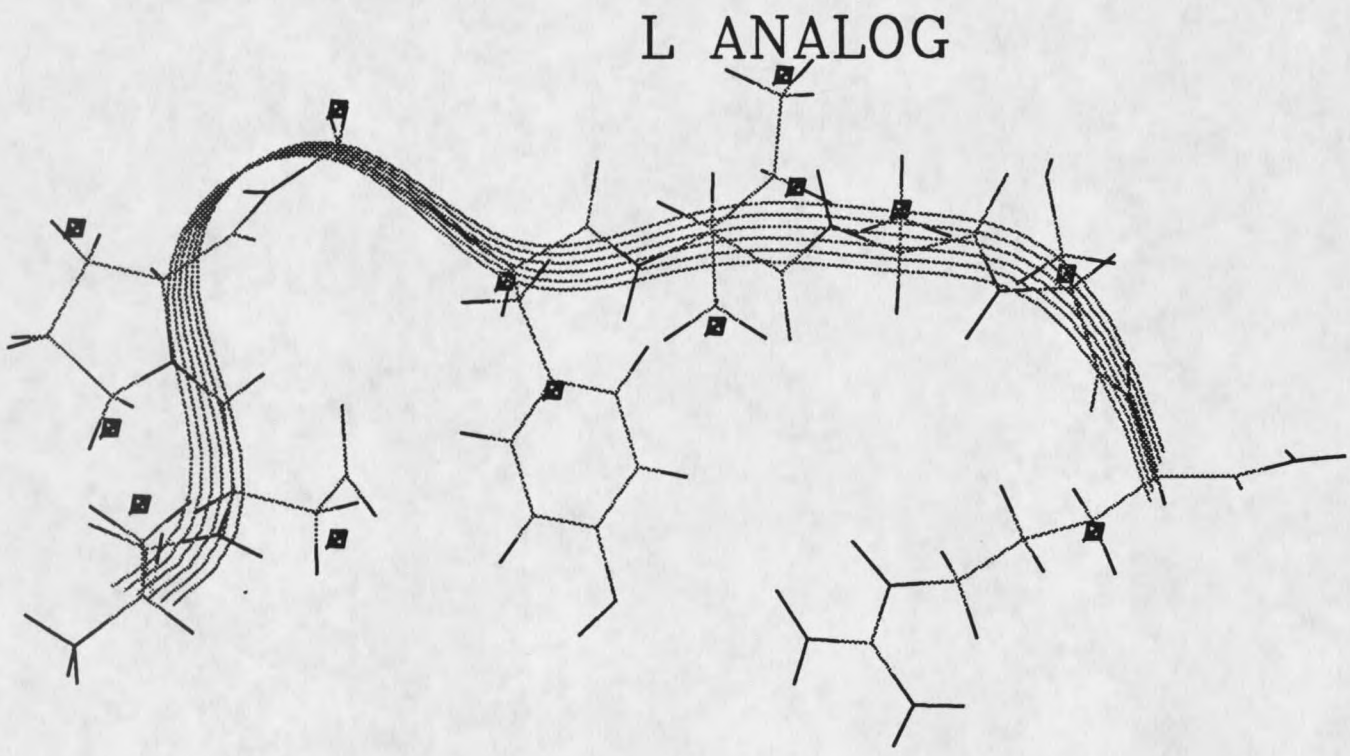

Figure 31. The L-analog Free in Solution.

The conformation adopted by the l-analog after 98.7 ps of molecular dynamics constrained by free in solution NOESY derived distance constraints.

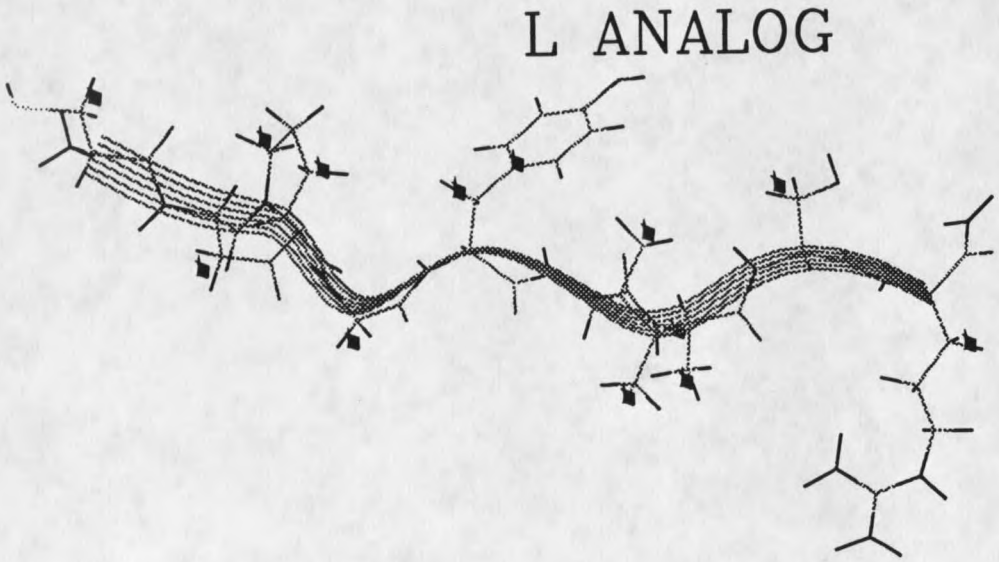

Unconstrained Molecular Dynamics

Incorporating distance constraints into MD could potentially restrict the exploration of conformation space by the peptides. In order to test whether or not the incorporation of distance constraints biased peptide 11 away from other conformations that might also possess good NOE agreement, molecular dynamics simulations of peptide 11 were performed without distance constraints. In the course of these unconstrained MD simulations peptide 11 adopted low energy conformations (Fig. 32) which possessed good NOE agreement (Fig. 33). The conformations with good NOE agreement generated by unconstrained molecular dynamics were somewhat similar to the conformations generated by constrained molecular dynamics (Figs. 34-35). If the unconstrained molecular dynamics simulations had generated peptide 11 conformations with good NOE agreement that differed greatly from the conformations generated by the constrained molecular dynamics simulations, then it would have been clear that the NOE derived distance constraints had prevented the constrained MD simulations from adequately exploring conformation space. However, the conformations with good NOE agreement generated by unconstrained MD were somewhat similar to the conformations generated by the constrained MD. This suggests that in the course of 100 ps of constrained molecular dynamics performed at 500 K that peptide 11 explored a significant portion of conformation space.

ϕ,ψ Plots of Free Peptide Conformations

The paths taken through conformation (ϕ,ψ) space of residue Asp_2-Arg_9 were monitored for the duration of constrained molecular dynamics simulations. The ϕ,ψ plots generated by MD using an extended conformation

Figure 32. Free Peptide 11 Energy During Unconstrained

The total kinetic and potential energy (Kcal) of peptide 11 as a function of the time (ps) elapsed by the molecular dynamics simulation.

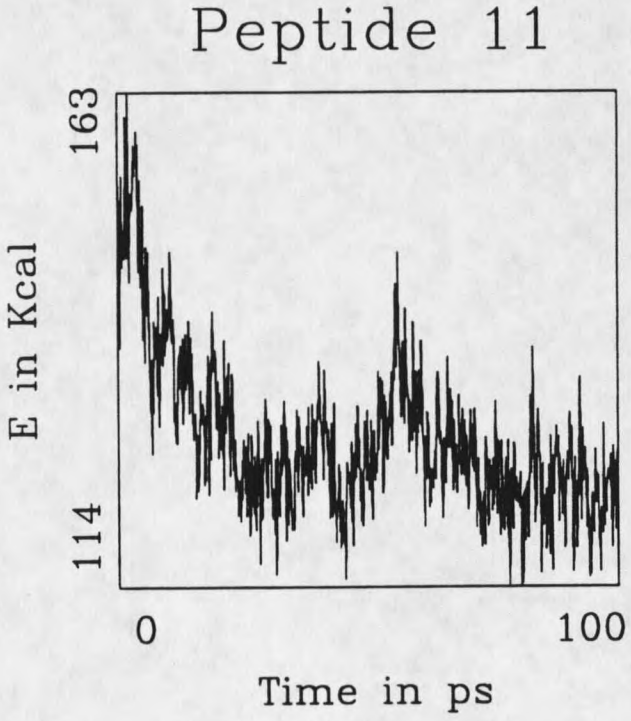

Figure 33. NOE Deviation During Unconstrained Molecular Dynamics of Peptide 11.

The total deviation in Å of peptide 11 inter-proton distances from the free in solution NOESY derived distance constraints as a function of the time elapsed by the unconstrained molecular dynamics simulation.

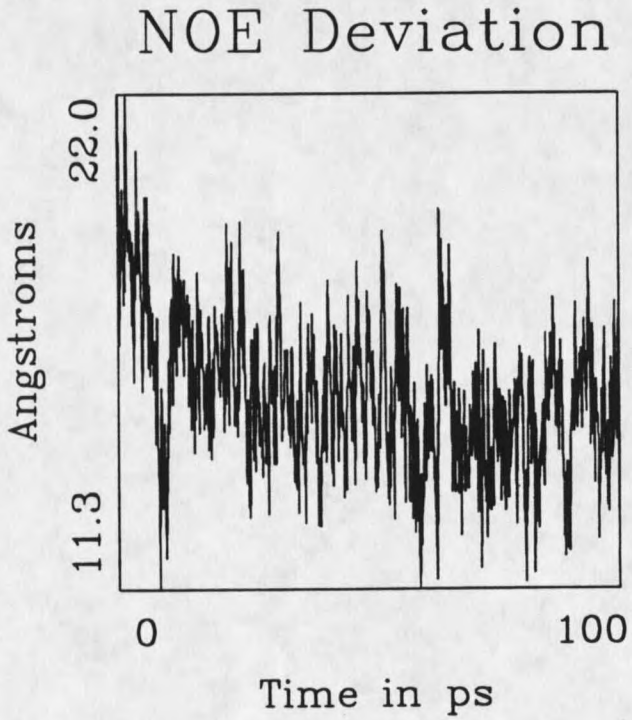

Figure 34. Conformation of Peptide 11 Generated by Unconstrained Molecular Dynamics.

The conformation adopted by peptide 11 after 9.4 ps of unconstrained molecular dynamics.

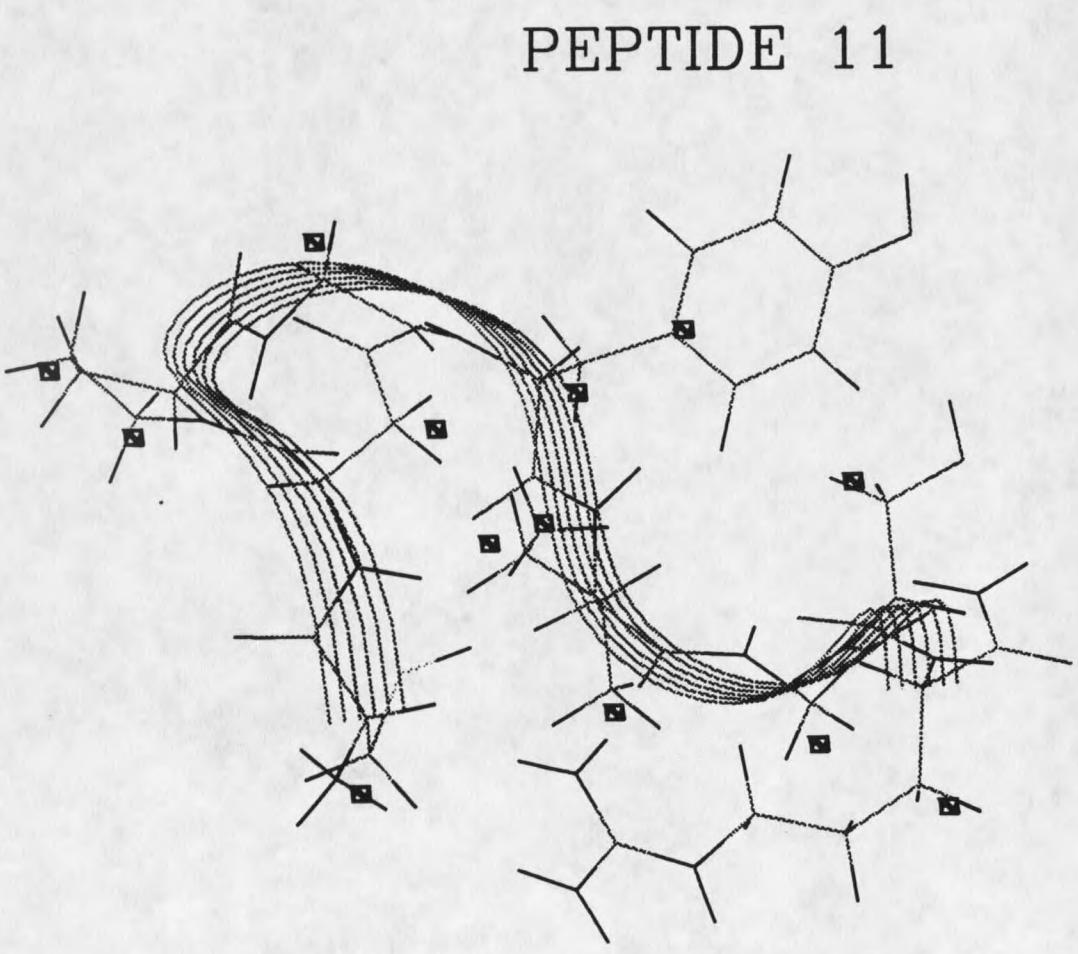

Figure 35. Conformation of Peptide 11 Generated by Unconstrained Molecular Dynamics.

The conformation adopted by peptide 11 after 81.4 ps of unconstrained molecular dynamics.

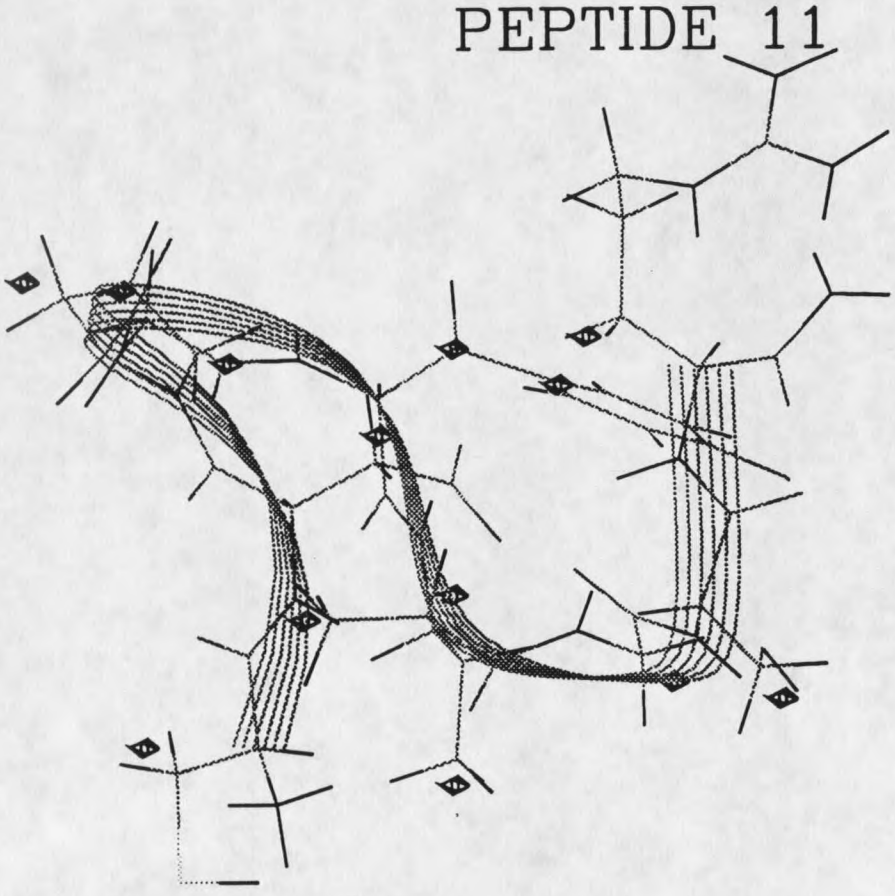

of the peptides as the starting structure are shown in Figures 36-38. When left and right handed helices, which start the amino acids in quadrants III and I, respectively, were used as starting structures, the amino acid residues were observed to quickly adopt conformations similar to those generated by MD which used an extended starting structure (data not shown).

Cys_1 does not possess a ϕ angle and was omitted from this analysis. Except for X_7, the paths through conformation space of the individual amino acid residues did not differ significantly between the three peptides studied when the same starting conformation was used. Gly_7 of peptide 11 explored all four quadrants of ϕ,ψ space as only glycine can do, but for much of the MD simulation Gly_7 of peptide 11 possessed a conformation corresponding to quadrant IV ($0 \leq \phi \leq 180$, $-180 \leq \psi \leq 0$) of ϕ,ψ space. Ala_7 of the d-analog also possessed a quadrant IV conformation, while Ala_7 of the l-analog was restricted to quadrant II ($-180 \leq \phi \leq 0$, $0 \leq \psi \leq 180$) and quadrant III ($-180 \leq \phi \leq 0$, $-180 \leq \psi \leq 0$) conformations.

The conformations of the enantiomeric alanines were anticipated due to their known steric properties. The Gly_7 conformation of peptide 11; however, could not have been predicted *a priori* as glycine can possess a conformation corresponding to any of the four quadrants of ϕ,ψ space. The preference of Gly_7 for the ϕ,ψ quadrant IV, which is the same backbone conformation adopted by Ala_7 of the d-analog, most likely results from the application of the NOESY derived distance constraints. In the unconstrained dynamics, Gly_7 did not favor any one region of ϕ,ψ conformation space (Fig. 39). The fact that the two biologically more active peptides were observed to possess a conformation unattainable by the less active analog implies that the

Figure 36. ϕ,ψ Plots of Free Peptide 11.

The backbone conformations adopted by the residues of peptide 11 in the course of molecular dynamics simulations constrained by free in solution NOESY derived distance constraints.

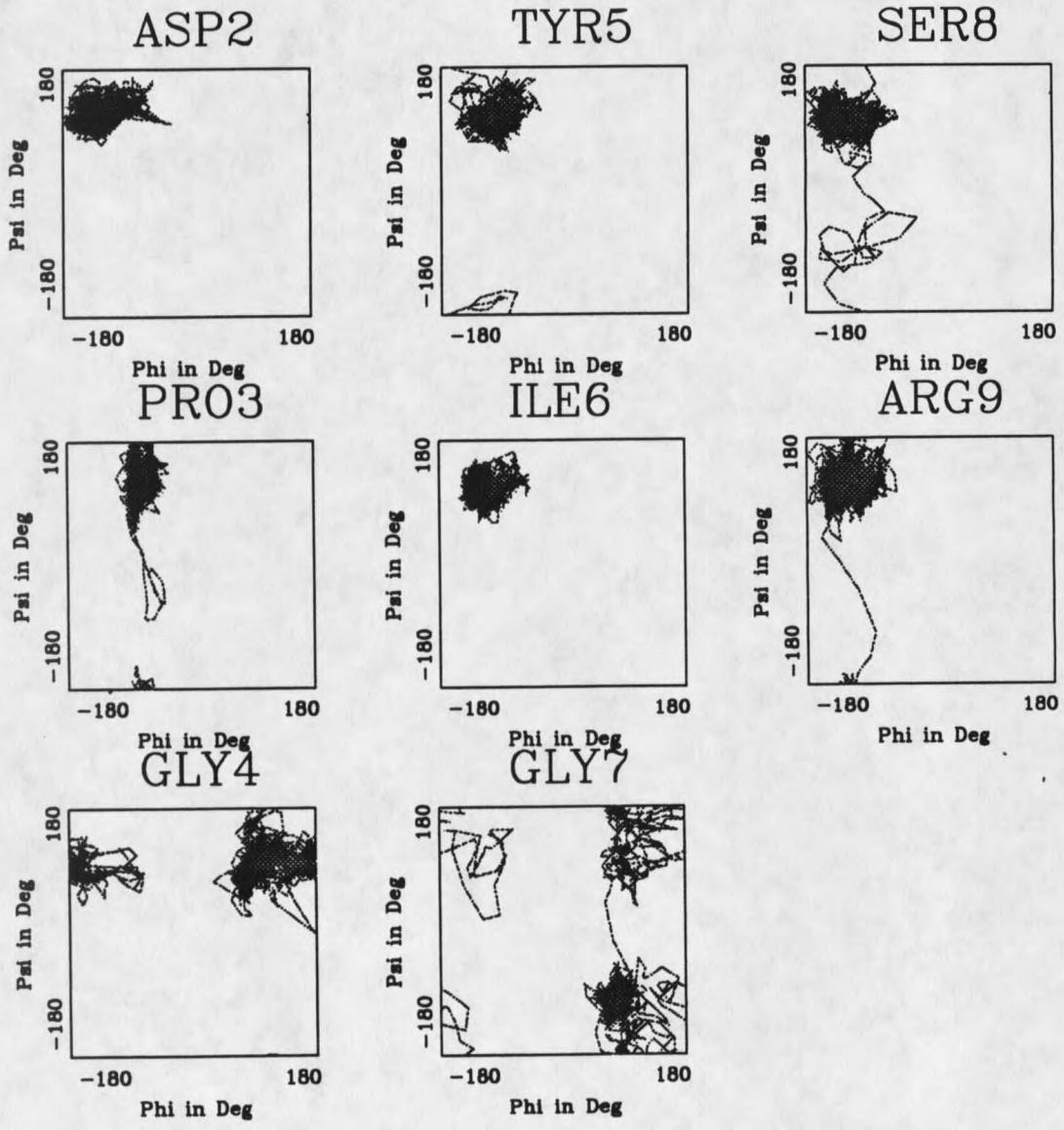

Figure 37. ϕ,ψ Plots of the D-analog Free in Solution.

The backbone conformations adopted by the residues of the d-analog in the course of molecular dynamics simulations constrained by free in solution NOESY derived distance constraints.

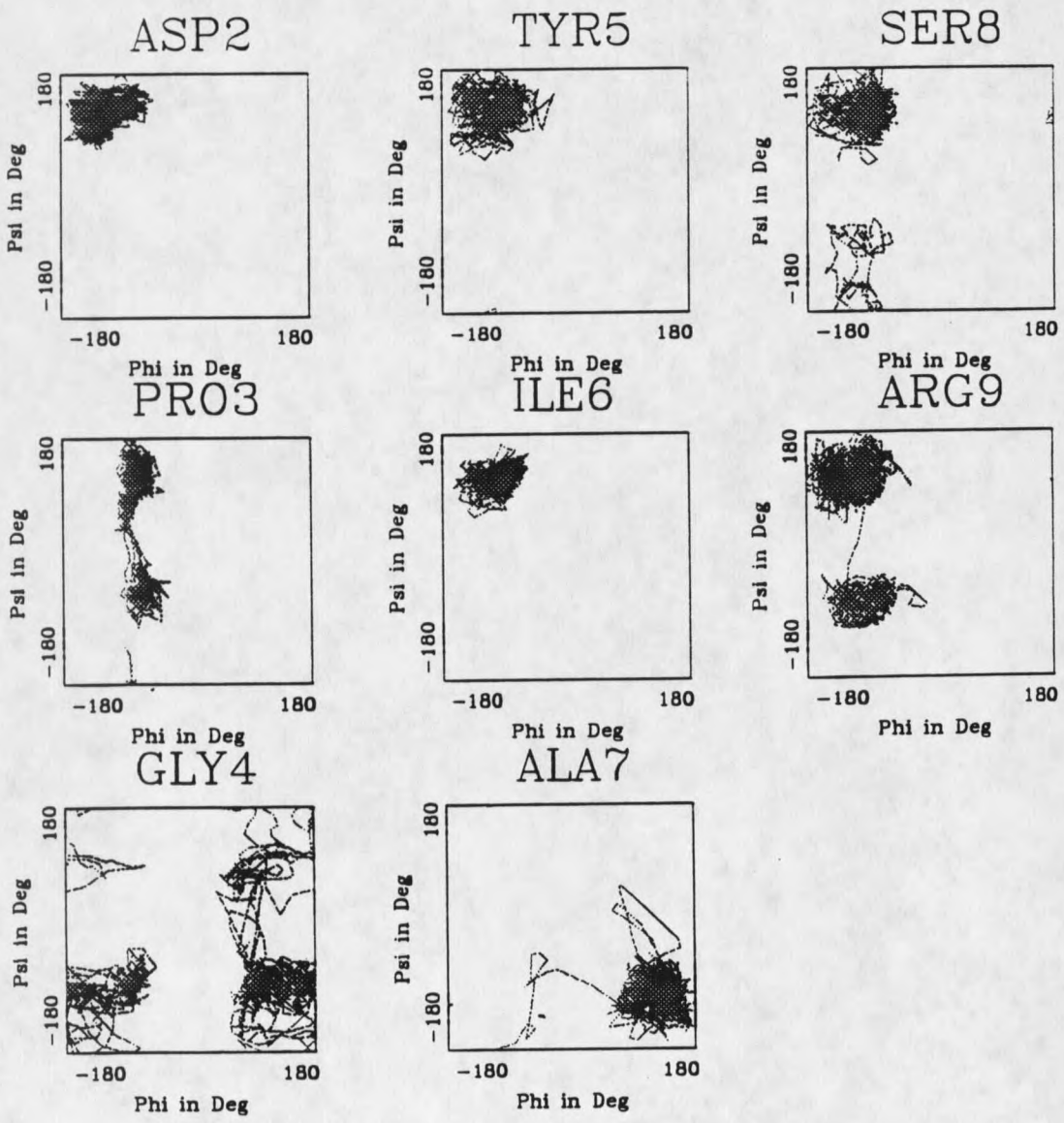

Figure 38. ϕ,ψ Plots of the L-analog Free in Solution.

The backbone conformations adopted by the residues of the l-analog in the course of molecular dynamics simulations constrained by free in solution NOESY derived distance constraints.

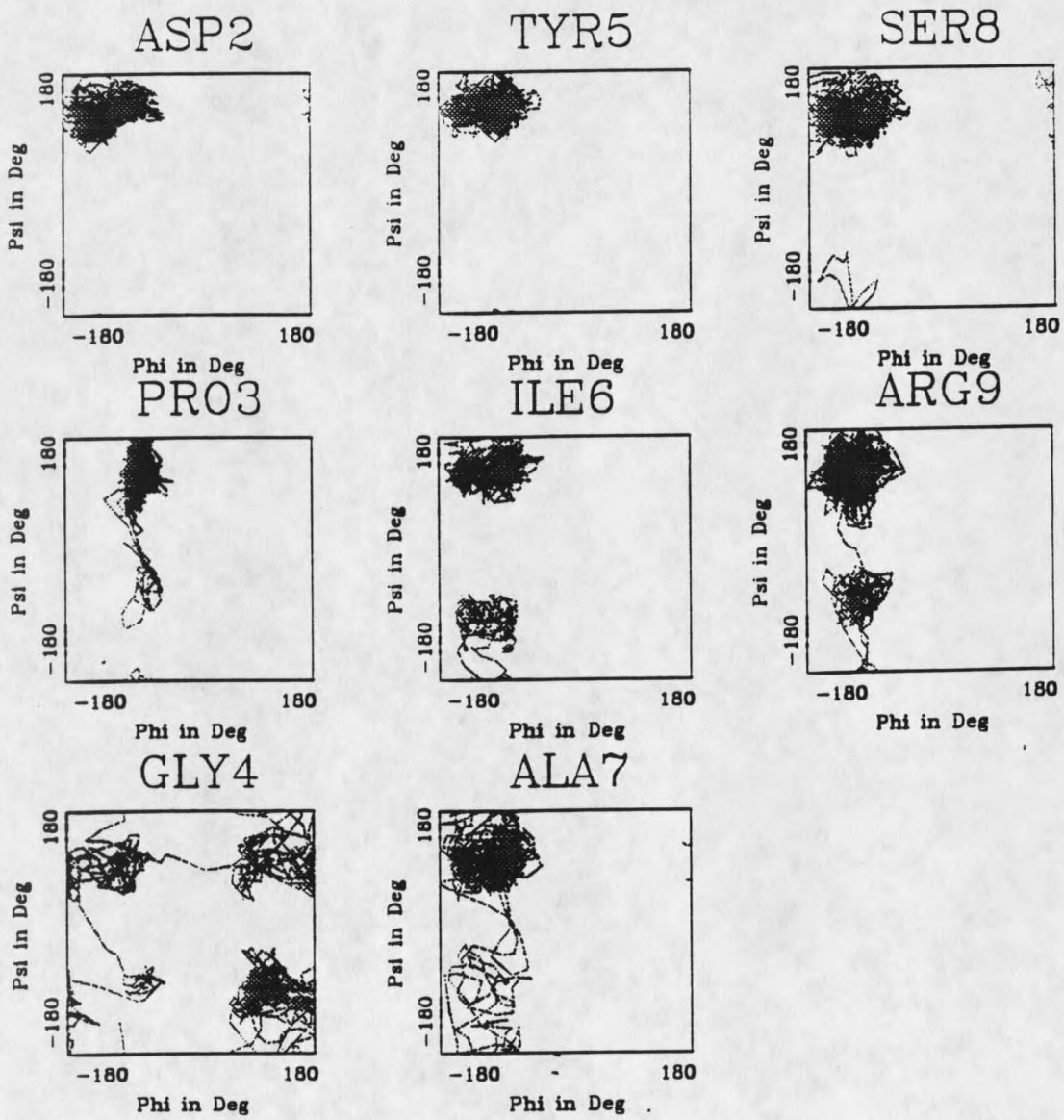

Figure 39. ϕ,ψ Plots of Free Peptide 11 Unconstrained.

The backbone conformations adopted by the residues of peptide 11 in the course of molecular dynamics simulations not constrained by free in solution NOESY derived distance constraints.

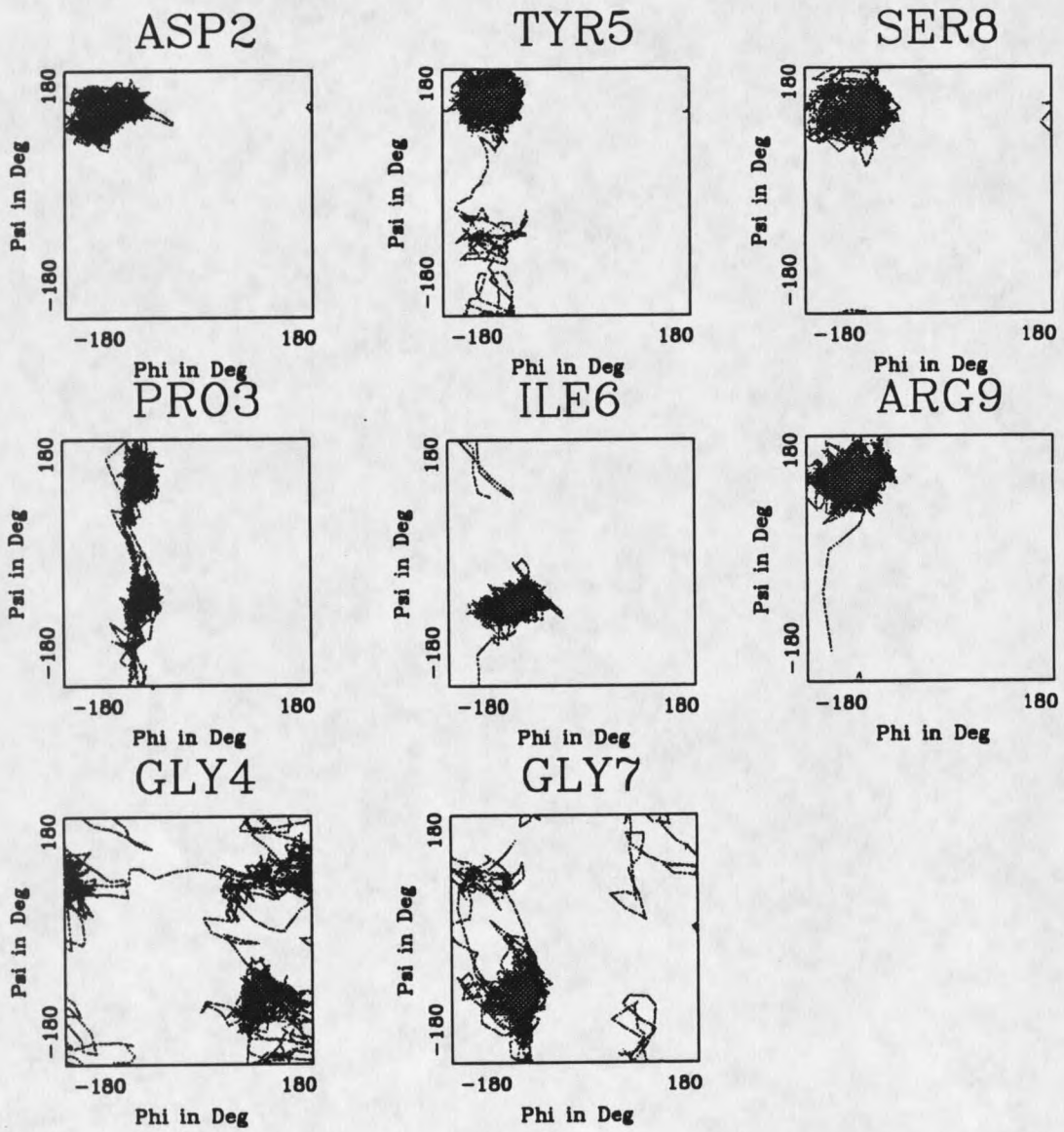

biologically active conformation of peptide 11 involves Gly_7 occupying quadrant IV of ϕ,ψ space. The dramatic similarity of the YIXSR regions of peptide 11 (Figs. 26-27) and the d-analog (Figs. 28-29) found in the NOE constrained MD implies that the greater biological activity of these peptides is a function of the observed bend around Gly_7 and d-Ala_7, respectively.

Observation of a DPGY Turn

In the course of molecular dynamics simulations, the DPGY region of peptide 11 (Figs. 27,34, and 35), the d-analog (Figs. 28-29), and the l-analog (Fig. 30), is observed to occasionally form a turn. Interestingly, the PG dipeptide sequence found in all three peptides has a high potential for β turn formation (Chou and Fasman, 1978), and short peptides with the PG dipeptide sequence, such as YPGDV, have previously been observed to possess relatively stable type II β turns when free in aqueous solution (Dyson *et al.*, 1988a).

The minimum necessary sequence for inhibition basement membrane matrix invasion is YIGSR (Iwamoto *et al.*, 1987). YIGSR-NH_2 and YI(dA)SR-NH_2 both inhibit invasion, while YI(lA)SR-NH_2 is completely inactive (Ostheimer *et al.*, 1992). However, when l-alanine is substituted for Gly_7 in peptide 11, CDPGYIGSR-NH_2, inhibition is reduced only from 80% to 45% of control at 100 μM of peptide. The residual activity of the l-analog and the fact that peptide 11, CDPGYIGSR-NH_2, is more active than YIGSR-NH_2 (Iwamoto *et al.*, 1987), implies that the CDPG region of these peptides may play a role in the interactions between the 67 kDa high-affinity laminin receptor and laminin. NMR spectroscopy of peptide 11, the d-analog, and the l-analog, discussed earlier, implies that the conformation of this region is similar in all

three peptides free in aqueous solution. The generation of a DPGY turn during MD in all three peptides is in agreement with predictions using the method of Chou and Fasman and the NMR observations of other peptides by Dyson *et al.* This evidence combined with the parallel NMR behavior of the three peptides in the DPGY region, suggests that the residual biological activity of the l-Ala$_7$ analog is the result of a DPGY β turn.

TRNOESY Experiments are Required

The combined results of NMR spectroscopy of the peptides free in solution and molecular dynamics simulations have generated conformations for peptide 11, the d-analog, and the l-analog, which are consistent with their biological activity. However, due to the limitations of NMR spectroscopy of short peptides free in aqueous solution, the structures presented cannot be considered a convincing elucidation of the biologically active conformations of peptide 11 and the d and l-analogs. In order to more fully elucidate the biologically active conformations of these peptides transferred nuclear Overhauser effect spectroscopy of the peptides was performed in the presence of the 67 kDa high-affinity laminin receptor. The results of the TRNOESY experiments are presented in the following chapter.

CHAPTER 4

THE RECEPTOR BOUND CONFORMATION OF PEPTIDE 11

NMR spectroscopy and molecular dynamics of peptide 11, the d-alanine$_7$ analog (d-analog), and the l-alanine$_7$ analog (l-analog) free in aqueous solution suggested that bends formed by DPGY and YIGSR were likely to play a role in the biological activity of peptide 11. In order to more fully elucidate the biologically active conformations of peptide 11 and the d-analog, and to explain the residual activity of the l-analog, transferred NOESY (TRNOESY) experiments were conducted on the three peptides in the presence of the 67 kDa high-affinity laminin receptor. The data generated from these experiments was incorporated into molecular dynamics simulations in order to investigate the receptor bound conformation of peptide 11 and the d and l-analogs.

Evidence for Binding of the Peptides to the Receptor

Prior to using the data generated by TRNOESY NMR experiments, it was necessary to establish that the peptides were binding to the 67 kDa high-affinity laminin receptor. Broadening of NMR resonance linewidth and changes in chemical shift values are often used to monitor peptide-receptor interactions (Landry and Gierasch, 1991, Landry *et al.*, 1992, Ni *et al.*, 1989a-1989c). However, with the low fraction of bound peptide (p_B) employed in the present work, the peptide chemical shift values and linewidths would be

expected to be dominated by the values of the free peptide (Campbell and Sykes, 1991a). Without these direct indicators of peptide-receptor interaction, receptor binding in the NMR experiment must be inferred from comparisons of the spectra in the presence (TRNOESY) and in the absence of receptor (NOESY). As will be discussed below, the TRNOESY spectra did exhibit significant differences from the NOESY spectra of the peptides free in solution.

The Chemical Shift Values of Cys_1 Protons in the Presence of Receptor Differ From Their Free in Solution Values

The chemical shifts of $Cys_1\alpha H$, $Cys_1\beta H^1$, and $Cys_1\beta H^2$ of peptide 11, the d-analog, and the l-analog free in solution and in the presence of receptor are presented in Table 6. Note that the pH at which these chemical shift values were measured differed from the pH at which the chemical shift values presented in Table 5 were measured. The pH of the various solutions is given in the table.

Table 6. Cys_1 Chemical Shifts

	peptide 11		d-analog		l-analog	
	free	bound	free	bound	free	bound
$C_1\alpha H$	4.22	4.15	4.29	4.10	4.22	4.08
$C_1\beta H^1$	3.03	3.01	3.08	2.99	3.00	2.96
$C_1\beta H^2$	3.22	3.17	3.28	3.11	3.18	3.10
pH	7.4	7.6	7.0	7.6	7.1	7.6

The composition of the free and receptor-bound solutions was identical except for the presence of the 67 kDa high-affinity laminin receptor in the

latter. The pH of the free peptide 11, d-analog, and l-analog solutions were 7.4, 7.0, and 7.1, respectively. The pH of the receptor solutions was 7.6. As the pK_a of the sulfur of monomeric cysteine is 8.33, it is possible that the small differences in pH of the free and the bound solutions could cause the observed change in Cys_1 proton chemical shift values. The formation of inter-peptide di-sulfide bonds could have also resulted in the observed difference in chemical shift.

Peptide Cross Relaxation Rates Are Faster in the Presence of Receptor

The long correlation times (τ_c) of large biopolymers (such as the 67 kDa high-affinity laminin receptor) increase the rate of NOE cross relaxation in bound ligands (Clore and Gronenborn, 1983, Campbell and Sykes, 1991a). Rapid rates of cross relaxation result in a rapid distribution of magnetization among connected protons. In the presence of the 67 kDa receptor, peptide 11, the d-analog, and the l-analog exhibited increased rates of cross relaxation. The increased rates of cross relaxation caused additional nuclear Overhauser effect cross relaxation pathways to affect the intensities of NOE intensities. The consequent deviation from linear buildup of NOE and TRNOE intensity is known as spin diffusion. The observation of increased rates of cross relaxation in all three peptides indicates that they bound the 67 kDa high-affinity laminin receptor.

NOESY of the peptides free in aqueous solution was performed with mixing times of 100, 200, and 400 ms. The intensity of the majority of NOEs increased as τ_m increased (Tables 6-8). However, as τ_m was increased from 200 to 400 ms, the intensity of some NOEs decreased, and many other NOEs failed

to exhibit a linear increase with increasing τ_m. A decrease in NOE intensity at longer τ_m is indicative of multi-step cross relaxation pathways. All free in solution NOEs that decreased in intensity when the mixing time was increased from 200 to 400 ms are noted in tables 6-8. Every instance of such a decrease involved intra-residue NOEs in which the inter-proton distance of the protons involved is known to be short. Examples included the NOEs between $Asp_2\beta H^1$-$Asp_2\beta H^2$, $Pro_3\gamma H_2$-$Pro_3\delta H_2$, $Tyr_5\alpha H$-$Tyr_5\beta H_2$, and $Ser_8\alpha H$-$Ser_8\beta H_2$. The presence of receptor greatly increased the amount of spin diffusion (Tables 9-11). In addition to the intra-residue proton pairs which exhibited spin diffusion in the free peptides, several inter-residue TRNOE intensities were affected by spin diffusion. Figures 40, 41, and 42 are representative of the inter-residue spin diffusion that resulted from increased rates of inter-residue cross relaxation exhibited by peptide 11, the d-analog, and the l-analog, respectively. The frequent occurrence of spin diffusion in the 400 ms TRNOESY experiments suggests that the peptides are binding the 67 kDa high-affinity laminin receptor. However, the fact that spin diffusion does not occur for $\tau_m \leq 200$, indicates that for the experimental conditions used, 200 ms is a "reasonable" mixing time (Campbell and Sykes, 1991b). Therefore, TRNOE intensities measured from experiments with $\tau_m \leq 200$ can be used to assess the bound conformation of peptide 11 and the d and l-analogs.

Table 7. Peptide 11 Free in Solution NOE Intensities as a Function of Mixing Time (τ_m).

	NOE intensity versus τ_m			
τ_m (ms)	100	200	400	SD[a]
$C_1\alpha H$-$C_1\beta H_2$	ZQ[b]	ZQ	ZQ	
$C_1\beta H^1$-$C_1\beta H^2$	-[c]	-	21.2	
$C_1\alpha H$-D_2NH	2.05	5.09	2.87	
$C_1\beta H_2$-D_2NH	-	-	2.11	
D_2NH-$D_2\alpha H$	ZQ	1.08	1.47	
D_2NH-$D_2\beta H^1$	-	-	2.75	
D_2NH-$D_2\beta H^2$	-	-	2.22	
$D_2\alpha H$-$D_2\beta H^1$	ZQ	ZQ	ZQ	
$D_2\alpha H$-$D_2\beta H^2$	ZQ	ZQ	ZQ	
$D_2\beta H^1$-$D_2\beta H^2$	45.0	46.4	41.2	*
$D_2\alpha H$-$P_3\delta H^1$	4.98	4.09	9.11	
$D_2\alpha H$-$P_3\delta H^2$	4.42	2.92	7.64	
$D_2\beta H^1$-$P_3\delta H^1$	-	-	-	
$D_2\beta H^1$-$P_3\delta H^2$	-	-	2.59	
$D_2\beta H^2$-$P_3\delta H^1$	-	-	-	
$D_2\beta H^2$-$P_3\delta H^2$	-	-	-	
$P_3\alpha H$-$P_3\beta H^1$	-	4.02	4.66	
$P_3\alpha H$-$P_3\beta H^2$	2.04	11.6	11.9	*
$P_3\alpha H$-$P_3\gamma H_2$	-	-	-	
$P_3\beta H^1$-$P_3\beta H^2$	25.0	33.0	31.9	*
$P_3\beta H^1$-$P_3\gamma H_2$	ZQ	ZQ	ZQ	
$P_3\beta H^2$-$P_3\gamma H_2$	ZQ	ZQ	ZQ	
$P_3\gamma H_2$-$P_3\delta H^1$	1.39	2.05	3.07	
$P_3\gamma H_2$-$P_3\delta H^2$	1.06	6.24	6.24	*
$P_3\alpha H$-G_4NH	-	4.83	8.27	
G_4NH-$G_4\alpha H$	3.56	14.8	10.6	*
G_4NH-Y_5NH	-	1.77	3.34	
$G_4\alpha H$-Y_5NH		5.15	10.1	
Y_5NH-$Y_5\alpha H$	ZQ	2.02	4.23	
Y_5NH-$Y_5\beta H_2$	0.68	3.93	5.76	
Y_5NH-$Y_52,6$	-	0.60	2.60	
$Y_5\alpha H$-$Y_5\beta H_2$	ZQ	15.2	10.7	*
$Y_5\alpha H$-$Y_52,6$	-	2.02	7.38	
$Y_5\beta H_2$-$Y_52,6$	noise[d]	16.6	26.0	

$Y_5$2,6-$Y_5$3,5	13.8	25.8	46.4	
Y_5NH-I_6NH	-	1.52	noise	
$Y_5\alpha$H-I_6NH	10.3	9.62	20.6	
$Y_5\beta H_2$-I_6NH	-	0.52	1.63	
$Y_5$2,6-I_6NH	-	0.26	noise	
I_6NH-$I_6\alpha$H	ZQ	ZQ	2.18	
I_6NH-$I_6\beta$H	-	2.07	4.91	
I_6NH-$I_6\gamma H_3$	-	-	0.69	
I_6NH-$I_6\gamma H^1$	-	-	2.35	
I_6NH-$I_6\gamma H^2$	-	-	2.26	
$I_6\alpha$H-$I_6\beta$H	ZQ	ZQ	2.41	
$I_6\alpha$H-$I_6\gamma H_3$	-	2.21	5.94	
$I_6\alpha$H-$I_6\gamma H^1$	-	-	1.95	
$I_6\alpha$H-$I_6\gamma H^2$	-	-	-	
$I_6\beta$H-$I_6\gamma H_3$	ZQ	9.37	9.11	*
$I_6\beta$H-$I_6\gamma H^1$	-	0.77	2.79	
$I_6\beta$H-$I_6\gamma H^2$	0.45	2.12	3.52	
$I_6\gamma H^1$-$I_6\gamma H^2$	26.7	42.0	39.5	*
I_6NH-G_7NH	-	0.75	1.17	
$I_6\alpha$H-G_7NH	5.47	8.79	13.7	
$I_6\beta$H-G_7NH	-	0.09	0.32	
$I_6\delta H_3$-G_7NH	-	-	1.00	
G_7NH-$G_7\alpha$H	4.10	5.07	10.3	
G_7NH-S_8NH	-	0.41	0.47	
$G_7\alpha$H-S_8NH	4.89	4.83	9.20	
S_8NH-$S_8\alpha$H	ZQ	ZQ	ZQ	
S_8NH-$S_8\beta H_2$	-	-	-	
$S_8\alpha$H-$S_8\beta H_2$	ZQ	4.73	ZQ	*
S_8NH-R_9NH	0.46	2.63	1.56	*
$S_8\alpha$H-R_9NH	1.15	2.16	4.07	
R_9NH-$R_9\alpha$H	ZQ	ZQ	ZQ	
R_9NH-$R_9\beta H^1$	-	0.91	0.80	*
$R_9\alpha$H-$R_9\beta H^1$	-	-	1.43	
$R_9\alpha$H-$R_9\beta H^2$	-	-	1.61	
$R_9\beta H^1$-$R_9\beta H^2$	11.5	36.1	10.8	*
$R_9\beta H^2$-$R_9\gamma H^2$	-	2.21	-	*
$R_9\gamma H_2$-$R_9\delta H_2$	ZQ	ZQ	ZQ	
R_9NH^1-R_9NH^2			102	

[a] If the NOE intensity was affected by spin diffusion (SD), then an asterisk (*) is placed in the column with the heading SD.

[b] If the cross peak was dominated by zero quantum (ZQ) coherence, then ZQ was substituted for NOE intensity.

[c] If an intra-residue or sequential NOE was absent, then a dash (-) was substituted for NOE intensity.

[d] If the intensity of a cross peak was not measureable due to overlap with t1 noise or the residual water signal, then the word noise was substituted for NOE intensity.

Table 8. D-analog Free in Solution NOE Intensities as a Function of Mixing Time (τ_m).

	NOE intensity versus τ_m			
τ_m (ms)	100	200	400	SD[a]
$C_1\alpha H$-$C_1\beta H_2$	ZQ[b]	ZQ	1.71	
$C_1\beta H^1$-$C_1\beta H^2$	overlap[c]			
$C_1\alpha H$-D_2NH	2.08	2.50	12.1	
$C_1\beta H_2$-D_2NH	-[d]	-	2.11	
D_2NH-$D_2\alpha H$	ZQ	ZQ	ZQ	
D_2NH-$D_2\beta H^1$	1.29	0.51	3.78	
D_2NH-$D_2\beta H^2$	-	-	1.80	*
$D_2\alpha H$-$D_2\beta H^1$	ZQ	2.38	5.16	
$D_2\alpha H$-$D_2\beta H^2$	ZQ	2.73	6.51	
$D_2\beta H^1$-$D_2\beta H^2$	7.75	34.4	29.9	*
$D_2\alpha H$-$P_3\delta H^1$	noise[e]	4.11	10.7	*
$D_2\alpha H$-$P_3\delta H^2$	noise	3.71	9.87	
$D_2\beta H^1$-$P_3\delta H^1$	-	-	-	
$D_2\beta H^1$-$P_3\partial H^2$	-	1.13	1.15	
$D_2\beta H^2$-$P_3\delta H^1$	-	-	-	
$D_2\beta H^2$-$P_3\delta H^2$	-	-	-	
$P_3\alpha H$-$P_3\beta H^1$	ZQ	1.54	2.63	
$P_3\alpha H$-$P_3\beta H^2$	ZQ	7.28	9.28	
$P_3\alpha H$-$P_3\gamma H_2$	-	0.97	-	
$P_3\beta H^1$-$P_3\beta H^2$	ZQ	12.3	24.0	
$P_3\beta H^1$-$P_3\gamma H_2$	-	-	-	
$P_3\beta H^2$-$P_3\gamma H_2$	ZQ	10.1	9.38	*
$P_3\gamma H_2$-$P_3\delta H^1$	ZQ	8.52	5.69	*
$P_3\gamma H_2$-$P_3\delta H^2$	ZQ	7.52	6.45	*
$P_3\alpha H$-G_4NH	1.95	5.69	12.2	
G_4NH-$G_4\alpha H$	4.05	12.3	16.9	
G_4NH-Y_5NH	1.51	0.93	3.81	
$G_4\alpha H$-Y_5NH	3.36	3.59	10.5	
Y_5NH-$Y_5\alpha H$	ZQ	1.16	4.98	
Y_5NH-$Y_5\beta H_2$	1.73	2.73	11.5	
Y_5NH-$Y_52,6$	-	0.96	1.06	
$Y_5\alpha H$-$Y_5\beta H_2$	ZQ	10.2	12.9	
$Y_5\alpha H$-$Y_52,6$	-	1.46	1.75	
$Y_5\beta H_2$-$Y_52,6$	3.58	11.0	20.3	
$Y_52,6$-$Y_53,5$	17.9	22.5	38.0	
Y_5NH-I_6NH	-	0.87	2.10	
$Y_5\alpha H$-I_6NH	6.26	5.67	18.1	
$Y_5\beta H_2$-I_6NH	-	2.51	2.00	*

$Y_5$2,6-I_6NH	-	-	-	
I_6NH-$I_6\alpha$H	ZQ	0.59	1.89	
I_6NH-$I_6\beta$H	0.65	3.30	5.87	
I_6NH-$I_6\gamma H_3$	-	-	-	
I_6NH-$I_6\gamma H^1$	-	0.60	1.63	
I_6NH-$I_6\gamma H^2$	-	0.84	1.51	
$I_6\alpha$H-$I_6\beta$H	ZQ	1.62	4.91	
$I_6\alpha$H-$I_6\gamma H_3$	-	1.55	3.32	
$I_6\alpha$H-$I_6\gamma H^1$	-	1.19	3.82	
$I_6\alpha$H-$I_6\gamma H^2$	-	-	1.53	
$I_6\beta$H-$I_6\gamma H_3$	-	7.46	12.8	
$I_6\beta$H-$I_6\gamma H^1$	-	9.77	5.70	*
$I_6\beta$H-$I_6\gamma H^2$	-	7.10	2.40	*
$I_6\gamma H^1$-$I_6\gamma H^2$	24.1	25.9	42.4	
I_6NH-A_7NH	3.20	0.76	1.93	
$I_6\alpha$H-A_7NH	2.82	4.57	16.2	
$I_6\beta$H-A_7NH	-	-	2.52	
$I_6\delta H_3$-A_7NH	-	1.71	0.49	*
A_7NH-$A_7\alpha$H	ZQ	1.54	3.36	
A_7NH-$A_7\beta H_3$	-	3.72	4.60	
A_7NH-S_8NH	-	-	2.78	
$A_7\alpha$H-S_8NH	3.10	4.48	18.6	
$A_7\beta H_3$-S_8NH	-	1.30	1.35	
S_8NH-$S_8\alpha$H	ZQ	1.00	7.45	
S_8NH-$S_8\beta H_2$	-	3.83	4.88	
S_8aH-$S_8\beta H_2$	ZQ	10.8	9.23	*
S_8NH-R_9NH	-	0.37	2.78	
$S_8\alpha$H-R_9NH	0.44	2.84	16.1	
R_9NH-$R_9\alpha$H	ZQ	2.61	1.39	*
R_9NH-$R_9\beta H^1$	-	2.94	3.00	*
$R_9\alpha$H-$R_9\beta H^1$	ZQ	0.84	0.25	*
$R_9\alpha$H-$R_9\beta H^2$	ZQ	1.92	3.30	
$R_9\beta H^1$-$R_9\beta H^2$	26.9	20.5	28.8	
$R_9\beta H^2$-$R_9\gamma H^2$	1.90	0.35	6.98	
$R_9\gamma H_2$-$R_9\delta H_2$	ZQ	1.33	-	*
$R_9NH_2{}^1$-$R_9NH_2{}^2$	333	73.7	158	

[a] If the NOE intensity was affected by spin diffusion (SD), then an asterisk (*) is placed in the column with the heading SD.

[b] If the cross peak was dominated by zero quantum (ZQ) coherence, then ZQ was substituted for NOE intensity.

[c] If a cross peak intensity was not measureable due to overlap with other peaks, then the word overlap was substituted for NOE intensity.

[d] If an intra-residue or sequential NOE was absent, then a dash (-) was substituted for NOE intensity.

[e] If the intensity of a cross peak was not measureable due to overlap with t1 noise or the residual water signal, then the word noise was substituted for NOE intensity.

Table 9. L-analog Free in Solution NOE Intensities as a Function of Mixing Time (τ_m).

	NOE intensity versus τ_m			
τ_m (ms)	100	200	400	SD[a]
$C_1\alpha H$-$C_1\beta H_2$	ZQ[b]	ZQ	ZQ	
$C_1\beta H^1$-$C_1\beta H^2$	overlap[c]			
$C_1\alpha H$-D_2NH	3.48	6.43	4.02	*
$C_1\beta H^1$-D_2NH	-[d]	-	-	
$C_1\beta H^2$-D_2NH	-	-	-	
D_2NH-$D_2\alpha H$	ZQ	1.04	2.89	
D_2NH-$D_2\beta H^1$	-	0.90	2.27	
D_2NH-$D_2\beta H^2$	-	2.60	1.00	*
$D_2\alpha H$-$D_2\beta H^1$	0.01	0.63	1.60	
$D_2\alpha H$-$D_2\beta H^2$	0.44	1.55	2.81	
$D_2\beta H^1$-$D_2\beta H^2$	18.7	31.8	34.3	*
$D_2\alpha H$-$P_3\delta H^1$	2.82	6.11	21.3	
$D_2\alpha H$-$P_3\delta H^2$	2.50	3.48	-	*
$D_2\beta H^1$-$P_3\delta H^1$	-	-	-	
$D_2\beta H^1$-$P_3\delta H^2$	-	-	-	
$D_2\beta H^2$-$P_3\delta H^1$	-	1.40	2.20	
$D_2\beta H^2$-$P_3\delta H^2$	-	-	-	
$P_3\alpha H$-$P_3\beta H^1$	ZQ	ZQ	2.13	
$P_3\alpha H$-$P_3\beta H^2$	1.25	4.31	7.88	
$P_3\alpha H$-$P_3\gamma H_2$	-	0.25	0.19	*
$P_3\beta H^1$-$P_3\beta H^2$	ZQ	17.5	24.0	
$P_3\beta H^1$-$P_3\gamma H_2$	ZQ	-	8.45	
$P_3\beta H^2$-$P_3\gamma H_2$	ZQ	2.16	7.85	
$P_3\gamma H_2$-$P_3\delta H^1$	ZQ	0.68	3.99	
$P_3\gamma H_2$-$P_3\delta H^2$	ZQ	3.84	3.83	*
$P_3\alpha H$-G_4NH	3.68	7.86	6.45	*
G_4NH-$G_4\alpha H$	5.36	11.9	7.28	*
G_4NH-Y_5NH	0.63	0.50	1.09	
$G_4\alpha H$-Y_5NH	6.79	12.4	6.26	*
Y_5NH-$Y_5\alpha H$	2.92	7.80	11.0	
Y_5NH-$Y_5\beta H_2$	2.20	11.5	15.4	
Y_5NH-$Y_52,6$	-	-	0.64	
$Y_5\alpha H$-$Y_5\beta H_2$	ZQ	2.31	13.2	
$Y_5\alpha H$-$Y_52,6$	1.24	1.98	4.11	
$Y_5\beta H_2$-$Y_52,6$	5.89	7.09	17.8	
$Y_52,6$-$Y_53,5$	5.80	20.4	37.9	
Y_5NH-I_6NH	-	-	-	
$Y_5\alpha H$-I_6NH	8.81	17.5	14.5	*

$Y_5\beta H_2$-I_6NH	-	-	-	
$Y_5$2,6-I_6NH	-	-	-	
I_6NH-$I_6\alpha$H	ZQ	0.66	2.09	*
I_6NH-$I_6\beta$H	2.47	6.22	3.23	*
I_6NH-$I_6\gamma H_3$	-	1.11	2.88	
I_6NH-$I_6\gamma H^1$	-	1.86	-	*
I_6NH-$I_6\gamma H^2$	-	1.53	0.80	*
$I_6\alpha$H-$I_6\beta$H	ZQ	ZQ	2.79	
$I_6\alpha$H-$I_6\gamma H_3$	-	-	0.88	*
$I_6\alpha$H-$I_6\gamma H^1$	-	1.21	-	*
$I_6\alpha$H-$I_6\gamma H^2$	-	-	-	
$I_6\beta$H-$I_6\gamma H_3$	ZQ	ZQ	10.2	
$I_6\beta$H-$I_6\gamma H^1$	-	4.76	0.35	*
$I_6\beta$H-$I_6\gamma H^2$	-	5.16	4.40	
$I_6\gamma H^1$-$I_6\gamma H^2$	25.7	39.0	25.6	*
I_6NH-A_7NH	-	-	0.14	
$I_6\alpha$H-A_7NH	4.51	13.1	11.9	
$I_6\beta$H-A_7NH	-	0.47	0.59	
$I_6\delta H_3$-A_7NH	-	-	0.43	
A_7NH-$A_7\alpha$H	ZQ	1.27	4.49	
A_7NH-$A_7\beta H_3$	2.72	6.98	4.80	*
A_7NH-S_8NH	-	-	0.50	
$A_7\alpha$H-S_8NH	4.75	10.5	12.2	
$A_7\beta H_3$-S_8NH	-	-	1.46	
S_8NH-$S_8\alpha$H	ZQ	1.07	3.82	
S_8NH-$S_8\beta H_2$	-	1.56	0.35	*
$S_8\alpha$H-$S_8\beta H_2$	3.78	8.97	12.5	
S_8NH-R_9NH	-	-	0.50	
$S_8\alpha$H-R_9NH	-	5.87	8.18	
R_9NH-$R_9\alpha$H	ZQ	ZQ	ZQ	
R_9NH-$R_9\beta H^1$	1.96	2.22	1.27	*
$R_9\alpha$H-$R_9\beta H^1$	ZQ	ZQ	1.11	
$R_9\alpha$H-$R_9\beta H^2$	-	ZQ	0.35	
$R_9\beta H^1$-$R_9\beta H^2$	5.28	18.2	13.5	*
$R_9\beta H^2$-$R_9\gamma H^2$	-	-	2.52	
$R_9\gamma H_2$-$R_9\delta H_2$	ZQ	ZQ	ZQ	
$R_9\delta H_2$-$R_9\varepsilon H_2$	ZQ	ZQ	ZQ	
$R_9\varepsilon$NH-R_9NH^2	-	-	-	
$R_9NH_2{}^1$-$R_9NH_2{}^2$	291	203	114	

[a] If the NOE intensity was affected by spin diffusion (SD), then an asterisk (*) is placed in the column with the heading SD.

[b] If the cross peak was dominated by zero quantum (ZQ) coherence, then ZQ was substituted for NOE intensity.

[c] If a cross peak intensity was not measureable due to overlap with other peaks, then the word overlap was substituted for NOE intensity.

[d] If an intra-residue or sequential NOE was absent, then a dash (-) was substituted for NOE intensity.

Table 10. Peptide 11 TRNOE Intensities as a Function of Mixing Time (τ_m).

	TRNOE intensity versus τ_m				
τ_m (ms)	50 ms	100ms	200ms	400 ms	SD[a]
$C_1\alpha H$-$C_1\beta H^1$	ZQ[b]	ZQ	ZQ	0.97	
$C_1\alpha H$-$C_1\beta H^2$	ZQ	ZQ	0.90	1.38	
$C_1\beta H^1$-$C_1\beta H^2$	ZQ	3.48	10.6	9.90	*
$C_1\alpha H$-D_2NH	-[c]	-	-	-	
$C_1\beta H^1$-D_2NH	-	-	-	-	
$C_1\beta H^2$-D_2NH	-	-	-	-	
D_2NH-D_2aH	-	-	-	-	
D_2NH-$D_2\beta H^1$	-	-	-	-	
D_2NH-$D_2\beta H^2$	-	-	-	-	
$D_2\alpha H$-$D_2\beta H^1$	ZQ	ZQ	0.85	1.23	
$D_2\alpha H$-$D_2\beta H^2$	ZQ	1.14	3.17	1.06	*
$D_2\beta H^1$-$D_2\beta H^2$	2.00	6.23	13.3	11.6	*
$D_2\alpha H$-$P_3\delta H^1$	-	noise[d]	1.08	2.91	
$D_2\alpha H$-$P_3\delta H^2$	-	noise	0.52	1.63	
$D_2\beta H^1$-$P_3\delta H^1$	-	-	-	0.59	
$D_2\beta H^1$-$P_3\delta H^2$	-	-	-	-	
$D_2\beta H^2$-$P_3\delta H^1$	-	-	-	1.14	
$D_2\beta H^2$-$P_3\delta H^2$	-	-	-	-	
$P_3\alpha H$-$P_3\beta H^1$	ZQ	ZQ	0.57	1.87	
$P_3\alpha H$-$P_3\beta H^2$	ZQ	ZQ	2.88	3.66	
$P_3\alpha H$-$P_3\gamma H_2$	-	-	-	1.04	
$P_3\beta H^1$-$P_3\beta H^2$	2.90	3.89	6.61	8.31	*
$P_3\beta H^1$-$P_3\gamma H_2$	ZQ	3.25	noise	4.28	
$P_3\beta H^2$-$P_3\gamma H_2$	ZQ	0.80	0.55	3.20	*
$P_3\gamma H_2$-$P_3\partial H^1$	ZQ	ZQ	1.42	2.73	
$P_3\gamma H_2$-$P_3\partial H^2$	ZQ	0.40	1.35	2.87	
$P_3\alpha H$-G_4NH	-	0.27	1.32	2.28	
G_4NH-$G_4\alpha H$	0.81	1.66	3.56	5.26	*
G_4NH-Y_5NH	0.18	1.04	0.85	0.96	*
Y_5NH-$Y_5\alpha H$	ZQ	ZQ	0.31	0.89	
Y_5NH-$Y_5\beta H_2$	-	1.36	1.69	3.36	
Y_5NH-$Y_52,6$	-	-	0.18	0.86	
$Y_5\alpha H$-$Y_5\beta H_2$	ZQ	ZQ	1.50	1.68	
$Y_5\alpha H$-$Y_52,6$	-	-	1.50	0.67	*
$Y_5\beta H_2$-$Y_52,6$	ZQ	0.55	1.95	6.53	
$Y_52,6$-$Y_53,5$	1.70	2.08	6.71	13.1	
Y_5NH-I_6NH	-	-	-	0.31	
$Y_5\alpha H$-I_6NH	1.00	1.05	3.35	4.46	
$Y_5\beta H_2$-I_6NH	-	-	-	0.33	
$Y_52,6$-I_6NH	-	-	-	0.38	

I_6NH-$I_6\alpha$H	ZQ	ZQ	0.41	0.43	*
I_6NH-$I_6\beta$H	-	0.94	1.67	0.82	*
I_6NH-$I_6\gamma H_3$	-	-	1.51	0.70	*
I_6NH-$I_6\gamma H^1$	-	-	-	-	
I_6NH-$I_6\gamma H^2$	-	-	1.43	0.22	*
$I_6\alpha$H-$I_6\beta$H	ZQ	ZQ	0.40	1.26	
$I_6\alpha$H-$I_6\gamma H_3$	-	-	-	0.34	
$I_6\alpha$H-$I_6\gamma H^1$	-	-	-	0.34	
$I_6\alpha$H-$I_6\gamma H^2$	-	-	-	0.33	
$I_6\beta$H-$I_6\gamma H_3$	ZQ	0.29	1.12	2.97	
$I_6\beta$H-$I_6\gamma H^1$	-	-	-	0.61	*
$I_6\beta$H-$I_6\gamma H^2$	-	-	1.66	0.94	*
$I_6\gamma H^1$-$I_6\gamma H^2$	2.20	3.64	7.77	7.74	*
I_6NH-G_7NH	-	0.32	0.41	0.26	*
$I_6\alpha$H-G_7NH	0.29	0.61	2.03	2.48	
$I_6\beta$H-G_7NH	-	-	-	0.32	
$I_6\delta H_3$-G_7NH	-	-	-	-	
G_7NH-$G_7\alpha$H	0.35	0.38	2.54	5.54	
G_7NH-S_8NH	-	-	-	-	
$G_7\alpha$H-S_8NH	-	-	0.40	0.69	
S_8NH-$S_8\alpha$H	ZQ	ZQ	0.24	0.15	*
S_8NH-$S_8\beta H_2$	-	-	0.50	1.11	
$S_8\alpha$H-$S_8\beta H_2$	-	ZQ	0.52	0.57	*
S_8NH-R_9NH	-	-	-	-	
$S_8\alpha$H-R_9NH	-	-	0.44	0.53	*
R_9NH-$R_9\alpha$H	ZQ	ZQ	0.12	0.21	
R_9NH-$R_9\beta H^1$	-	-	-	-	
$R_9\alpha$H-$R_9\beta H^1$	-	ZQ	0.32	-	*
$R_9\alpha$H-$R_9\beta H^2$	-	ZQ	0.60	-	*
$R_9\beta H^1$-$R_9\beta H^2$	1.75	3.91	3.63	1.13	*
$R_9\beta H^2$-$R_9\gamma H^2$	-	-	0.34	-	*
$R_9NH_2{}^1$-$R_9NH_2{}^2$	30.1	16.7	7.48	-	

[a] If the TRNOE intensity was affected by spin dissusion (SD), then an asterisk was placed in the column with the heading SD.

[b] If the cross peak was dominated by zero quantum (ZQ) coherence, then ZQ was subsitituted for TRNOE intensity.

[c] If an intra-residue or sequential TRNOE was absent, then a dash (-) was substituted for TRNOE intensity.

[d] If the intensity of a cross peak was not measureable due to overlap with t1 noise or the residual water signal, then the word, noise, was substituted for TRNOE intensity.

Table 11. D-analog TRNOE Intensities as a Function of Mixing Time (τ_m).

	TRNOE intensity versus τ_m				
τ_m (ms)	50	100	200	400	SD[a]
$C_1\alpha H$-$C_1\beta H^1$	-[b]	ZQ[c]	-	1.21	
$C_1\alpha H$-$C_1\beta H^2$	-	ZQ	-	2.30	
$C_1\beta H^1$-$C_1\beta H^2$	-	2.51	13.4	10.6	*
$C_1\alpha H$-D_2NH	-	-	-	-	
$C_1\beta H^1$-D_2NH	-	-	-	-	
$C_1\beta H^2$-D_2NH	-	-	-	-	
D_2NH-$D_2\alpha H$	-	-	-	-	
D_2NH-$D_2\beta H^1$	-	0.27	-	-	
D_2NH-$D_2\beta H^2$	-	0.56	-	-	
$D_2\alpha H$-$D_2\beta H^1$	-	1.23	noise[d]	4.64	
$D_2\alpha H$-$D_2\beta H^2$	-	1.49	noise	3.67	
$D_2\beta H^1$-$D_2\beta H^2$	1.37	8.80	25.3	9.76	*
$D_2\alpha H$-$P_3\delta H^1$	-	2.00	noise	1.17	*
$D_2\alpha H$-$P_3\delta H^2$	-	2.47	noise	0.95	*
$D_2\beta H^1$-$P_3\delta H^1$	-	-	0.41	0.74	
$D_2\beta H^1$-$P_3\delta H^2$	-	-	0.65	1.03	
$D_2\beta H^2$-$P_3\delta H^1$	-	-	1.64	-	
$D_2\beta H^2$-$P_3\delta H^2$	-	-	-	-	
$P_3\alpha H$-$P_3\beta H^1$	0.10	0.42	2.28	1.37	*
$P_3\alpha H$-$P_3\beta H^2$	0.29	1.49	5.70	3.13	*
$P_3\alpha H$-$P_3\gamma H_2$	-	0.76	0.63	1.06	
$P_3\beta H^1$-$P_3\beta H^2$	0.60	6.49	12.0	7.28	*
$P_3\beta H^1$-$P_3\gamma H_2$	-	-	0.90	2.79	
$P_3\beta H^2$-$P_3\gamma H_2$	-	0.51	1.55	2.16	
$P_3\gamma H_2$-$P_3\delta H^1$	-	1.00	3.92	3.24	*
$P_3\gamma H_2$-$P_3\delta H^2$	-	1.35	4.09	2.15	*
$P_3\alpha H$-G_4NH	-	0.76	4.82	1.89	*
G_4NH-$G_4\alpha H$	0.34	3.27	8.76	5.60	*
G_4NH-Y_5NH	-	0.62	0.77	1.06	
$G_4\alpha H$-Y_5NH	-	0.94	4.66	2.09	
Y_5NH-$Y_5\alpha H$	-	ZQ	ZQ	0.90	
Y_5NH-$Y_5\beta H_2$	-	1.40	3.74	2.71	*
Y_5NH-$Y_52,6$	-	0.38	0.34	0.72	
$Y_5\alpha H$-$Y_5\beta H_2$	ZQ	ZQ	1.12	3.28	
$Y_5\alpha H$-$Y_52,6$	-	-	-	1.40	
$Y_5\beta H_2$-$Y_52,6$	-	2.88	8.54	6.91	*
$Y_52,6$-$Y_53,5$	ZQ	3.98	15.4	11.4	*
Y_5NH-I_6NH	-	-	-	0.36	
$Y_5\alpha H$-I_6NH	0.19	1.29	5.14	2.94	*
$Y_5\beta H_2$-I_6NH	-	-	-	0.85	
$Y_52,6$-I_6NH	-	-	-	0.67	

I_6NH-$I_6\alpha H$	-	ZQ	1.84	3.26	
I_6NH-$I_6\beta H$	-	0.48	1.36	1.28	*
I_6NH-$I_6\gamma H_3$	-	0.45	-	0.13	
I_6NH-$I_6\gamma H^1$	-	0.31	-	0.43	
I_6NH-$I_6\gamma H^2$	-	-	-	0.38	
$I_6\alpha H$-$I_6\beta H$	-	ZQ	4.03	1.26	*
$I_6\alpha H$-$I_6\gamma H_3$	-	-	1.14	1.06	
$I_6\alpha H$-$I_6\gamma H^1$	-	-	-	0.30	
$I_6\alpha H$-$I_6\gamma H^2$	-	-	-	0.71	
$I_6\beta H$-$I_6\gamma H_3$	-	1.13	5.93	3.84	*
$I_6\beta H$-$I_6\gamma H^1$	-	-	-	0.70	
$I_6\beta H$-$I_6\gamma H^2$	-	-	3.11	3.22	
$I_6\gamma H^1$-$I_6\gamma H^2$	1.02	6.55	22.5	6.33	*
I_6NH-A_7NH	0.26	0.49	1.67	1.07	*
$I_6\alpha H$-A_7NH	-	1.14	5.77	2.46	*
$I_6\beta H$-A_7NH	-	0.15	0.97	0.80	*
$I_6\delta H_3$-A_7NH	-	-	-	-	
A_7NH-$A_7\alpha H$	-	ZQ	1.47	1.14	*
A_7NH-$A_7\beta H_3$	-	1.24	3.23	1.71	*
A_7NH-S_8NH	-	-	-	-	
$A_7\alpha H$-S_8NH	0.28	0.57	1.87	0.87	*
$A_7\beta H_3$-S_8NH	-	-	-	-	
S_8NH-$S_8\alpha H$	-	0.26	1.55	-	*
S_8NH-$S_8\beta H_2$	-	-	-	-	
$S_8\alpha H$-$S_8\beta H_2$	-	1.23	3.37	1.64	*
S_8NH-R_9NH	-	0.49	0.76	0.15	*
$S_8\alpha H$-R_9NH	-	-	2.84	0.88	*
R_9NH-$R_9\alpha H$	-	ZQ	1.58	0.33	*
R_9NH-$R_9\beta H^1$	-	-	0.74	-	
$R_9\alpha H$-$R_9\beta H^1$	-	ZQ	ZQ	0.71	
$R_9\alpha H$-$R_9\beta H^2$	-	-	-	1.38	
$R_9\beta H^1$-$R_9\beta H^2$	2.00	8.13	25.7	6.67	*
$R_9\beta H^1$-$R_9\varepsilon NH$	-	-	2.58	-	
$R_9\varepsilon NH$-R_9NH^2	-	ZQ	3.41	0.68	*
$R_9NH_2{}^1$-$R_9NH_2{}^2$	7.41	8.93	-	-	

[a] If the TRNOE intensity was affected by spin dissusion (SD), then an asterisk was placed in the column with the heading SD.

[b] If an intra-residue or sequential TRNOE was absent, then a dash (-) was substituted for TRNOE intensity.

[c] If the cross peak was dominated by zero quantum (ZQ) coherence, then ZQ was subsitituted for TRNOE intensity.

[d] If the intensity of a cross peak was not measureable due to overlap with t1 noise or the residual water signal, then the word, noise, was substituted for TRNOE intensity.

Table 12. L-analog TRNOE Intensities as a Function of Mixing Time (τ_m).

	TRNOE intensity versus τ_m				
τ_m (ms)	50 ms	100ms	200ms	400 ms	SD[a]
$C_1\alpha H$-$C_1\beta H^1$	-[b]	0.47	-	1.25	
$C_1\alpha H$-$C_1\beta H^2$	-	0.60	-	1.57	
$C_1\beta H^1$-$C_1\beta H^2$	3.08	11.7	27.6	21.3	*
$C_1\alpha H$-D_2NH	-	-	-	-	
$C_1\beta H^1$-D_2NH	-	-	-	-	
$C_1\beta H^2$-D_2NH	-	-	-	-	
D_2NH-$D_2\alpha H$	-	-	-	-	
D_2NH-$D_2\beta H^1$	-	-	-	-	
D_2NH-$D_2\beta H^2$	-	-	-	-	
$D_2\alpha H$-$D_2\beta H^1$	ZQ[c]	ZQ	0.85	0.50	*
$D_2\alpha H$-$D_2\beta H^2$	ZQ	ZQ	1.21	1.03	*
$D_2\beta H^1$-$D_2\beta H^2$	1.62	11.7	13.7	12.0	*
$D_2\alpha H$-$P_3\delta H^1$	-	0.24	3.03	2.89	*
$D_2\alpha H$-$P_3\delta H^2$	-	0.93	1.73	1.77	*
$D_2\beta H^1$-$P_3\delta H^1$	-	-	-	-	
$D_2\beta H^1$-$P_3\delta H^2$	-	-	0.40	-	
$D_2\beta H^2$-$P_3\delta H^1$	-	-	1.02	0.70	*
$D_2\beta H^2$-$P_3\delta H^2$	-	-	-	-	
$P_3\alpha H$-$P_3\beta H^1$	-	0.37	0.74	1.41	
$P_3\alpha H$-$P_3\beta H^2$	-	1.49	2.42	3.33	
$P_3\alpha H$-$P_3\delta H_2$	-	-	-	0.62	
$P_3\beta H^1$-$P_3\beta H^2$	0.50	6.55	8.36	8.23	*
$P_3\beta H^1$-$P_3\delta H_2$	-	ZQ	0.90	5.39	
$P_3\beta H^2$-$P_3\delta H_2$	-	1.39	1.32	2.46	
$P_3\gamma H_2$-$P_3\delta H^1$	-	0.81	2.41	1.38	*
$P_3\gamma H_2$-$P_3\delta H^2$	-	1.12	2.62	3.00	*
$P_3\alpha H$-G_4NH	-	0.73	3.08	0.99	*
G_4NH-$G_4\alpha H$	0.22	3.46	5.79	6.04	*
G_4NH-Y_5NH	-	0.45	1.45	0.92	*
Y_5NH-$Y_5\alpha H$	-	0.90	1.11	5.11	
Y_5NH-$Y_5\beta H_2$	-	1.75	3.25	3.88	
Y_5NH-$Y_52,6$	-	0.56	0.96	0.61	*
$Y_5\alpha H$-$Y_5\beta H_2$	-	1.81	2.33	4.20	
$Y_5\alpha H$-$Y_52,6$	-	-	0.78	1.40	
$Y_5\beta H_2$-$Y_52,6$	-	2.24	5.36	6.24	*
$Y_52,6$-$Y_53,5$	1.25	6.74	10.3	10.7	*
Y_5NH-I_6NH	-	-	-	-	
$Y_5\alpha H$-I_6NH	-	2.47	4.00	3.24	*
$Y_5\beta H_2$-I_6NH	-	-	-	0.26	
$Y_52,6$-I_6NH	-	-	-	0.50	
I_6NH-$I_6\alpha H$	-	ZQ	0.92	0.75	*

I_6NH-$I_6\beta H$	-	0.75	1.38	1.34	*
I_6NH-$I_6\gamma H_3$	-	-	0.95	-	
I_6NH-$I_6\gamma H^1$	-	0.33	-	-	
I_6NH-$I_6\gamma H^2$	-	0.32	0.24	-	
$I_6\alpha H$-$I_6\beta H$	-	ZQ	ZQ	1.06	
$I_6\alpha H$-$I_6\gamma H_3$	-	ZQ	0.53	1.52	
$I_6\alpha H$-$I_6\gamma H^1$	-	-	0.17	-	
$I_6\alpha H$-$I_6\gamma H^2$	-	-	0.15	-	
$I_6\beta H$-$I_6\gamma H_3$	-	-	-	-	
$I_6\beta H$-$I_6\gamma H^1$	-	-	-	0.49	
$I_6\beta H$-$I_6\gamma H^2$	-	-	2.21	1.59	*
$I_6\gamma H^1$-$I_6\gamma H^2$	0.33	5.67	7.79	5.90	*
I_6NH-A_7NH	-	-	1.02	0.30	*
$I_6\alpha H$-A_7NH	-	1.44	3.71	4.37	
$I_6\beta H$-A_7NH	-	-	1.40	0.83	*
$I_6\delta H_3$-A_7NH	-	-	0.70	0.50	*
A_7NH-$A_7\alpha H$	-	0.15	0.86	1.09	*
A_7NH-$A_7\beta H_3$	-	0.60	2.27	2.00	*
A_7NH-S_8NH	-	-	-	-	
$A_7\alpha H$-S_8NH	-	1.34	2.15	2.38	*
$A_7\beta H_3$-S_8NH	-	-	0.52	0.89	
S_8NH-$S_8\alpha H$	-	ZQ	1.17	0.34	*
S_8NH-$S_8\beta H_2$	-	-	1.04	1.03	*
$S_8\alpha H$-$S_8\beta H_2$	-	0.79	1.96	0.71	*
S_8NH-R_9NH	-	-	-	-	
$S_8\alpha H$-R_9NH	-	0.14	1.73	0.97	*
R_9NH-$R_9\alpha H$	-	ZQ	-	-	
R_9NH-$R_9\beta H^1$	-	-	1.40	0.48	*
$R_9\alpha H$-$R_9\beta H^1$	-	-	0.26	0.30	
$R_9\alpha H$-$R_9\beta H^2$	-	-	0.17	0.63	
$R_9\beta H^1$-$R_9\beta H^2$	0.57	3.39	4.59	3.85	*
$R_9\beta H^2$-$R_9\gamma H^2$	-	-	0.39	1.03	
$R_9NH_2{}^1$-$R_9NH_2{}^2$	6.22	15.9	5.82	-	

[a] If the TRNOE intensity was affected by spin dissusion (SD), then an asterisk was placed in the column with the heading SD.

[b] If an intra-residue or sequential TRNOE was absent, then a dash (-) was substituted for TRNOE intensity.

[c] If the cross peak was dominated by zero quantum (ZQ) coherence, then ZQ was subsitituted for TRNOE intensity.

Figure 40. Peptide 11 Ile_6NH-Gly_7NH NOE and TRNOE Intensity as a Function of Mixing Time (τ_m).

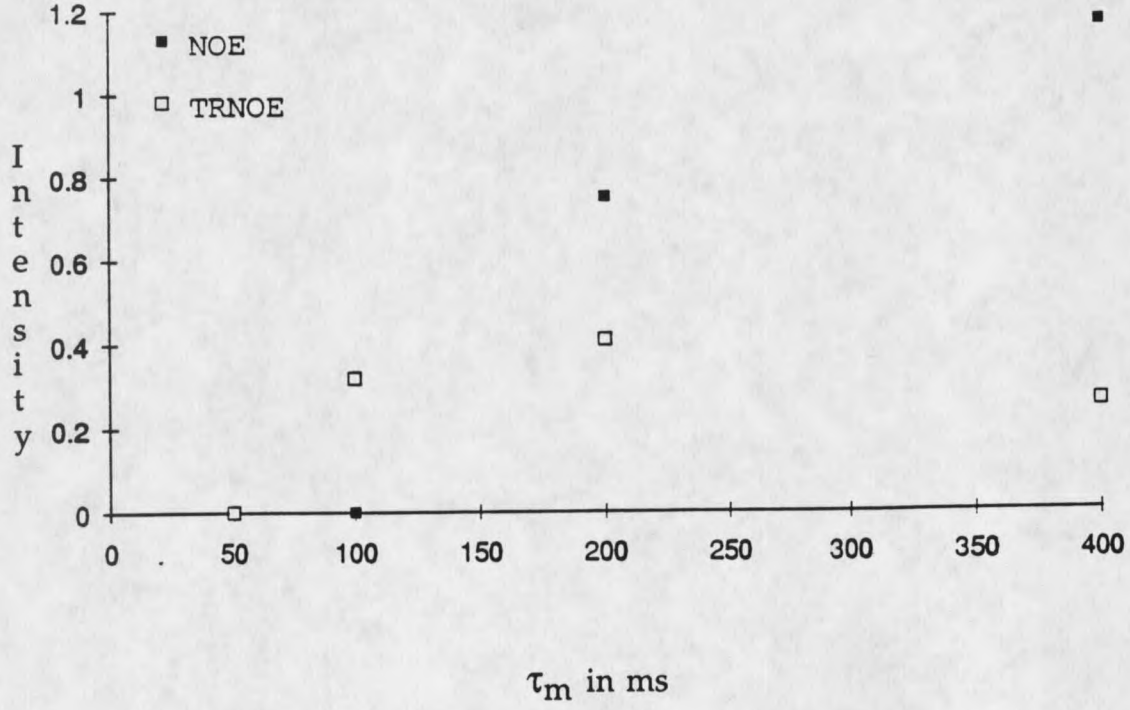

Figure 41. D-analog Ala7αH-Ser8NH NOE and TRNOE Intensity as a Function of Mixing Time (τ_m).

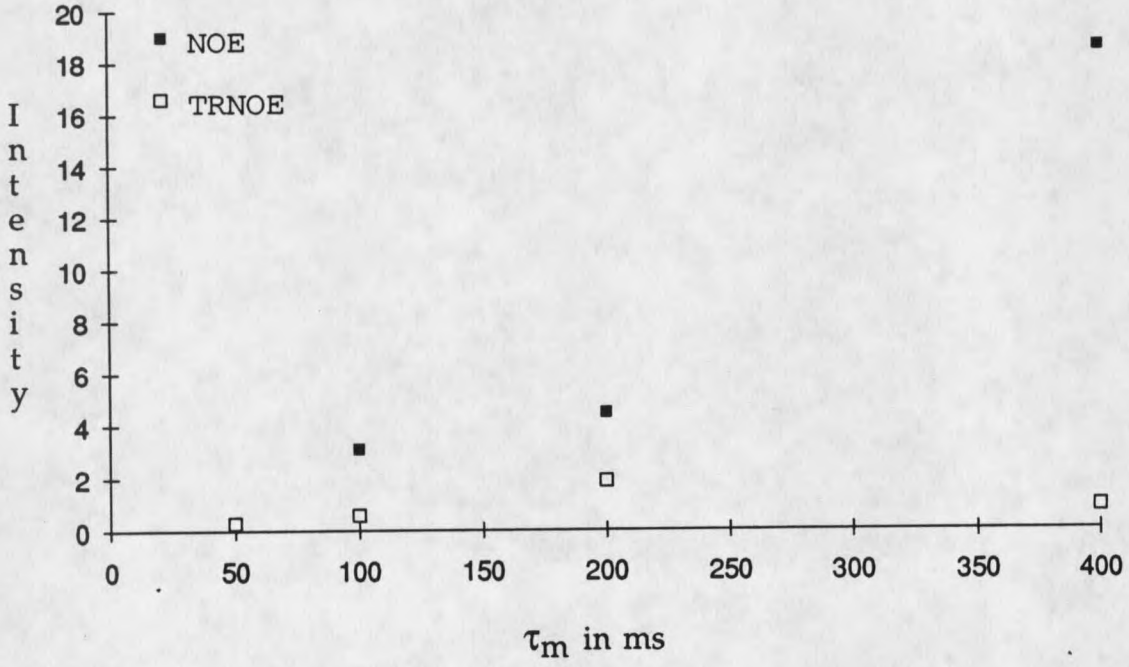

Figure 42. L-analog Ser8αH-Arg9NH NOE and TRNOE Intensity as a Function of Mixing Time (τ_m).

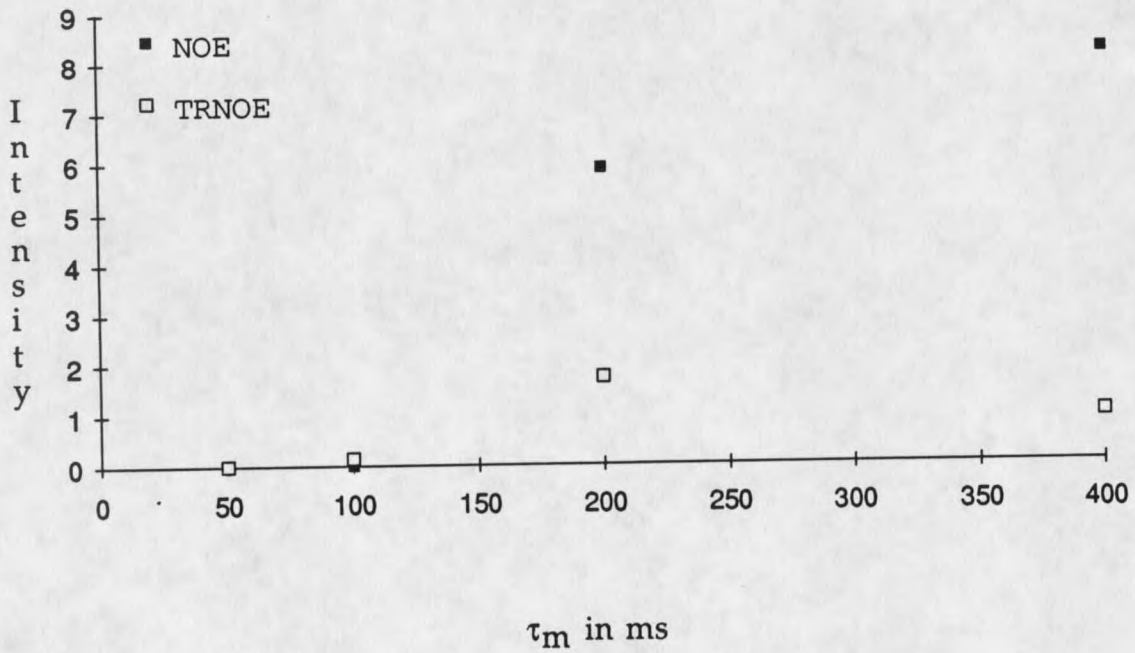

Relative NOE and TRNOE Intensities Differed Considerably

The NOE connectivity of peptide 11, the d-analog, and the l-analog free in solution was typical of that of short, linear peptides. The free peptide NOE intensities were averaged over all compact conformers. Because multiple conformers exist, all sequential inter-residue NOEs are exhibited. In contrast, NOE intensities in the presence of receptor (ie. TRNOE intensities) are expected not to be an average, but rather to be dominated by the bound conformation of the peptide (Clore and Gronenborn, 1983, Campbell and Sykes, 1991b). Consequently, if the inter-residue TRNOE intensities of peptide 11 and the d and l-analogs differ from their corresponding NOE intensities, then this would imply that the conformation of the peptide observed by TRNOESY is in fact the bound conformation.

The relative inter-residue NOE and TRNOE intensities of peptide 11 and the d and l-analogs differed significantly. The differences for each peptide are presented in tables 12-14. Prior to performing this comparison it was necessary to classify the NOE and TRNOE intensities as strong, medium, or weak based on comparisons of NOESY and TRNOESY experiments performed with different mixing times. If a NOE was first detectable at a t_m of 100, 200, or 400 ms, then it was classified as strong, medium, or weak, respectively. If a TRNOE was first detectable at a τ_m of 50, 100, or 200 ms, then it was classified as strong, medium, or weak, respectively.

The inter-residue NOEs of the free peptide are evenly distributed. Essentially every sequential inter-residue NOE is present. In contrast, several sequential inter-residue TRNOEs are either weak or absent. Absence of an inter-residue TRNOE can only result from the peptide adopting an inflexible

compact conformation. The fact that the patterns of TRNOESY intensity differ significantly from the patterns of NOESY intensity suggest that the data of the TRNOESY spectra is representative of the bound conformation. The secondary structures implied by the observed pattern of inter-residue sequential TRNOESY connectivities are discussed below. It is reasonable to assume that binding to the receptor forces peptide 11, the d-analog, and the l-analog into one conformation. However, it is possible that the peptides could bind the receptor in more than one conformation. Further study utilizing techniques such as spectral back-calculation is necessary in order to try and understand the precision of the bound conformation.

J^3Coupled Protons Exhibited Zero Quantum Coherence

At short mixing times (τ_m < 200 ms) a significant fraction of J^3 coupled protons displayed zero-quantum (ZQ) coherence. ZQ coherence is the through bond magnetization transfer pathway that can be recognized by the anti-phase multiplets of COrrelation SpectroscopY (COSY). ZQ coherence was reduced but still persisted even when τ_m was randomly varied by 20 ms for all mixing times (Macura *et al.*, 1981). The X_iNH-$X_i\alpha H$ and $X_i\alpha H$-$X_i\beta H$ were particularly prone to possessing ZQ coherence at short τ_m. Because ZQ coherence is a through bond exchange of magnetization, the resultant cross peaks convey no information regarding r_{ij}.

In addition to X_iNH-$X_i\alpha H$ and $X_i\alpha H$-$X_i\beta H$ cross peaks, the side chain proton cross peaks of P_3 and I_6 were ZQ dominated through τ_m = 200 ms. Interestingly, arginine did not behave as these other long side chains. The arginine side chain protons exhibited neither through bond coherence nor

Table 13. The Effect of Receptor Binding on Peptide 11 Inter-residue NOE

	Free	Effect	Bound
$C_1\alpha H$-D_2NH	S	↓	0
$C_1\beta H_2$-D_2NH	0	=	0
$D_2\alpha H$-$P_3\delta H^1$	S	↓	M
$D_2\alpha H$-$P_3\delta H^2$	S	↓	M
$D_2\beta H^1$-$P_3\delta H^1$	0	=	0
$D_2\beta H^1$-$P_3\delta H^2$	0	=	0
$D_2\beta H^2$-$P_3\delta H^1$	W	=	W
$D_2\beta H^2$-$P_3\delta H^2$	0	=	0
$P_3\alpha H$-G_4NH	M	=	M
G_4NH-Y_5NH	M	↑	S
$G_4\alpha H$-Y_5NH	S	↓	M
Y_5NH-I_6NH	M	↓	0
$Y_5\alpha H$-I_6NH	S	=	S
$Y_5\beta H_2$-I_6NH	M	↓	0
$Y_52,6$-I_6NH	M	↓	0
I_6NH-G_7NH	M	=	M
I_6aH-G_7NH	S	=	S
$I_6\beta H$-G_7NH	M	↓	0
$I_6\delta H_3$-G_7NH	W	↓	0
G_7NH-S_8NH	M	↓	0
$G_7\alpha H$-S_8NH	S	↓	W
S_8NH-R_9NH	S	↓	0
$S_8\alpha H$-R_9NH	S	↓	W

Table 14. The Effect of Receptor Binding on D-analog Inter-residue NOE Intensity.

	Free	Effect	Bound
$C_1\alpha H$-D_2NH	S	↓	0
$C_1\beta H_2$-D_2NH	0	=	0
$D_2\alpha H$-$P_3\delta H^1$	S	↓	M
$D_2\alpha H$-$P_3\delta H^2$	S	↓	M
$D_2\beta H^1$-$P_3\delta H^1$	0	↑	W
$D_2\beta H^1$-$P_3\delta H^2$	0	↑	W
$D_2\beta H^2$-$P_3\delta H^1$	M	↓	W
$D_2\beta H^2$-$P_3\delta H^2$	0	=	0
$P_3\alpha H$-G_4NH	S	↓	M
G_4NH-Y_5NH	S	=	S
$G_4\alpha H$-Y_5NH	S	↓	M
Y_5NH-I_6NH	M	↓	0
$Y_5\alpha H$-I_6NH	S	=	S
$Y_5\beta H_2$-I_6NH	M	↓	0
$Y_52,6$-I_6NH	0	=	0
I_6NH-A_7NH	S	=	S
$I_6\alpha H$-A_7NH	S	=	M
$I_6\beta H$-A_7NH	W	↑	M
$I_6\delta H_3$-A_7NH	M	↓	0
A_7NH-S_8NH	W	↓	0
$A_7\alpha H$-S_8NH	S	=	S
$A_7\beta H_3$-S_8NH	M	↓	0
S_8NH-R_9NH	M	=	M
$S_8\alpha H$-R_9NH	S	↓	W

Table 15. The Effect of Receptor Binding on L-analog Inter-residue NOE Intensity.

	Free	Effect	Bound
$C_1\alpha H$-D_2NH	S	↓	0
$C_1\beta H_2$-D_2NH	0	=	0
$D_2\alpha H$-$P_3\delta H^1$	S	↓	M
$D_2\alpha H$-$P_3\delta H^2$	S	↓	M
$D_2\beta H^1$-$P_3\delta H^1$	0	=	0
$D_2\beta H^1$-$P_3\delta H^2$	0	↑	W
$D_2\beta H^2$-$P_3\delta H^1$	M	↓	W
$D_2\beta H^2$-$P_3\delta H^2$	0	=	0
$P_3\alpha H$-G_4NH	S	↓	M
G_4NH-Y_5NH	S	↓	M
$G_4\alpha H$-Y_5NH	S		
Y_5NH-I_6NH	0	=	0
$Y_5\alpha H$-I_6NH	S	↓	M
$Y_5\beta H_2$-I_6NH	0	=	0
$Y_52,6$-I_6NH	0	=	0
I_6NH-A_7NH	W	=	W
$I_6\alpha H$-A_7NH	S	↓	M
$I_6\beta H$-A_7NH	M	↓	W
$I_6\delta H_3$-A_7NH	W	=	W
A_7NH-S_8NH	W	↓	0
$A_7\alpha H$-S_8NH	S	↓	M
$A_7\beta H_3$-S_8NH	W	=	W
S_8NH-R_9NH	W	↓	0
$S_8\alpha H$-R_9NH	S	↓	W

through space NOE cross relaxation. Arginine side chain cross peaks were conspicuously absent from spectra of both the free and bound peptides. The fact that receptor binding did not generate arginine side chain TRNOEs suggests that in the bound conformation, the Arg_9 side chain is exposed to the solvent. The fact that the Arg_9 side chain NH_2 protons are observed to exchange with the solvent (Tables 6-11) is additional evidence that the Arg_9 side chain is exposed to the solvent when the peptides are both free and bound.

Conformations of the Peptides in the Presence of Receptor

The different forms of protein secondary structure (ie. a helices, b sheets, and turns) exhibit distinct patterns of NOE connectivity (Billeter et al., 1982, Wüthrich, 1986). In the presence of receptor peptide 11, the d-analog, and the l-analog, exhibit patterns of NOE connectivity consistent with the formation of distinct secondary structures.

DPGY of All Three Peptides Forms a Type II β Turn in the Receptor Bound Conformation

A type II β turn is indicated by the presence of strong $d_{aN}(i,i+1)$, $d_{Na}(i+1,i+1)$, and $d_{NN}(i+1,i+2)$ NOEs and the absence of a $d_{NN}(i,i+1)$ NOE (Billeter et al., 1982). Optimally, the $d_{aN}(i,i+2)$ will also be present, though detection of this NOE will be more difficult as the distance between these two protons in a type II turn is 3.3 Å.

In peptide 11 and the d and l-analogs, the TRNOEs $P_3\alpha H$-G_4NH, $G_4\alpha H$-G_4NH, and G_4NH-Y_5NH, are strong for all mixing times including τ_m = 50 ms. This suggests that DPGY of all three peptides forms a type II β turn. The

existence of this type of turn would be virtually confirmed if the absence of the $d_{NN}(i,i+1)$ TRNOE and the presence of the $d_{aN}(i,i+2)$ TRNOE could be detected. However, Pro_3 lacks an amide proton so the $P_3\alpha H$-G_4NH TRNOE must be absent. The $P_3\alpha H$-Y_5NH TRNOE, which was expected to be difficult to detect, was not observed.

If DPGY formed a type II β turn, then the amide proton of Tyr_5 would be hydrogen bonded to the backbone carbonyl of Asp_2. The chemical shift of the hydrogen bonded amide proton of a type II β turns is approximately 8 ppm (Pease, 1979, Gierasch, 1981, reviewed by Rose *et al.*, 1985). In peptide 11, the d-analog, and the l-analog the chemical shifts of Tyr_5NH 8.05, 7.99, and 8.04 ppm, respectively. These values all represent a significant shift of 0.13-0.19 ppm upfield of the tyrosine amide random coil chemical shift. The upfield chemical shift of Tyr_5NH combined with the pattern of Pro_3, Gly_4, and Tyr_5 TRNOESYs observed strongly suggest the presence of a DPGY type II β turn. The formation of such a turn would be in accordance with the predictions of Chou and Fasman (1977) and the observations of Dyson *et al.* (1988a) discussed in Chapter 3.

YIGSR of Peptide 11 Forms a Bend in the Receptor Bound Conformation

Peptide 11 exhibits strong Y_5aH-I_6NH, $d_{aN}(i,i+1)$, I_6NH-I_6aH, $d_{Na}(i,i)$, I_6NH-G_7NH, $d_{NN}(i+1,i+2)$ TRNOEs, and no Y_5NH-I_6NH $d_{NN}(i,i+1)$ TRNOEs (Table 12). This sequential TRNOE pattern suggests the presence of a DYIG type II b turn, which is supported by the Gly_7 chemical shift value of 7.99 ppm. The only sequential connectivity in the GSR region of peptide 11 are medium intensity G_7aH-S_8NH and S_8aH-R_9NH TRNOEs. The absence of other forms

of sequential connectivity suggests that GSR adopts an extended conformation (Billeter *et al.*, 1982). TRNOESY of peptide 11 in the presence of the receptor suggests that the YIGSR region forms an open bend consisting of GYIG turn followed by the more extended conformation of the GSR region.

YIASR of the D-analog Forms a Bend

As was the case with peptide 11, the $Y_5\alpha H$-I_6NH, I_6NH-$I_6\alpha H$, and I_6NH-G_7NH TRNOEs are all medium or strong, and the Y_5NH-I_6NH TRNOE is absent from the d-analog in the presence of receptor (Table 13). This pattern of NOE connectivity is consistent with a type II β turn. However, the chemical shift of Ala_7 is 8.47 ppm, which is not consistent with a tight turn stabilizing hydrogen bond between the carbonyl of Gly_4 and the amide of Ala_7. The backbone conformation consistent with both the pattern of TRNOEs and the Ala_7NH chemical shift value of 8.47 ppm is a loose turn, or in other words, a bend.

YIASR of the L-analog is in an Extended Conformation

The pattern of sequential backbone TRNOEs of the l-analog indicates that its YIASR conformation differs significantly from the conformation of peptide 11 and the d-analog. Unlike peptide 11 and the d-analog which exhibit distinct groupings of $d_{NN}(i,i+1)$ and $d_{\alpha N}(i,i+1)$ TRNOEs, the l-analog exhibits no medium or strong $d_{NN}(i,i+1)$ TRNOEs and consistently medium $d_{aN}(i,i+1)$ TRNOEs for the length of the YIASR region. In addition, the l-analog exhibits I_6bH-A_7NH, $I_6\delta H_3$-A_7NH, and $A_7\beta H_3$-S_8NH TRNOEs. The d-analog does not exhibit any of these TRNOEs, and peptide 11 exhibited only a weak $I_6\beta H$-G_7NH TRNOE. This sequential backbone NOE pattern is

indicative of an extended conformation (Billeter *et al.*, 1982, Wüthrich, 1986).

Generation of Candidate Receptor Bound Conformations by Molecular Dynamics

TRNOEs were converted into ranges of inter-proton distance and incorporated into molecular dynamics (MD) simulations as described in Chapter 2: Materials and Methods. Conformations of peptide 11, the d-analog, and the l-analog are presented in figures 43-44, 45-46, and 47-48, respectively. All three peptides exhibited similar DPGY type II b turn. Peptide 11 and the d-analog possessed similar YIXS bends, while the YIASR region of the l-analog possessed a more extended structure.

The DPGY turn and the YIXSR bend indicated by their patterns of NOE connectivity are clearly present in the conformations of peptide 11 and the d-analog. However, the relative positions of these structures is not certain. While the bends of peptide 11 were consistently found to orient themselves to yield an "S" shaped molecule (Figs. 43-44), the d-analog bends were observed to form a "W" (Fig. 45) as well as an "S" shaped molecule (Fig. 46). The "S" shape favored by peptide 11 is most likely the bound conformation; however, the instances of "W" shaped d-analog make structural assignment less than certain. It is possible that the "S" and "W" shaped conformations that both peptide 11 and the d-analog adopt in the course of molecular dynamics simulations possess biological activity.

Constrained molecular dynamics of the l-analog readily generated a DPGY type II b turn and the extended YIASR conformation that was indicated by its sequential NOE connectivity (Figs. 47-48). The similarity in DPGY regions of the three molecules again supports the notion that the residual

Figure 43. Peptide 11 Bound to the Receptor.

The conformation adopted by peptide 11 after 75.3 ps of molecular dynamics constrained by TRNOESY derived distance constraints.

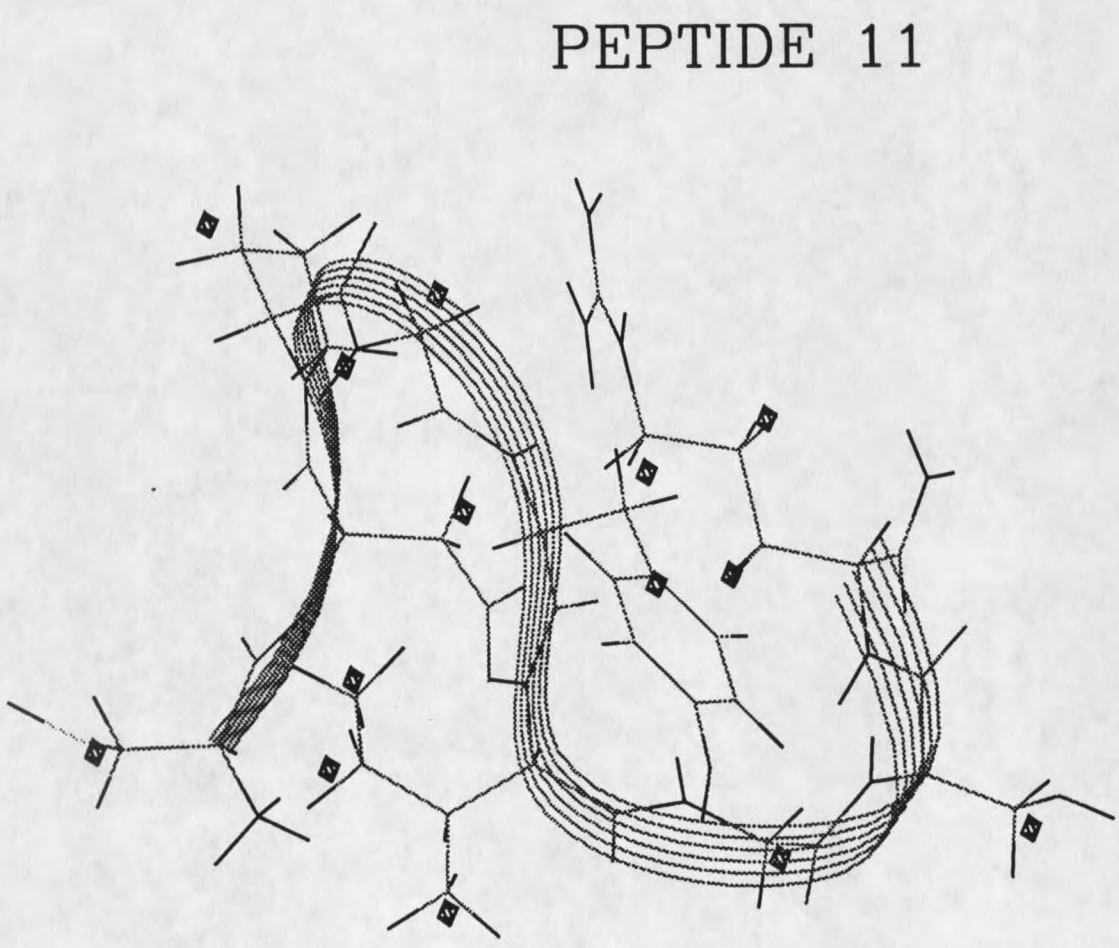

Figure 44. Peptide 11 Bound to the Receptor.

The conformation adopted by peptide 11 after 97.1 ps of molecular dynamics constrained by TRNOESY derived distance constraints.

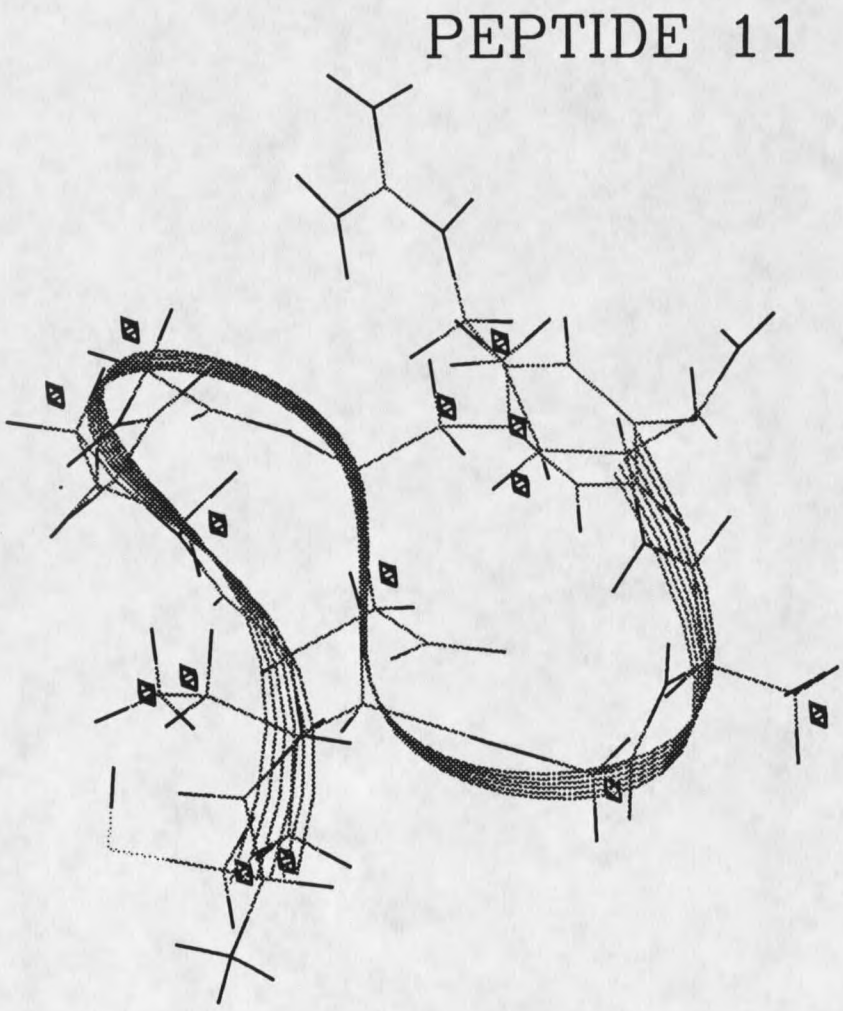

Figure 45. The D-analog Bound to the Receptor.

The conformation adopted by the d-analog after 28.7 ps of molecular dynamics constrained by TRNOESY derived distance constraints.

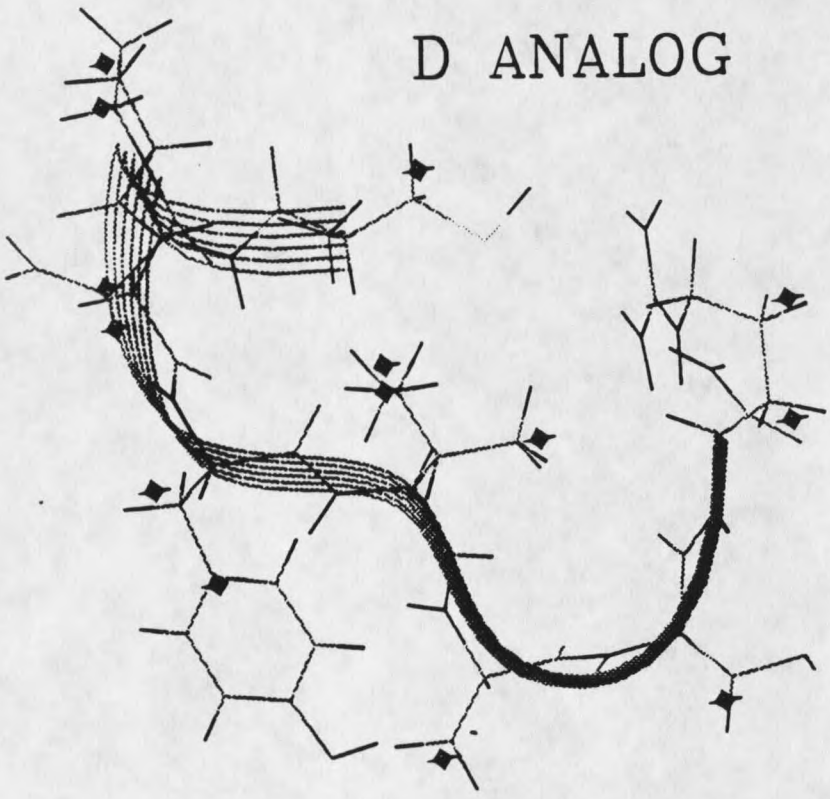

Figure 46. The D-analog Bound to the Receptor.

The conformation adopted by the d-analog after 85.1 ps of molecular dynamics constrained by TRNOESY derived distance constraints.

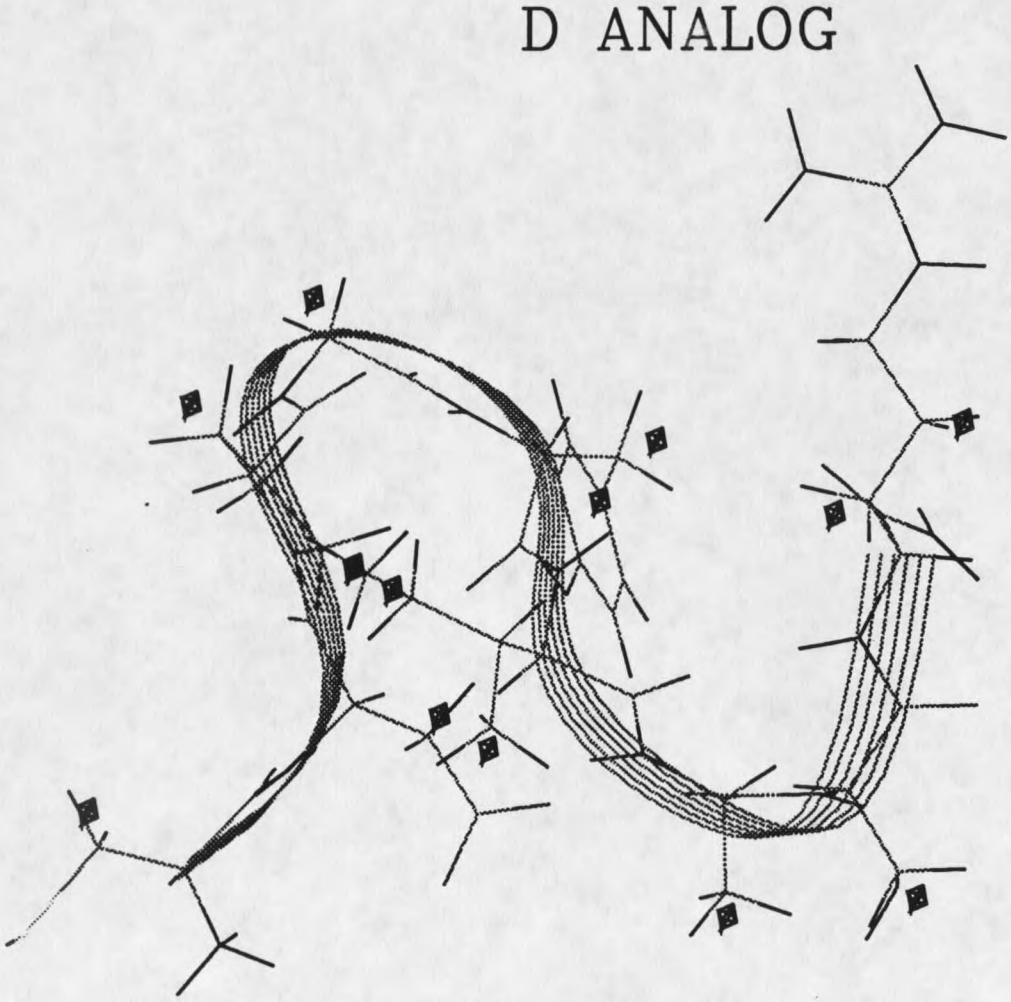

Figure 47. The L-analog Free Bound to the Receptor.

The conformation adopted by the l-analog after 52.9 ps of molecular dynamics constrained by TRNOESY derived distance constraints.

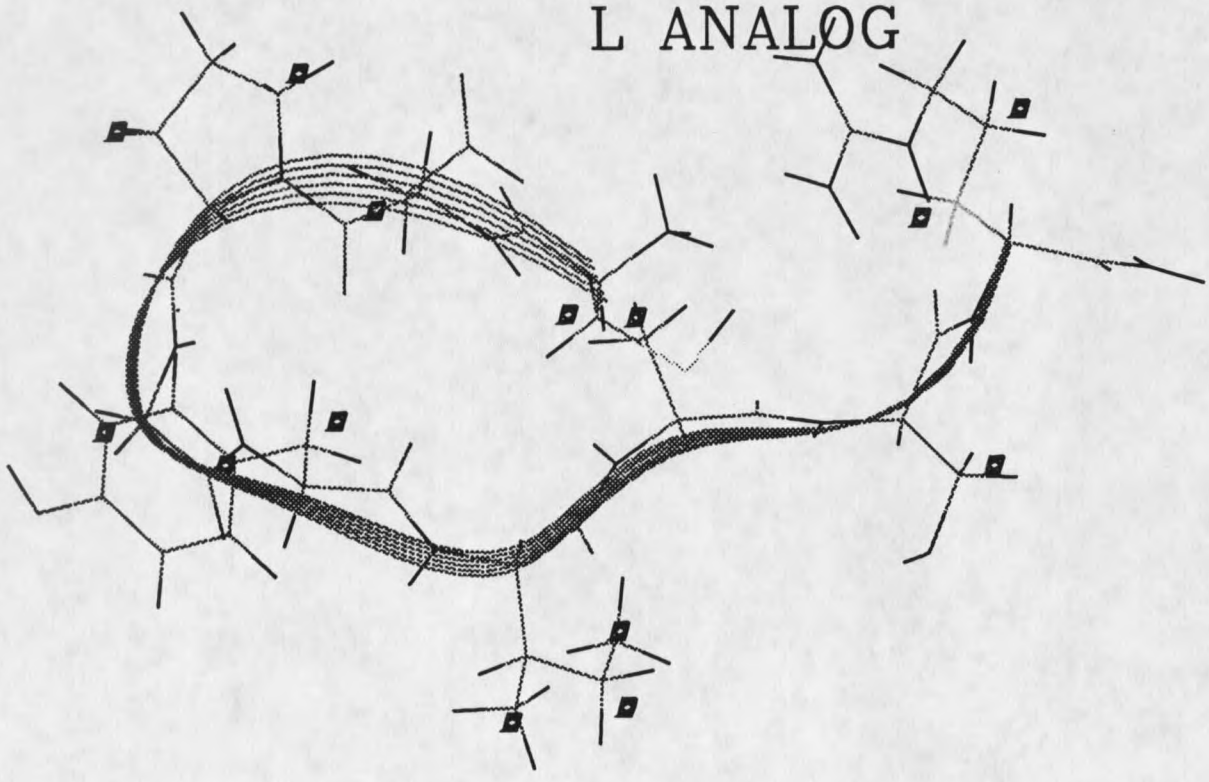

Figure 48. The L-analog Bound to the Receptor.

The conformation adopted by the l-analog after 81.4 ps of molecular dynamics constrained by TRNOESY derived distance constraints.

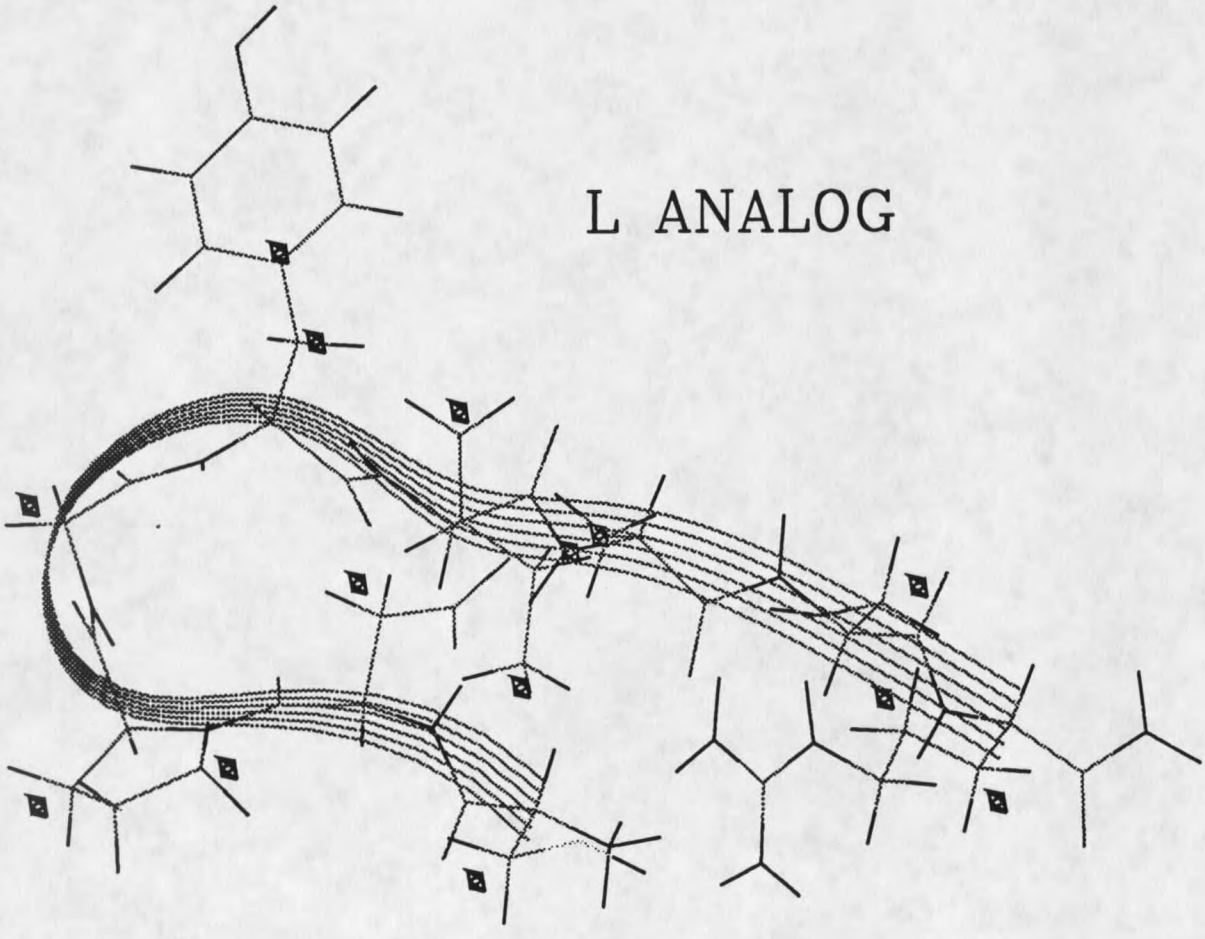

biological activity of the l-analog results from its ability to form a type II β turn in this region. The correspondence of the candidate bound structures of peptide 11, the d-analog, and the l-analog is discussed in the following chapter.

CHAPTER 5

DISCUSSION

Candidates for the biologically active conformation of peptide 11, the d-alanine$_7$ analog (d-analog), and the l-alanine$_7$ analog (l-analog) have been generated by using a combination of single amino acid substitution, NMR spectroscopy, and molecular dynamics simulations. The conformations generated by molecular dynamics simulations are consistent with the NMR data; however, the agreement between the structure of the peptides and their known function has yet to be fully discussed. The sequence of peptide 11 has been manipulated in many ways. If the conformations presented previously are to be considered representative of the biological active conformation of peptide 11, then these conformations must be consistent with and explain the activity or inactivity that results from each change in the sequence of peptide 11.

The Activity of the D-analog and Peptide 11 are Equal

Substitution of d-alanine for Gly$_7$ of peptide 11 results in a peptide which is equal in activity to the native peptide at high concentrations (Fig. 2). Molecular dynamics constrained by NOESY and TRNOESY derived inter-proton distance constraints generated structures for the d-analog and peptide 11 which exhibited very similar bends in the DPGY and YIXSR regions of the two peptides. The equal activity of these two peptides is thought to result

from their ability to adopt very similar conformations.

YIXSR Conformations of Peptide 11 and the D-analog With Good NOE Agreement Match the Predictions of Brandt-Rauf *et al.*

The ϕ and ψ angles of the YIXSR regions of the receptor bound conformations of peptide 11 and the d-analog presented in figures 36 and 38, respectively, agree well with the ϕ,ψ values predicted by Brandt-Rauf *et al.* and differ significantly from the values predicted by McKelvey *et al.*, as shown in Table 15. Brandt-Rauf et al. predicted that Gly_7 of peptide 11 possessed a conformation corresponding to the D* region of a Zimmerman plot. In the peptide structures proposed in this work, the conformations of the pivotal Gly_7 and Ala_7 of the more active peptide 11 and d-analog agree exactly with the prediction of the conformation of this residue by Brandt-Rauf *et al.* in that their conformations correspond to the D* region of a Zimmerman plot (Table 15).

Table 16. Predictions of YIXSR Conformation.

	Conformation versus Amino Acid Residue.				
	Y	I	X	S	R
Peptide 11	C	D	D*	D	D
d-analog	F	C	D*	C	A
Brandt-Rauf	C	D	D*	D	D
McKelvey	CA	A	A	F	C/E

As Brandt-Rauf *et al.* successfully predicted the type of turn found in the receptor bound conformation of the YIGSR region of peptide 11, it is

possible that their predictions concerning other aspects of the peptide structure are correct as well. Brandt-Rauf *et al.* predicted that the arginine side chain of YIGSR (Arg_9 in peptide 11 and the d and l-analogs) stabilized the YIGSR bend by forming hydrogen bonds with the backbone carbonyl of tyrosine (Tyr_5 in peptide 11 and the d and l-analogs). As arginines frequently act as stabilizing elements in proteins (Mrabet *et al.*, 1992), it is quite possible that this prediction is valid. The role played by Arg_9 in peptide 11 will be discussed below.

YIGSR-$NH_2$and YI(dA)SR-NH_2 are Active, YI(lA)SR-NH_2 is Inactive

Substitution of l-alanine for the glycine of YIGSR results in a peptide, YI(lA)SR-NH_2, that is unable to inhibit the migration of metastatic cells *in vitro* (Ostheimer et al., 1992). Structures generated for the l-analog, CDPGYI(lA)SR-NH_2 (Figs. 30-31 and 47-48), suggest that the inactivity of YI(lA)SR-NH_2 results from its inability to form the same YIXSR bend as either peptide 11 or YI(dA)SR-NH_2.

The disruption of a glycine centered bend has been previously reported. In the first 20 amino acids of the Aα chain of human fibrinogen there is a type II β turn about Gly_{12} (Ni *et al.*, 1989a,b,c). In order for this turn to form, the glycine ϕ angle must be in the range: $0^\circ \leq \phi \leq 180^\circ$. This range corresponds to quadrants I and IV of a Ramachandran plot and/or the *-ed quadrants of a Zimmerman plot. In a naturally occurring mutation, which results in a blood clotting disorder, the Gly_{12} is replaced by a valine (Ménaché, 1983). Valine substitution reduces the biological activity of the peptide, because its bulky side chain sterically prevents the formation of the type II β turn, which

Ni *et al.*, 1989c found to be present in the native structure. The substitution of l-alanine for glycine and consequent disruption of the YIXSR-NH_2 bend is completely analogous to the valine substitution in the fibrinogen peptide studied by Ni *et al.*

The l-analog, CDPGYI(lA)SR-NH_2, Possesses Residual Activity

Unlike YI(lA)SR-NH_2, which is completely inactive, the l-analog of the full 9 residue native peptide 11 is approximately 50% as active as native peptide 11 (Fig. 2). The reduction in activity appears to result from the inability of the l-analog to adopt the same bend in its YIASR as the active peptide 11. The residual activity of the l-analog is believed to result from the ability of the DPGY region of the molecule to form the same type II β turn as peptide 11 (Figs. 34-35 and 43-44) and the d-analog (Figs. 28-29 and 45-46) in that region.

Cys_1 is Required for the CDPG Region of Peptide 11 to Effectively Bind the Receptor

Removal of Cys_1 from CDPGYIGSR yields a less active peptide (Graf et al., 1987b). Interestingly, the peptides DPGYIGSR and YIGSR are equally active in promoting cell attachment and in competing with the entire laminin molecule for the 67 kDa high-affinity lamin receptor (Graf et al., 1987b). Apparently, the DPG residues of the longer peptide do not increase its activity indicating that Cys_1 is necessary for the binding of the CDPG region of peptide 11 to the receptor. Additional evidence for the requirement of Cys_1 comes from the substitution of serine for the Cys_1 of peptide 11 that demonstrates the peptide, SDPGYIGSR-NH_2, to be incapable of inhibiting the

migration of metastatic cells *in vitro* (Fig. 49) (J.R. Starkey, unpublished data). The sensitivity of peptide 11 to the serine for Cys_1 substitution suggests that binding of the receptor to peptide 11 involves Cys_1 directly.

TRNOESY and molecular dynamics of peptide 11, the d-analog, and the l-analog suggest the presence of a DPGY type II β turn in the bound conformation of peptide 11 and the d and l-analogs. It is possible that this turn is crucial to the correct presentation of Cys_1 to the receptor. The performance of two experiments could confirm whether or not the role of the turn is to present Cys_1 to the receptor. The biological activity of the peptide, DPGYI(lA)SR-NH_2, could be assayed. If the presentation of Cys_1 is essential, then this peptide should be completely inactive. In addition, the biological activity of the peptide, CDP(lA)YI(lA)SR-NH_2, could be assayed. If a type II β turn is necessary for the correct presentation of Cys_1 to the receptor, then this peptide should be completely inactive as well.

Unfortunately, the ambiguity concerning the presence of inter-peptide di-sulfide bonds in the NMR samples necessitates that arguements concerning the biological role of Cys_1 be considered speculative. Before conclusions can be drawn considering the biological role of Cys_1 in peptide 11 both the biological assays and the NMR spectroscopy of peptide 11 need to be performed in the presence of a reducing agent in order to guarantee that it is the properties of the monomer that are being observed.

Arg$_9$Stabilizes the YIXSR Bend

Several manipulations of the peptide 11 and YIGSR sequences indicate the importance of R_9 to their biological activity. In YIGSR, the substitution of

Figure 49. SDPGYIGSR-NH_2 is Inactive.

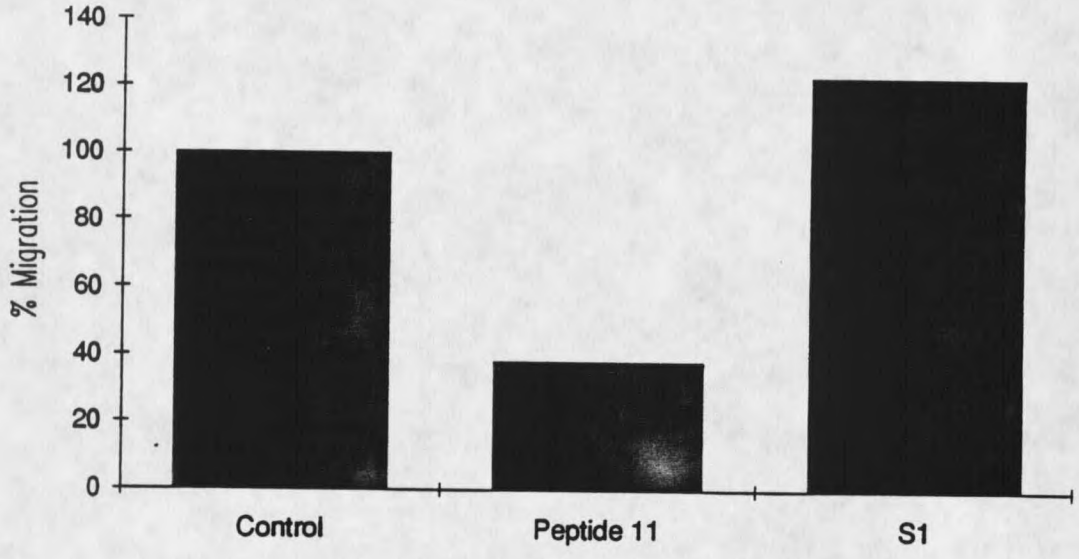

glutamic acid for arginine yields an inactivate peptide, YIGSE (Graf *et al.*, 1987b). Interestingly, the peptide YIGSK, in which the similar amino acid lysine has been substituted for arginine, is completely inactive as well.

Comparison of the NOESY and TRNOESY spectra of peptide 11 and the d and l-analogs indicates that the conformational properties of Arg_9 do not differ significantly between the free and the bound states of the peptides (Chapter 4). The similarity of free and bound states implies that binding of the YIXSR regions of peptide 11 and the d-analog does not bring Arg_9 into direct contact with the receptor.

If Arg_9 did not interact directly with the receptor, then it would be free to perform the stabilizing role (Mrabet *et al.*, 1992) proposed by Brandt-Rauf *et al.* Brandt-Rauf *et al.* suggested that the arginine side stabilized the YIGSR bend by hydrogen bonding to the backbone carbonyl of the tyrosine. YIGSE and YIGSK are less active because they lack the stabilizing arginine. It is interesting that the substitution of the long, positively charged side chain of lysine for arginine results in an inactive peptide. Apparently, multiple polar contacts, which only arginine can form, are necessary to stabilize the bend.

If the role of Arg_9 was to stabilize the YIXSR bend, then the greater activity that results from amidinating the carboxy terminus might be explained as well. Leaving the carboxy terminus of peptide 11 unprotected, ie. CDPGYIGSR, results in a negative charge in proximal to the positively charged side chain of Arg_9. The presence of this charge could readily draw the Arg_9 side chain away from the YIGSR bend. Without the Arg_9 side chain in a position to stabilize the YIGSR bend, the peptide would adopt its biologically active conformation less frequently and consequently be less active.

Unfortunately, the Arg_9 did not possess any inter-residue TRNOEs, which would have permitted the assignment of its conformation relative to the remainder of peptide 11. However, the abundance of biological data clearly supports the prediction of Brandt-Rauf *et al.*, that the side chain of Arg_9 stabilizes the YIGSR bend.

IGSR is Inactive

Deletion of tyrosine from YIGSR yields an inactive peptide (Graf et al., 1987b). This implies that the tyrosine ring participates in receptor binding. However, as Brandt-Rauf *et al.* suggested that arginine stabilized the YIGSR bend by binding to the backbone carbonyl oxygen of tyrosine, the inactivity of IGSR could result from the inability of the peptides to form a stable bend.

How the Receptor Binds Peptide 11

Both NMR and biological data indicate that binding of the receptor possibly involves direct contact between Cys_1 and the receptor and no contact between Arg_9 and the receptor. A survey of the "S" shaped conformations of peptide 11 (Figs. 35 and 43-44) and the d-analog (Figs. 29 and 46) reveals that it is possible to present Cys_1 to the receptor and simultaneously direct Arg_9 away from the receptor. This could be accomplished if Cys_1 and I_6X_7 of the YIXSR turn were on the contact interface with the receptor.

Conclusion

A candidate for the biologically active conformation of peptide 11 has been generated by incorporation TRNOESY ^1H-^1H NMR data into molecular dynamics simulations. Comparison of the native peptide to mono-

substituted analogs provided insights as to the structural characteristics necessary for biological activity. The proposed biologically active conformation of native peptide 11 is consistent with and able to explain the relative activities of all known modified peptide sequences derived from the native peptide 11 sequence. The excellent agreement between the proposed structure and the known function of peptide 11 suggests that the candidate conformation presented in this work is likely to be the conformation of peptide 11 that inhibits cell adhesion by binding to the 67 kDa high-affinity laminin receptor. However, the accuracy of the proposed structure will not be fully specified until the structure can be refined with back-calculations and the activity of an analog with a synthetically locked conformation is compared to the activity of native peptide 11.

REFERENCES

Balaram, P., Bothner-By, A.A., and Dadok, J. (1972a). Negative Nuclear Overhauser Effects as Probes of Macromolecular Structure. *J. Am. Chem. Soc.* **94**, 4015-4017.

Balaram, P., Bothner-By, A.A., and Breslow, E. (1972b). Localization of Tyrosine at the Binding Site of Neurophysin II by Negative Nuclear Overhauser Effects. *J. Am. Chem. Soc.* **94**, 4017-4018.

Bax, A. (1989). Homonuclear Hartman-Hahn Experiments. *Methods in Enzymology* **176**, 151-168.

Bax, A. and Davis, D.G. (1985a). Practical Aspects of Two-Dimensional Transverse NOE Spectroscopy. *J. Mag. Res.* **63**, 207-213.

Bax, A. and Davis, D.G. (1985b). MLEV-17 Based Two-Dimensional Homonuclear Magnetization Transfer Spectroscopy. *J. Mag. Res.* **65**, 255-360.

Beck, K., Hunter, I., and Engel, J. (1990). Structure and Function of Laminin: Anatomy of a Multidomain Glycoprotein. *FASEB J.* **4**, 148-160.

Billeter, M., Braun, W., and Wüthrich, K. (1982). Sequential Resonance Assignments in Protein 1H Nuclear Magnetic Resonance Spectra. *J. Mol. Biol.* **155**, 321-346.

Bodenhausen, G., Vold, R.L., and Vold, R.R. (1980). Multiple Quantum Spin Echo Spectroscopy. *J. Mag. Res.* **37**, 93.

Bogusky, M.J., Naylor, A.M., Pitzenberger, S.M., Nutt, R.F., Brady, S.F., Colton, C.D., Sisko, J.T., Anderson, P.S., and Veber, D.F. (1992). NMR and Molecular Modelling Characterization of RGD Containing Peptides. *Int. J. Peptide Protein Res.* **39**, 63-76.

Bothner-By, A.A., Stephens, R.L., Lee, J., Warren, C.D. and Jeanloz, R.W. (1984). Structure Determination of a Tetrasaccharide: Transient Nuclear Overhauser Effects in the Rotating Frame. *J. Am. Chem. Soc.* **106**, 811-813.

Brandt-Rauf, P.W., Pincus, R.P., Carty, R.P. Lubowsky, J., Avitable, M., Carucci, J., and Murphy, R.B. (1989). Conformation of the Metastasis-Inhibiting Laminin Pentapeptide. *J. Prot. Chem.* **8**, 149-157.

Brooks, B.R., Bruccoleri, R.E., Olafson, B.D., States, D.J., Swaminathan, S., and Karplus, M. (1983). *J. Comput. Chem.* **4**, 187-217.

Bundi, A. and Wüthrich, K. (1979). ^{1}H NMR parameters of the common amino acid residues measured in aqueous solutions of the linear tetrapeptides H-Gly-Gly-X-L-Ala-OH. *Biopolymers* **18**, 285-297.

Burke, C., Mayo, K.H., Skubitz, A.P.N., and Furcht, L.T. (1991). ^{1}H NMR and CD Secondary Structure Analysis of Cell Adhesion Promoting Peptide F-9 from Laminin. *J. Biol. Chem.* **266**, 19407-19412.

Campbell, A.P. and Sykes, B.D. (1991a). Theoretical Evaluation of the Two-Dimensional Transferred Nuclear Overhauser Effect. *J. Mag. Res.* **93**, 77-92.

Campbell, A.P. and Sykes, B.D. (1991b). Interaction of Troponin I and Troponin C: Use of the Two-dimensional Nuclear Magnetic Resonance Transferred Nuclear Overhauser Effect to Determine the Structure of the Inhibitory Troponin I Peptide When Bound to Skeletal Troponin C. *J. Mol. Biol.* **222**, 405-421.

Cavanagh, J., and Rance, M. (1990). Sensitivity Improvement in Isotropic Mixing (TOCSY) Experiments. *J. Mag. Res.* **88**, 72-85.

Chou, P.Y. and Fasman, G.D. (1978). Prediction of the Secondary Structure of Proteins from their Amino Acid Sequence. *Adv. Enzymol. Relat. Areas Mol. Biol.* **48**, 45-148.

Chung, A. E., Jaffe, R., Freeman, I. L., Vergnes, J. P., Braginski, J. E., and Carlin, B. (1979). Properties of a Basement Membrane-Related Glycoprotein Synthesized in Culture by a Mouse Embryonal-Carcinoma Derived Cell Line. *Cell* **16**, 277-281.

Clore, G.M. and Gronenborn, A.M. (1983). Theory of the Time Dependent Transferred Nuclear Overhauser Effect: Applications to Structural Analysis of Ligand-Protein Complexes in Solution. *J. Mag. Res.* **53**, 423-442.

Clore, G.M.. Gronenborn, A.M., Carlson, G., and Meyer, E.F. (1986). Stereochemistry of Binding of the Tetrapeptide Acetyl-Pro-Ala-Pro-Tyr-NH2 to Porcine Pancreatic Elastase. *J. Mol. Biol.* **190**, 259-267.

Dyson, H.J., Rance, M., Houghten, R.A., Lerner, R.A., and Wright, P.E. (1988a). Folding of Immunogenic Peptide Fragments of Proteins in Water Solution: I. Sequence Requirements for the Formation of Reverse Turn. *J. Mol. Biol.* **201**, 161-200.

Dyson, H.J., Rance, M., Houghten, R.A., Wright, P.E., and Lerner, R.A. (1988b). Folding of Immunogenic Peptide Fragments of Proteins in Water Solution: II. The Nascent Helix. *J. Mol. Biol.* **201**, 201-217.

Engel, J., Odermatt, E., Engel, A., Madri, J., Furthmayr, H., Rohde, H. H., and Timpf, R. (1981). Shapes, Domains, Organizations and Flexibility of Laminin and Fibronectin, Two, Multifunctional Proteins of the Extracellular Matrix. *J. Mol. Biol.* **150**, 97-120.

Fesik, S.W., Bolis, G., Sham, H.L., and Olejniczak, E.T. (1987) Structure Refinement of a Cyclic Peptide from Two-Dimensional NMR Data and Molecular Modelling. *Biochemistry* **26**, 1851.

Gierasch, L.M., Deber, C.M., Madison, V., Niu, C.H., and Elkan, R.B. (1981) Conformations of (X-L-Pro-Y)c Cyclic Hexapeptides. Preferred β-Turn Conformers and Implications for β Turns in Proteins. *Biochemistry* **20**, 4730-4738.

Goodman, S.L. (1992). α6β1 Integrin and Laminin E8: An Increasingly Complex Simple Story. *Kidney Int.* **41**, 650-656.

Graf, J., Iwamoto, Y., Sasaki, M., Robey, F. A., and Yamada, Y. (1987a). Identification of an amino acid sequence in Laminin mediating cell attachment, chemotaxis, and receptor binding. *Cell* **48**, 989-996.

Graf, J., Ogle, R.C., Robey, F.A., Sasaki, M., Martin, G.R., Yamada, Y., and Kleinman, H.K. (1987b). A pentapeptide from the laminin B1 chain mediates cell adhesion and binds the 67 000 laminin receptor. *Biochemistry* **26**, 6896-6900.

Grathwol, C. and Wüthrich, K. (1981). NMR Studies of the Rates of Proline *Cis-Trans* Isomerization in Oligopeptides. *Biopolymers* **20**, 2623-2633.

Iwamoto, Y., Robey, F.A., Graf, J., Sasaki, M., Kleinman, H.K., Yamada, Y., and Martin, G.R. (1987). YIGSR, a Synthetic Laminin Pentapeptide, Inhibits Experimental Metastasis Formation. *Science* **238**, 1132-1134.

Jeener, J., Meier, B.H., Bachman, P., and Ernst, R.R. (1979) Investigation of Exchange Processes by Two-Dimensional NMR Spectroscopy. *J. Chem. Phys.* **11**, 4546-4553.

Kessler, H., Gehrke, M., and Griesinger, C. (1988) Two-Dimensional NMR Spectroscopy: Background and Overview of the Experiments. *Angew. Chem. Int. Ed. Engl.* **27**, 490-536.

Kleinman, H.K., McGarvey, M.L., Hassel, J.R., Star, V.L., Cannon, F.B., Lauise, G.W., and Martin, G.R. (1986) Basement Membrane Complexes with Biological Activity. *Biochemistry* **25**, 312-318.

Kramer, R.H., Vu, M., Cheng, Y.-F., and Ramos, D.M. (1991) Integrin Expression in Malignant Melanoma. *Cancer and Metastasis Reviews* **10**, 49-60.

Landry, S.J. and Gierasch, L.M. (1991) The Chaperonin GroEL Binds a Polypeptide in an α-Helical Conformation. *Biochemistry* **30**, 7359-7362.

Landry, S.J., Jordan, R., McMacken, R., and Gierasch, L.M. (1992) Different Conformations for the Same Polypeptide Bound to Chaperones DnaK and GroEL. *Nature* **355**, 455-457.

McKelvey, D.R., Brooks, C.L., and Mokotoff, M. (1991) A CHARMM Analysis of the Conformations of the Metastasis-Inhibiting Laminin Pentapeptide. *J. Prot. Chem.* **3**, 265-271.

Macura, S. and Ernst, R.R. (1980). Elucidation of Cross Relaxation in Liquids by Two-Dimensional NMR Spectroscopy. *Mol. Phys.* **41**, 95-117.

Macura, S., Huang, Y., Suter, D., and Ernst, R.R. (1981) Two-Dimensional Chemical Exchange and Cross-Relaxation Spectroscopy of Coupled Nuclear Spins. *J. Mag. Res.* **43**, 259-281.

Marion, D. and Wüthrich, K. (1983). Application of Phase Sensitive Two-Dimensional Correlated Spectroscopy (COSY) for Measurements of 1H-1H Spin-Spin Coupling Constants in Proteins. *Biochem. Biophys. Res. Commun.* **113**, 967-974.

Mayo, K.H., Burke, C., Lindon, J.N., Kloczewiack, M. (1990) ^{1}H NMR Sequential Assignments and Secondary Structure Analysis of Human Fibrinogen γ-Chain C-Terminal Residues 385-411. *Biochemistry* **29**, 3277-3286.

Mayo, K.H., Parra-Diaz, D., McCarthy, J.B., and Chelberg, M. (1991). Cell Adhesion Promoting Peptide GVKGDKGNPGWPGAP from the Collagen Type IV Triple Helix: Cis/trans Proline-Induced Multiple ^{1}H NMR Conformations and Evidence for a KG/PG Multiple Turn Repeat Motif in the All-trans Proline State. *Biochemistry* **30**, 8251-8267.

Mrabet, N.T., Van den Broeck, A., Van den Brande, I., Stanssens, P., Laroche, Y., Lambeir, A., Matthijssens, G., Jenkins, J., Chiadmi, M., van Tilbeurgh, H., Rey, F., Janin, J., Quax, W.J., Lasters, I., De Maeyar, M., and Wodax, S.J. (1992). Arginine Residues as Stabilizing Elements in Proteins. *Biochemistry* **31**, 2239-2253.

Neuhaus, D. and Keeler, J. (1986). "False" Transverse NOE Enhancements in CAMELSPIN Spectra. *J. Mag. Res.* **68**, 568-574.

Ni, F., Konishi, Y., Frazier, R.B., and Scheraga, H.A. (1989a). High-Resolution NMR Studies of Fibrinogen-like Peptides in Solution: Interaction of Thrombin with Residues 1-23 of the Aα Chain of Human Fibrinogen. *Biochemistry* **28**, 1989.

Ni, F., Meinwald, Y.C., Vásquez, M, and Scheraga, H.A. (1989b). High-Resolution NMR studies of Fibrinogen-like Peptides in Solution: Structure of a Thrombin-Bound Peptide Corresponding to Residues 7-16 of the Aα Chain of Human Fibrinogen. *Biochemistry* **28**, 3094-3105.

Ni, F., Konishi, Y., Bullock, L.D., Rivetna, M.N., and Scheraga (1989c). High-Resolution NMR Studies of Fibrinogen-like Peptide in Solution: Structural Basis for the Bleeding Disorder Caused by a Single Mutation of Gly(12) to Val(12) in the Aα Chain of Human Fibrinogen Rouen. *Biochemistry* **28**, 3106-3119.

Olejniczak, E.T., Gample, R.T., Jr., Rockway, T.W., and Fesik, S.W. (1988) Study of the Solution Conformation of Rat Atrial Natriuretic Factor 7-23 in Sodium Dodecyl Sulfate Micelles. *Biochemistry* **27**, 7124-7131.

Ostheimer, G.J., Starkey, J.R., Lambert, C.G., Helgerson, S.L., and Dratz, E.A. (1992). NMR Constrained Solution Structures for Laminin Peptide 11: Analogs Define Structural Requirements for Inhibition of Tumor Cell Invasion of Basement Membrane Matrix. *J. Biol. Chem.*, in press.

Pease, L.G., Niu, C.H., and Zimmerman, G. (1979) *J. Am. Chem. Soc.* **101**, 184-191.

Plateau, P. and Guéron, M. (1982). Exchangeable Proton NMR Without Baseline Distortion, Using New Strong-Pulse Sequence. *J. Am. Chem. Soc.* **104**, 7310-7311.

Ramos, D.M., Cheng, Y.F., and Kramer, R.H. (1991) *Invasion and Metastasis* **11**, 125-138.

Redfield, A.G. and Kuntz, S.D. (1975) *J. Mag. Res.* **19**, 250.

Reed, J., Hull, W.E., von der Lieth, C.-W., Kübler, D., Suhai, S., and Kinzel, V. (1988). Secondary Structure of the Arg-Gly-Asp Recognition Site in Proteins Involved in Cell-Surface Adhesion. *Eur. J. Biochem.* **178**, 141-154.
Repesh, L.A. (1989) A New in vitro Assay for Quantitating Tumor Cell Invasion. *Invasion and Metastasis* **9**, 193-208.

Rose, G.D., Gierasch, L.M., and Smith, J.A. (1985) Turns in Peptides and Proteins. *Adv. Prot. Chem.* **37**, 1-99.

Scheraga, H.A. (1984) *Carlsberg Res. Commun.* 49, 1-55.

Starkey, J.R. (1990) Cell-matrix Interactions During Tumor Invasion. *Cancer and Metastasis Reviews* **9**, 113-123.

Terranova, V.P., Rao, C.N., Kalebi, T., Margulies, I.M., and Liotta, L.A. (1983) Laminin Receptor on Human Breast Carcinoma Cells. *Proc. Natl. Acad. Sci. USA* **80**, 444-448.

Timpl, R., Rohde, H., Gehron Robey, P., Rennard, S.I., Foidart, J.M., and Martin, G.R. (1979) Laminin - a Glycoprotein from Basement Membrane. *J. Biol. Chem.* **254**, 9933-9937.

Wewer, U.M., Lance, A.L., Jaye, M. Ricca, G.A., Drohan, W.N., Claysmith, A.P., Rao, C.N., Wirth, P., Coligan, J.E., Albrechisen, R., Mudryj, M., and Sobel, M.E. (1986) Altered Levels of Laminin Receptor mRNA in Various Human Carcinoma Cells that have Different Abilities to Bind Laminin. *Proc. Natl. Acad. Sci. USA* **83**, 7137-7141.

Wishart, D.S., Sykes, B.D., and Richards, F.M. (1992) The Chemical Shift Index: A Fast and Simple Method for the Assignment of Protein Secondary Structure through NMR Spectroscopy. *Biochemistry* **31**, 1647-1651.

Wright, P.E., Dyson, J., and Lerner, R.A. (1988). Conformation of Peptide Fragments of Proteins in Aqueous Solution: Implications for Initiation of Protein Folding. *Biochemistry* **27**, 7167-7174.

Wüthrich, K., Billeter, M., and Braun, W. (1984). Polypeptide Secondary Structure Determination by Nuclear Magnetic Resonance Observation of Short Proton-Proton Distances. *J. Mol. Biol.* **180**, 715-740.

Wüthrich, K. (1986). *NMR of Proteins and Nucleic Acids*, John Wiley & Sons, New York.

Wüthrich, K. (1989). Protein Strcuture Determination in Solution by NMR Spectroscopy. *J. Biol. Chem.* **265**, 22059-22062.

Zimmerman, S.S., Pottle, M.S., Nemethy, G., and Scheraga, H.A. (1977). Conformational Analysis of the 20 Naturally Occurring Amino Acid Residues Using ECEPP. *Macromolecules* **10**, 1-9.